Aerodynamic Forces and Heat Transfer of Sphere and Sharp Cone In Hypersonic Flow

A Project Presented to

The Faculty of the Aerospace Engineering Program

San Jose State University

In Partial Fulfillment of the Requirements

for the

Degree of Master of Science

In

Aerospace Engineering

by

Josue Lopez
May 2014

ABSTRACT

Aerodynamic Forces and Heat Transfer of A Sphere and Sharp Cone In Hypersonic Flow

By

Josue Lopez

Computational Fluid Dynamics (CFD) has become a very useful tool when it comes to simulating a flow over a blunt body at any Mach number. Some programs do not yield very good results at hypersonic velocities, due to the high temperatures and the reactions of the flow involving the high temperature chemistry. The CFD software in this analysis is STAR CCM+, which is capable of simulating hypersonic flow and account for chemistry at high velocities. The scope of this project is to calculate lift, drag and heat transfer using Newtonian and modified Newtonian to compare to Computational Fluid Dynamics simulations. The comparison will be from a range of Mach numbers from Mach 5 to Mach 15 in intervals of 5. The geometries analyzed will be a sphere and cone of various semi-apex angles. As the semi-apex angle varies, the shock detachment distance also varies affecting the heat transferred to the nose of vehicle. The goal is to compare the accuracy in between analytical and CFD simulation results to observe which method yields better results when comparing to experimental data.

Table of Contents

List of Figures

List of Tables

Nomenclature

θ - Angle at which a surface is inclined with respect to the free stream in Newtonian Theory.

α - Angle of attack

ε - Semi-apex angle of a circular sharp cone

β - Wave angle for exact oblique shock theory in Eq. 8

ϕ - Angle between a normal to the surface and free stream in Newtonian Theory and Meridian angle when looking at a cone, from the base or the sharp end, at an angle of attack

Introduction

Hypersonic flight has been a major topic in the field of Aerospace Engineering ever since flight has been an interest to man. It all started in the early 1900s with the Wright brothers, by designing and building the first aircraft that was able to sustain flight. Throughout the years, there has been substantial research to improve flight conditions, and flight capabilities in the hypersonic regime. Hypersonic flight is labeled as the regime when the flow (or a vehicle) travels five times the speed of sound or faster (Mach ≥ 5) although nothing out of the ordinary occurs at Mach 5, as it is the case at Mach 1 with the sonic boom. In hypersonic velocity regime, there are certain physical flow phenomena that are very important as the Mach number increases to higher values. At times some of the phenomena may become an important aspect at Mach 3 and sometimes at around Mach 7. Hypersonic velocities are not very common in aircraft; they are mostly seen in re-entry vehicles when they enter the atmosphere. For example, the Apollo lunar capsule reached a velocity greater than Mach 36 as it re-entered the atmosphere. Recently hypersonic flight has been considered for aircraft, and some prototypes have been tested by the United States Air Force, such as the X-51A Waverider.

As Mach number increases so does the temperature, and some of the phenomena that takes place is the dissociation of certain elements in the flow. Temperatures surrounding the vehicle can reach +3,000 K, which was the case for the Apollo lunar capsule when it re-entered the atmosphere [5]. Temperatures are a major concern for re-entry vehicles; the temperatures need to be controlled to be able to keep the vehicle safe as well as the crew. Heat transfer considerations need to be addressed very seriously

when dealing with hypersonic velocity, which is why the geometrical shape of a hypersonic vehicle is important, as well as for drag consideration in aircraft.

The scope of this paper is to analyze various geometrical shapes (vehicles) using Newtonian and Modified Newtonian theories to obtain lift/drag coefficients and heat transfer data at various Mach numbers. The cone shape will also be analyzed at an angle of attach to compare to the accuracy of computational fluid dynamic simulations in a hypersonic flow regime.

Literature Review

The reasoning behind this project is based on the interest for hypersonic velocity flight. It is a topic that has been highly researched since the early 1900's and there has been much speculation about it in the 21st century; which has caught the attention of many. Although technology is very advanced, there are no aircrafts that can travel at hypersonic speed or even at supersonics speeds on a regular basis. If commercial aircraft could travel at hypersonic speeds nothing would be the same; general population would travel from one side of the planet to the other without much difficulty. Many engineering applications rely on the computer to carry on many of the complicated and tedious array of calculations needed to decipher certain problems. Although the computer is a very helpful and powerful tool, sometimes it is not very accurate on certain applications due to its complexity. If it's too complicated for a computer to carry on the calculations, it is definitely impossible, or near impossible, to do it by hand. In the branch of Aerospace Engineering, when trying to model a flow, computational fluid dynamics simulation programs are used. The programs are chosen depending on the regime that it's being analyzed and the accuracy of the results vary. The simulations do not yield very accurate results in aerodynamic, nor heat transfer data for hypersonic regimes, due to the complexity of the physics involved with the flow. It is very difficult to account for all major disciplines simultaneously, when analyzing hypersonic vehicles in terms of their aerodynamics. The simulations are not always good, but for certain flow regimes the simulations are very accurate, which is why computational fluid dynamics simulation programs are used.

Typically during the conceptual design process of a hypersonic entry vehicle, various methods are employed to improve the speed of the computational simulations. One of the methods tends to be panel methods in conjunction with Newtonian flow theory to obtain some aerodynamic characteristic at hypersonic velocities. Using alternative methods comes at the expense of a small reduction in reliability of the method and the limited amount of vehicle shapes that can be analyzed using these alternative methods. The geometrical shapes used in panel methods are generally chosen among shapes that provide the necessary aerodynamics performance, such as lift and drag for certain mission requirements. Computational fluid dynamics has more substantial requirements to analyze a given vehicle [2].

Given that computational fluid dynamics simulations do not yield very accurate results for hypersonic flow, due to the complicated physical phenomena involved, research has been done on comparing the accuracy of computational fluid dynamics programs with experimental data gathered from a hypersonic shock tunnel for a given blunt body prototype vehicle. The objective of the research is to validate the codes of computational fluid dynamic programs by comparing the results to experimental data and Newtonian theory. The subject used is a 60^{o} blunt cone prototype at $\alpha = 0^{o}$. The methodology for the validation of the CFD code was to calculate aerodynamic forces and convective heat transfer rates using Newtonian and Modified Newtonian theories. The same data was collected from a wind tunnel using the prototype, and finally the same data was obtained using a CDF simulator. The experiment took place in a hypersonic shock tunnel HST2 with a flow of Mach 5.75. The equipment used was an accelerometer-based three-component balance system to obtain the coefficient of drag, and platinum thin-film

gauges attached to the surface of the prototype to obtain the convective heat transfer to the body. The computational based program used for the simulations was an Axi-Symmetric Navier-Stokes simulator.

The results generated from all three methods were very satisfactory in accordance to the objective of the research. The theoretical, Newtonian and modified Newtonian theories, calculations of the coefficient of drag differed from the experimental value by 6%, while the computational value over predicted the coefficient by 9% from the experimental data. For the convective heat transfer rate, the measured value was 11% higher than the theoretical value, and the computational value was 2% lower at the stagnation point. The results obtained from the study were satisfactory to validate the code used in the computational program to simulate hypersonic flow and generate reasonable values. Although the computational simulator over predicted the drag coefficient, it was within a reasonable margin in which the safety factor for any design will account for the error. For the convective heat transfer rate the computational value was only 2% lower than the experimental value, being a really good result since heat transfer is very important at hypersonic velocities [2].

Theory

Hypersonic flight has become of great interest today, and new vehicle concept designs are being developed to travel at high Mach numbers. Hypersonic aerodynamics is very important due to certain physical phenomena that do not occur at lower supersonic speeds. The flow field in hypersonic flight is dominated by the phenomena, which involves high temperature flow dynamics. Unlike subsonic and supersonic flows, hypersonic flow is nonlinear and the hypersonic aspect of a flow may become important at Mach 3. Moreover, as Mach numbers increases the phenomena becomes more critical.

Newtonian theory was investigated at the end of the seventeenth century, before thermodynamics, kinetic theory and viscous stresses were developed, which is why some of the analyses and results may be in error in comparison to today's knowledge in the subject. At the time Sir Isaac Newton did not have an intuition of the shock wave or the shock layer, and he did not realize the flow velocity necessary for compressibility to dominate the flow field. Sir Isaac Newton's approach was from a set of basic laws and a theoretical model of a physical problem leading to a solution for the problem. Therefore, Newtonian theory is often used to estimate the pressure distribution over a surface of a body in hypersonic flow.

Newtonian Theory

The oldest and most commonly used method in the realm of hypersonic flow is Newtonian theory. The well known Newtonian sine-squared law is used in local surface inclination methods. Considering a surface inclined at angle θ to the free stream, the flow comprises of an infinite number of particles that impact the surface and then travel

tangentially to the surface. At the moment of impact, particles lose their normal component but are able to keep the tangential component. The rate of change of the normal component of momentum is equal to the force applied on the surface by the impact. This is shown in Fig. 1, where the free stream velocity normal to the surface is $V_\infty \sin\theta$.

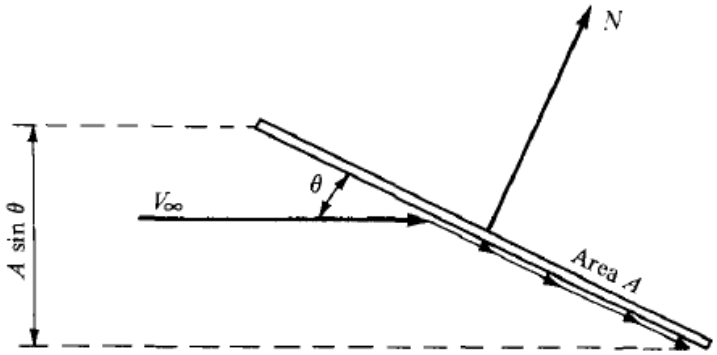

Figure 1: Representation of Newtonian impact theory

If the area of the surface is A, the mass flow component on the surface is $\rho_\infty A \sin\theta\, V_\infty$. Therefore, the rate of change of momentum is

(mass flow) * (change in normal component of velocity)

$$(\rho_\infty V_\infty A \sin\theta) * (V_\infty \sin\theta) = \rho_\infty V_\infty^2 A \sin^2\theta$$

Which then yields Newton's second law, the force normal to the surface:

$$N = \rho_\infty V_\infty^2 A \sin^2\theta \qquad \text{Eq. (1)}$$

The force acts as the rate of change of momentum, and the force per unit area can be characterized as:

$$\frac{N}{A} = \rho_\infty V_\infty^2 \sin^2\theta \qquad \text{Eq. (2)}$$

Considering the normal force per unit area in terms on aerodynamics, Newton's model adopts a stream of particles moving parallel towards the surface, with a rectilinear motion with no random motion. It is known that moving gas is composed of random motion of the particles, as well as guided motion. Also, the static free stream pressure p_∞ is measured from random motion particles only. Therefore, the guided motion particles in the model are the result of the normal force per unit area (N/A). Accounting for the pressure of random motion and guided motion particles, the force per unit area can be denoted as the pressure difference above p_∞, explicitly $p - p_\infty$. Consequently, equation 2 can be written as:

$$p - p_\infty = \rho_\infty V_\infty^2 \sin^2\theta \qquad \text{Eq. (3)}$$

Equation 3 can also be ascribed in terms of the pressure coefficient $C_p = (p - p_\infty) / \frac{1}{2} \rho_\infty V_\infty^2$ as:

$$\frac{p - p_\infty}{\frac{1}{2}\rho_\infty V_\infty^2} = 2sin^2\theta$$

Which can also be expressed as:

$$C_p = 2\sin^2\theta \qquad \text{Eq. (4)}$$

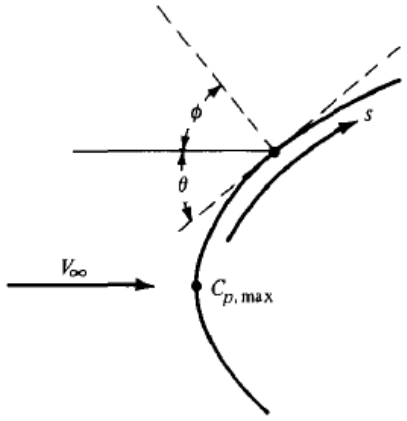

Figure 2: Angle distinction for Newtonian theory

Newton's sine-squared law states that the pressure coefficient is proportional to the sine square of the angle between a tangent to the surface and to the free stream. Newtonian theory can also be expressed in terms of the angle between a normal to the surface and free stream, and the angle is represented by ϕ as shown in Figure 2. In terms of ϕ, Equation 4 becomes:

$$C_p = 2\cos^2\phi \qquad \text{Eq. (5)}$$

The physical meaning for the theory can be derived from hypersonic oblique shock relations for C_p with free stream conditions.

$$C_p = \frac{4}{\Upsilon+1}\left[sin^2\beta - \frac{1}{M_\infty^2}\right] \qquad \text{Eq. (6)}$$

Equation 7 is given after taking the limit as the Mach number increases to infinity:

$$C_p = \frac{4}{\Upsilon+1}\left[sin^2\beta\right] \qquad \text{Eq. (7)}$$

Considering that the heat capacity ratio (Υ) goes to 1 as the Mach number goes to infinity, Equation 8 is derived from taking both limits as $M_\infty \to \infty$ and $\gamma \to 1$ yields:

$$C_p = 2\sin^2\beta \qquad \text{Eq. (8)}$$

Equation 8 results from the exact oblique shock theory, and for the moment β is the wave angle, not the deflection angle. Considering the density relation for exact oblique shock, Equation 9:

$$\frac{\rho_2}{\rho_\infty} = \frac{(\Upsilon+1)M_\infty^2\sin^2\beta}{(\Upsilon-1)M_\infty^2\sin^2\beta+2} \qquad \text{Eq. (9)}$$

Equation 10 was derived as the limit of M_∞ goes to infinity:

$$\frac{\rho_2}{\rho_\infty} = \frac{(\gamma+1)}{(\gamma-1)} \qquad \text{Eq. (10)}$$

In addition to $M_\infty \to \infty$, also $\gamma \to 1$, resulting in equation 11:

$$\frac{\rho_2}{\rho_\infty} \to \infty \qquad \text{Eq. (11)}$$

As shown in Equation 11, the density behind the shock is very large, and the shock wave follows the shape along the body surface. This is good for $M_\infty \to \infty$ and small deflection angles.

$$\frac{\beta}{\theta} = \frac{(\gamma+1)}{2} \qquad \text{Eq. (12)}$$

Considering that $\gamma \to 1$, $M_\infty \to \infty$, and θ and β are small then $\beta = \theta$ and the shock wave rests on the body, and the results becomes Equation 4:

$$C_p = 2\sin^2\theta \qquad \text{Eq. (4)}$$

The Newtonian model of fluid flow accounts for the particles that impact the frontal area of the body only, since the particles cannot turn around and impact the back area of the body. Therefore, the back area of the body does not have any impact pressure, and the pressure on this area can be assumed to be ambient, $p = p_\infty$. Consequently, the pressure coefficient on the back area is zero.

Modified Newtonian Theory

The maximum pressure, as well as maximum pressure coefficient (C_p), occurs at the stagnation point. Whereas in a blunt body it will be at $\theta = \pi/2$ and $\phi = 0$, with a $C_p = 2$. Maximum pressure coefficient occurs as $M_\infty \to \infty$, at a normal shock wave at hypersonic speeds. The flow across a normal shock can be described by:

$$p_\infty + \rho_\infty V_\infty^2 = p_2 + \rho_2 V_2^2 \qquad \text{Eq. (13)}$$

Across a normal shock wave the flow velocity decreases such that the flow behind the shock wave is subsonic. At hypersonic speed it can be assume that $(\rho_\infty V_\infty^2) >> (\rho_2 V_2^2)$, resulting in a limiting circumstance as $M_\infty \rightarrow \infty$, where:

$$p_2 - p_\infty = \rho_\infty V_\infty^2$$

or

$$C_p = \frac{p2 - p\infty}{\frac{1}{2}\rho_\infty V_\infty^2} = 2 \qquad \text{Eq. (14)}$$

The maximum pressure coefficient occurs for an infinite Mach value, for a large but finite Mach number the coefficient of pressure is less than 2. The maximum C_p occurs at the stagnation point, and can be denoted as $C_{p,max}$ as in Figure 2. For a given M_∞, $C_{p,max}$ can be calculated using normal shock wave theory using:

$$C_{p,max} = \frac{2}{\gamma M_\infty^2}\left(\frac{p_{0,2}}{p_\infty} - 1\right) \qquad \text{Eq. (15)}$$

Downstream of the stagnation point the C_p can be presumed to follow the sine-squared theory by Newtonian theory, classified as:

$$C_p = C_{p,max}\sin^2\theta \qquad \text{Eq. (16)}$$

In terms of blunt bodies, Modified Newtonian theory, Equation 16, is more accurate than Newtonian theory, Equation 4.

Impact Theory Modified

As previously mentioned, Newtonian Theory assumes the Mach value to be very high and the value of specific heat ratio to be unity, which yield Eq. 4. This equation only accounts for the angle of attack, and when dealing with circular geometries with varying semi-apex angles Eq. (4) may not be adequate for the analysis. Therefore, several modifications have been done to Eq. (4) in order to incorporate the semi-apex angle and the meridian angle along the circular shape, to define the pressure coefficient at any given point in the shape as a function of angle of attack and semi-apex angle. In Eq. (4) the value of θ is the local angle of attack to the free stream, and for a cone the value of $\sin\theta$ is given by:

$$\sin\theta = \sin\varepsilon * \cos\alpha + \cos\varepsilon * \sin\alpha * \cos\phi \qquad \text{Eq. (17)}$$

Where, ε is the semi-apex angle in a circular cone, α is the angle of attack with respect to the free stream flow, and ϕ is the meridian angle measured from the windward. Given that more angles are introduced into the equation, the angle referred to as the angle of attack is changed from θ to α, as it is typically know as. This expression was derived using shock layer theory in an approach to derive an approximation for the pressure coefficient involving the semi-apex angle, angle of attack and meridian angle. The approximations were by Laval, Cheng and Guiraud, and the full derivation can be found in ref. [7].

Heat Transfer

Aerodynamic heating is a key element in hypersonic flow. As the velocity climbs into the hypersonic regime, heat flux increases to the cubed of the velocity. The shock wave formed due to hypersonic velocities reaches very high temperatures by the flow

impact where the air elements dissociate. The temperature in the shock wave can reach beyond 9000 K, to the point of ionization of Oxygen (O_2) and Nitrogen (N_2) at very high Mach values. The shock layer thickness formed gives some cooling time/distance before reaching the surface of the body. Typically, the temperature that reaches the body is significantly smaller than the shock wave temperature; since the usual method of aerodynamic heating from shock layer to the surface is by means of thermal conduction. Therefore, a greater shock layer thickness can be achieved by having a blunted body, which in return yields a smaller heat flux. However, at hypersonic velocities the shock layer temperature becomes extremely hot to the point that it also emits thermal radiation, which turns out to be the dominant source of heat transfer at temperatures higher than 1000 K on the shock layer. Consequently, as the shock layer reaches ionization temperatures thermal radiation becomes a substantial portion of the heat transferred to the body surface, and convective heating is negligible.

For a slender sharp cone the oblique shock wave is very close to the body. The shock layer between the shock wave and the body is very thin. A major interaction between the inviscid flow behind the shock and viscous boundary layer on the surface occurs as a result of a thin shock layer. As a result that hypersonic vehicles usually fly at high altitudes where density is low, the boundary layer becomes thicker, which in some cases is of the same magnitude as the shock layer thickness. Thermal conduction is a physical characteristic of viscous flow in addition to friction. Where friction dissipates heat over a body, which comes in kinetic energy from the moving flow, and the flow velocity is decreased as an effect of friction. The loss of kinetic energy resurfaces as internal energy of the fluid, causing the temperature to rise. Hence, aerodynamic heating

is an important value to consider for hypersonic flight. In this paper, the heat transfer of a sphere and a sharp cone are being approximated analytically. The heat transfer rate equation used for a sphere was the following:

$$\dot{q}_s = \rho_\infty^{1/2} * {V_\infty}^3 * (1.83 * 10^8) * R^{-1/2}(1 - \frac{h_w}{h_0}) \quad [\text{W/cm}^2] \qquad \text{Eq. (18)}$$

Where R is the radius of the sphere, V_∞ and ρ_∞ are the free stream velocity and density respectively. The static enthalpy and enthalpy at the wall are defined by h_0 and h_w respectively. For a sharp cone a similar equation was used, where the equation is a function of the semi apex angle, ε, and cord length, x:

$$\dot{q}_c = 4.03 * 10^{-5} \sqrt{\frac{\rho_\infty * cos\varepsilon}{x}} * {V_\infty}^{3.2} * sin\varepsilon * (1 - \frac{h_w}{h_0}) \quad [\text{W/m}^2] \qquad \text{Eq. (19)}$$

The values for h_0 are as follows for sphere and cone respectively:

$$h_0 = h_\infty + 0.5\ {V_\infty}^2$$

$$h_0 = h_\infty + 0.4\ {V_\infty}^2$$

Where the free stream enthalpy is equivalent to the specific heat of the free stream, times the free stream temperature, $h_\infty = C_p * T_\infty$.

STAR CCM+

The STAR-CCM+ software is an engineering physics simulator within a single integrated package with multiple tools. In the acronym STAR-CCM+, the "CCM" stands for "computational continuum mechanics", where the application employs a client-server architecture to allow users to solve problems from a lightweight computer, and the heavy math algorithm, is done on a remote machine. This type of application allows for computational time to be reduced substantially.

STAR-CCM+ is an entire engineering processor used for solving problems involving

flow (of fluids or solids), heat transfer, and stress. It is composed of a suite of integrated components that is combined in order to provide a software that is able to address a wide variety of modeling needs, such as:

- 3D-CAD modeler
- CAD embedding
- Surface preparation tools
- Automatic meshing technology
- Physics modeling
- Turbulence modeling
- Post-processing
- CAE integration

STAR-CCM+ is based on object-oriented programming, which is designed to handle large models using an architecture meshes, solves and post-processes over multiple computing resources without requiring additional effort from the user.

The object-oriented programming nature of the code can be seen in the user interface. An object tree is provided for each simulation, containing object representations of all the data associated with the simulation. The objects presented on the simulation tree are located on the server, which can run as either a serial or a parallel process. A client interface connects to a server, and displays the simulation objects available on that server.

3D-CAD Modeler

3D-CAD is a feature-based parametric solid modeler within STAR-CCM+ that allows geometry to be built for CFD simulation. The geometry created with 3D-CAD is stored as 3D-CAD models, which can then be converted to geometry parts for integration with the meshing and simulation process. A major feature of 3D-CAD is design

parameters, which allows the user to modify the 3D-CAD model from outside of 3D-CAD. Another benefit is that it allows the user to solve for a particular geometry, change the size of one or more components, and quickly re-run the case.

CAD Embedding

STAR-CCM+ simulations can be set up, runned and post-processed using other CAD and PLM environments such as SolidWorks, CATIA V5, Pro/ENGINEER, and NX. CFD results are linked directly to the CAD geometry (a process called associativity). After any modification in the CAD model the simulation results can be updated by using the "update solution" button.

Surface Preparation Tools

One of STAR-CCM+'s main components is an automated process that links a powerful surface wrapper to the manufacturers unique meshing technology. The surface wrapper significantly reduces the time spent on surface cleanup and, for problems that involve large assemblies of complex geometry parts, reduces the entire meshing process to hours instead of days.

This method works by 'shrink-wrapping' a high-quality triangulated surface mesh onto any geometrical model, closing holes in the geometry and joining disconnected and overlapping surfaces, providing a single manifold surface that can be used to automatically generate a computational mesh without user intervention. STAR-CCM+ also includes a set of surface-repair tools which allows users to interactively improve the quality of imported or wrapped surfaces, offering the choice of a completely automatic repair, user control, or a combination of both.

Automatic Meshing Technology

This tool in STAR-CCM+'s single integrated process provides a fast, and automatic route from complex CAD to CFD mesh. Advanced automatic meshing technology can generate a polyhedral or predominantly hexahedral control volumes. The use of a polyhedral mesh has proven to be more accurate for fluid-flow problems than a hexahedral or tetrahedral mesh of a similar size (number of cells); meanwhile, it is considerably more difficult to create. This meshing technology offers a combination of speed, control, and accuracy. For problems involving multiple frames of reference, fluid-structure interaction and conjugate heat transfer, STAR-CCM+ can automatically create conformal meshes across multiple physical domains.

An important part of mesh generation for accurate CFD simulation is the near-wall region, or extrusion-layer mesh. STAR-CCM+ automatically produces a high-quality extrusion layer mesh on all walls in the domain. In addition, the user can control the position, size, growth-rate, and number of cell layers in the extrusion-layer mesh.

Physics Models

Some of the STAR-CCM+'s physics modeling capabilities include:

Solvers

- Segregated
- Coupled
- Finite volume solid stress

Time

- Steady state
- Implicit and explicit unsteady
- Harmonic balance

Turbulence

- RANS
- RSM
- LES/DDES
- Lamina-turbulent transition

Compressibility

- Ideal Gas
- Real Gas

Heat transfer

- Conjugate heat transfer (CHT)
- Multiband and gray thermal surface to surface radiation
- Solar radiation
- Discrete ordinates radiation (DOM) including participating media

Multiphase

- Lagrangian particle tracking
- VOF (incompressible and compressible)
- Cavitation & boiling
- Eulerian multiphase
- De-icing & De-fogging
- Melting & solidification

Moving Mesh

- Dynamic Fluid Body Interaction (DFBI or 6DOF)
- Rigid body motion
- Mesh morphing
- Multiple reference frames (MRF)

Combustion & chemical reaction

- Reaction kinetics

- Eddy break up (EBU)
- Presumed probability density function (PPDF)
- Complex chemistry
- Ignition
- NOx modeling

Distributed Resistance (Porous media)

- Anisotropic
- Orthotropic
- User defined
- Porous baffles

Turbulence Modeling

In addition to its provision for inviscid and laminar flow, STAR-CCM+ has a comprehensive range of turbulence models:

- k-epsilon (Standard, V2F, Realizable, Two-layer)
- k-omega (Standard, SST and BSL)
- Reynolds Stress (RSM – linear and quadratic)
- Spalart-Allmaras Turbulence models
- Boundary-layer transition
- Large Eddy Simulation (LES)
- Detached Eddy Simulation (DES, in the new Delayed Detached Eddy Simulation or DDES formulation)

Post-processing

STAR-CCM+ contains a suite of post-processing tools designed to enable the user to obtain maximum value and understanding resulting from the CFD simulation. This includes scalar and vector scenes, streamlines, scene animation, numerical reporting, data plotting, import and export of table data, and spectral analysis of acoustical data.

CAE Integration

Several third-party analysis packages can be coupled with STAR-CCM+ to further extend the range of possible simulations available. Co-simulation is possible using Abaqus, GT-Power, WAVE and OLGA, and file-based coupling is possible for other tools such as Radtherm, NASTRAN and ANSYS.

Modeling High Speed Flows

At high Mach numbers, extreme temperatures occur along with dissociation, or ionization, of the gas must be considered. The Mach number regimes, and the appropriate models to use, vary by gas and upstream temperature and pressure. For air however, the following general guidelines can be used:

Up to Mach 3 a calorically perfect gas assumption, namely ideal gas with constant specific heats, can be used.

From Mach 3-10 a thermally perfect gas assumption, namely ideal gas with temperature-varying specific heats, can be used.

From Mach 10-30, the dissociation needs to be modeled more accurately, so a real gas model and chemically reacting flow is used. The gas dissociation can be modeled by using finite rate chemistry models in the code, where the user will need to supply the reactions and reaction mechanisms. This will provide the correct specific heats and gamma values.

Any flow above Mach 30, involving dissociation, requires solving the Navier-Stokes equations together with the Maxwell equations, which are not inherently supported in STAR-CCM+.

Eulerian- Lagrangian Multiphase

Multiphase modeling allows solving the flow and thermal fields of two or more different materials simultaneously. Interactions between the materials can be considered with the materials being solid, liquid or gas.

The Eulerian Multiphase model (EMP) can be used for dispersed multiphase flows including bubbly, droplet and particle flows. This modeling approach is used where incompressible or compressible techniques would require excessively large meshes to resolve the free surfaces.

Lagrangian multiphase modeling tracks idealized particles or groups of particles (parcels) through the domain. These particles may be solid, fluid (droplets) or gaseous (bubbles). The interaction with the continuous phase may be either one or two way coupled, including the effects of turbulence, heat, mass and momentum transfer if so required.

Physics Models

- Three Dimensional
- Steady
    - Controls the size of the local time-steps being used in the time-marching procedure. For steady simulations, the local time-step is used by the pseudo time-step associated with the iterations. For transient simulation, the local time-step is used within a time-step.

- Gas (Air with density and dynamic viscosity of each altitude)
- Coupled Flow
    - Solves the conservation equations for mass and momentum simultaneously using a time- (pseudo-time-) marching approach. The preconditioned form of the governing equations used by the Coupled Flow model makes it suitable for solving incompressible and isothermal flows.

This formulation is robust for solving flows with dominant source terms, such as rotation. Another advantage of the coupled flow solver is that CPU time scales linearly with cell count; in other words, the convergence rate does not deteriorate, as the mesh is refined.

The coupled algorithm yields more robust and accurate solutions in compressible flow, particularly in the presence of shocks

- Real Gas
- Coupled Energy (Used to determined heat transfer)
- Turbulent
    - Accurate prediction of turbulent flow calculates quantities such as drag, and heat transfer. For most engineering analyses, the main interest is in the prediction of the mean (averaged) flow field. The effect of the fluctuations, around the average or filtered flow field, is included using a turbulence model.

- SST K-Omega model
    - Two transport equations are solved, the turbulent eddy-viscosity is defined as a function of the *turbulent kinetic energy* (k) with the turbulent dissipation rate replaced by the *specific dissipation rate* (omega) in the definition of the turbulent eddy-viscosity. The method mainly focuses in separated flows, low-Reynolds number (i.e. transitional) flows, or when the solution of the very near-wall physics is of prime importance.

- Reynolds-Averaged Navier-Stokes
    - The RANS equations are the time-averaged equations of motion for fluid flow. The RANS equations are primarily used to describe turbulent flows.

- All y+ Wall Treatment Three types of wall treatment are provided depending on the turbulence model that is chosen for the simulation:
    - The all-y+ wall treatment is a hybrid treatment that attempts to emulate the

high-y+ wall treatment for coarse meshes and the low-y+ wall treatment for fine meshes and is also formulated in order to produce reasonable answers for meshes of intermediate resolution (that is, when the wall-cell centroid falls within the buffer region of the boundary layer, where 5<y+<30).

In the case of a turbulence model using a two-layer approach, a modified all-y+ wall-treatment is applied to account for the fact that only the turbulence production is solved to the wall. The turbulence production term at the wall is determined with the all-y+ wall treatment. The turbulence dissipation rate term however becomes a function of wall-distance in the near-wall layer, which is then is blended smoothly with values computed from solving the transport equation away from the wall.

Meshing

The type of meshing used was trimmer mesh. This type of mesh is more efficient at putting cells in the desired areas. A trimmer mesh with the grid lines aligned with the flow often provides the most efficient approach to getting good results. Typical trimmer meshes contain 4-40 million cells, depending on the complexity of the geometry and flow field, and the near-wall treatment.

The type of cell used in the meshing was prism layer. This type of meshing layer yields a good resolution of the boundary layer is critical; therefore the thickness of the prism layer should be designed such that the entire boundary layer is contained within it. The use of wall functions rather than integrating to the wall can be appropriate (for SST K-Omega turbulence model) depending on factors, including:

- Desired accuracy
- Relative importance of skin friction drag
- Importance of transition

- Existence/importance of separation/reattachment on smooth boundaries
- For integrating to the wall, 20-30 prism layers are typically used, with the near-wall y+ being on the order of 1
- For wall functions, 5-8 prism layers are typically used, with the near-wall y+ being on the order of 50-150

Methodology

Determining aerodynamic forces and heat transfer data on a sphere and cone is the objective to accomplish. The sphere is the same from any angle, meaning it cannot be put at an angle of attack because it yields the same result, it is only being evaluated for the drag coefficient and heat transfer. The cone is evaluated at various semi-apex angles, and angles of attack. The cone does not yield a lift coefficient at zero angle of attack, only when the angle of attack is greater than zero.

Drag Coefficient of a Sphere

Returning to the concept of Newtonian impact theory, a body in a fluid flow only accounts for the particles that impact the frontal area of the body since the particles cannot turn around and impact the back area of the body. Therefore, the back area of the body does not have any impact pressure, and the pressure on this area can be assumed to be ambient, $p = p_\infty$. Hence, the impact area on a sphere is only the frontal area, a hemisphere. The drag is calculated by integrating over the front half of the sphere, substituting the difference of surface pressure and free stream pressure. The pressure differences are substituted using Newtonian Theory equation, listed as Eq. (4). Once the drag is obtained it can be non-dimensionalized to determine the drag coefficient. The analytical calculations can be found in Appendix 1.

Heat Transfer of a Sphere

Heat transfer was determined by obtaining the heat flux utilizing Eq. (18) for a sphere. The heat transfer varies as the Mach number increase, as well as the radius of the sphere increases. The free stream conditions used were at sea level; such as temperature, pressure and density. The temperature at the shock wave depended on the Mach and radius of the sphere, which determines the shock layer thickness. As the radius of the sphere varies, the shock layer thickness varies as well having an effect on the heat flux into the sphere. When the shock layer is greater there is more air in between the detached shock wave and the surface of the body, which could help reduce the heat flux, as there is a larger heating of the air and smaller heating of the body.

Lift and Drag Coefficients of a Sharp Cone

As already mentioned, a body in a fluid flow only accounts for the particles that impacts the frontal area and the back area does not have any impact pressure. When a sharp cone is at zero angle of attack, the whole cone has an impact pressure; hence it also has a coefficient of pressure. As the cone is at zero angle of attack the flow impact is the same everywhere. The drag coefficient for a cone at zero angle of attack can be determined using Newtonian theory by determining the drag force due to pressure over the total surface area of the cone.

When the cone is at an angle of attack the flow will impact the entire cone as well as if the angle of attack is smaller or equal to the semi apex angle of the cone. Once the angle of attack is greater than the semi apex angle, the top part of the cone will not be impacted by the fluid flow, therefore that section of the cone will have a $C_p = 0$, as is it defined in Newtonian theory. The pressure coefficient at any point in the cone can be

determined by using Eq. (4) and Eq. (17), which is a function of the semi-apex angle in a circular cone, ε, angle of attack, α, and the meridian angle, ϕ, measured from the windward to leeward. The angle at which the flow does not impact the surface is determined by:

$$\cos^{-1}\left[\frac{-\tan\varepsilon}{-\tan\alpha}\right] \qquad \text{Eq. (20)}$$

Eq. (20) is the limit at which the pressure coefficient is integrated to determine the coefficient of normal force and lift coefficient. The complete analytical calculations to determine coefficients of lift and drag can be found in Appendix 1.

Heat Transfer of a Sharp Cone

The heat flux for a cone was determined as a function of the semi-apex angle, using Eq. (19). To determine the enthalpy it was necessary to use oblique shock theory and exact method tables from ref [4] and [5] to determine the temperature at the shock with respect to the free stream temperature. As the Mach value increases, the temperature at the shock wave also increases having an effect on the static enthalpy used to determine the heat flux. The free stream conditions used were sea level, such as the density and pressure.

STAR CCM+ Set Up

Procedure

The first step in the simulation is creating the geometry and determining a domain where the flow will be analyzed. In the cases simulated, the object being analyzed (sphere or cone) was placed inside a domain (box) where each side is specified as an inlet, outlet or symmetry. The domain was significantly larger, about 20 times the length on each

side, than the object of interest to avoid the walls to have an affect on the final results.

The second step was to set up the boundary conditions of the domain, with an inlet, outlet, symmetry plane(s), wall(s) and far field. The far field boundary is set to 'free stream' boundary condition type. Angles of attack are defined by changing the far field boundary condition flow direction, not the orientation of the body. Half-body with a symmetry plane was used to reduced simulation time.

The thirds step, proceeding from the boundary conditions, is to set up the physics and meshing initial conditions on the geometry and boundary conditions of the domain. The initial conditions for the set ups being analyzed were as follows:

- Three Dimensional
- Steady
- Gas (Air with density and dynamic viscosity of each altitude)
- Coupled Flow
- Real Gas
- Coupled Energy (Used to determined heat transfer)
- Turbulent
- SST K-Omega model
- Reynolds-Averaged Navier-Stokes
- All y+ Wall Treatment

The fourth step, once all the initial conditions have been specified, is to proceed and do the surface mesh followed by a volume mesh of the geometry and domain. The mesh will be accomplished using all the initial condition values specified in the previous step.

The fifth step is to specify the data to be collected from the simulation using the 'reports' tab on the drop tree, such as the lift (cone), drag and heat transfer coefficients.

Results

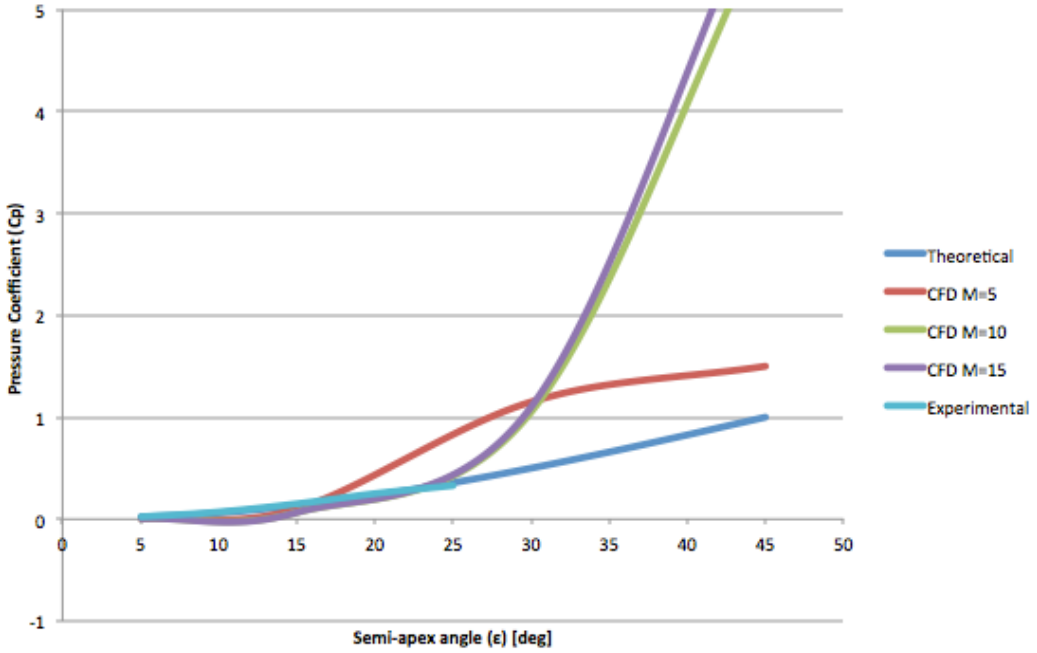

Figure 3: Pressure Coefficient distribution as a function of sharp cone Semi-apex angle (ε), comparing various methods at zero angle of attack ($\alpha = 0^{o}$)

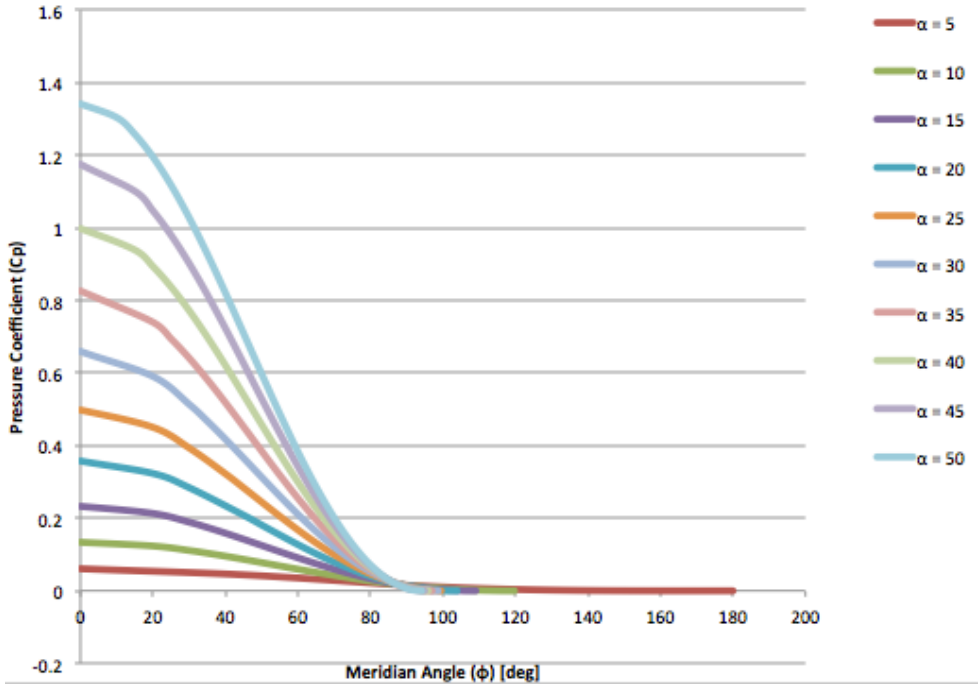

Figure 4: Pressure Coefficient distribution as a function of meridian angle (ϕ) for a five-degree semi-apex angle cone ($\varepsilon=5^{o}$) at various angles of attack (α)

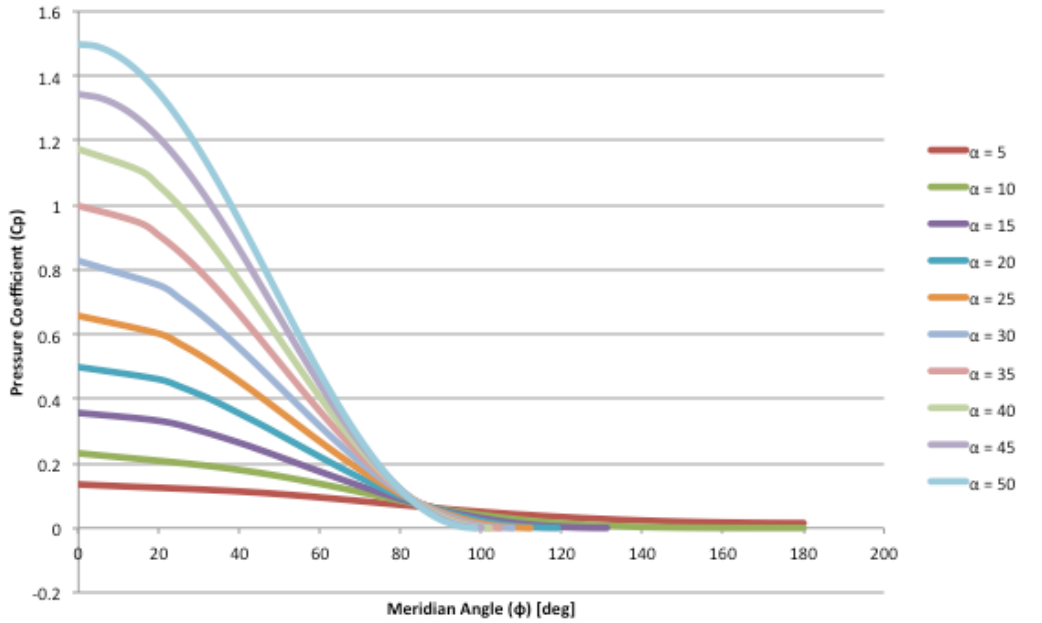

Figure 5: Pressure Coefficient distribution as a function of meridian angle (ϕ) for a ten-degree semi-apex angle cone (ε=10^{o}) at various angles of attack (α)

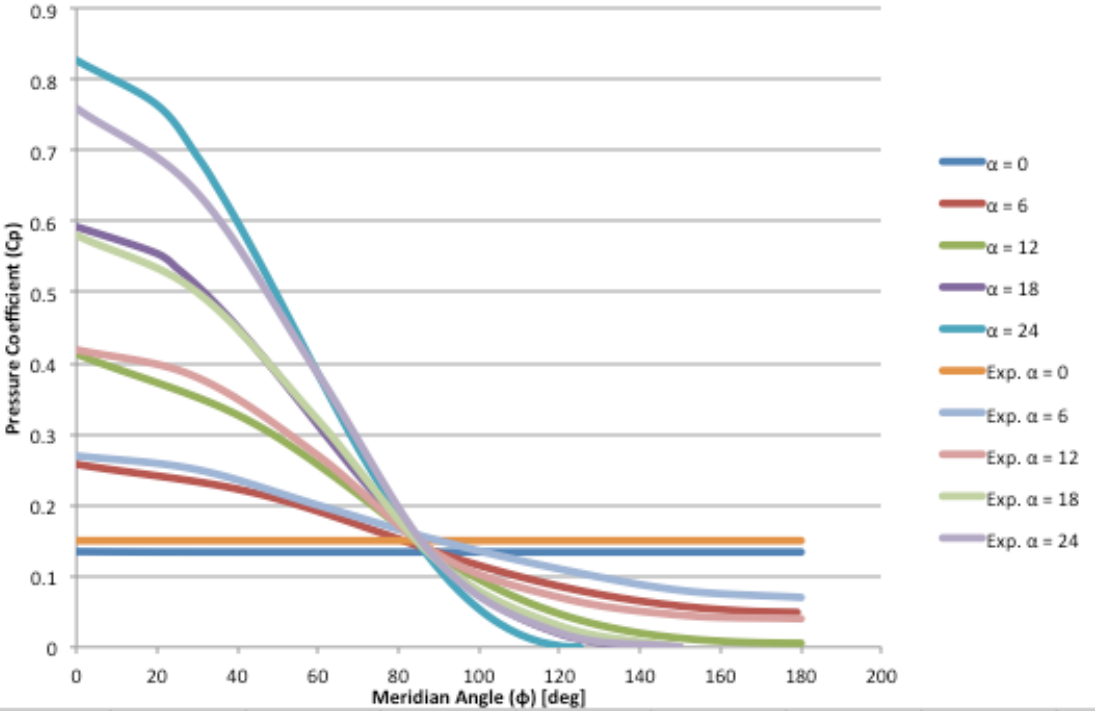

Figure 6: Pressure Coefficient distribution as a function of meridian angle (ϕ) for a fifteen-degree semi-apex angle cone (ε=15^{o}) at various angles of attack (α)

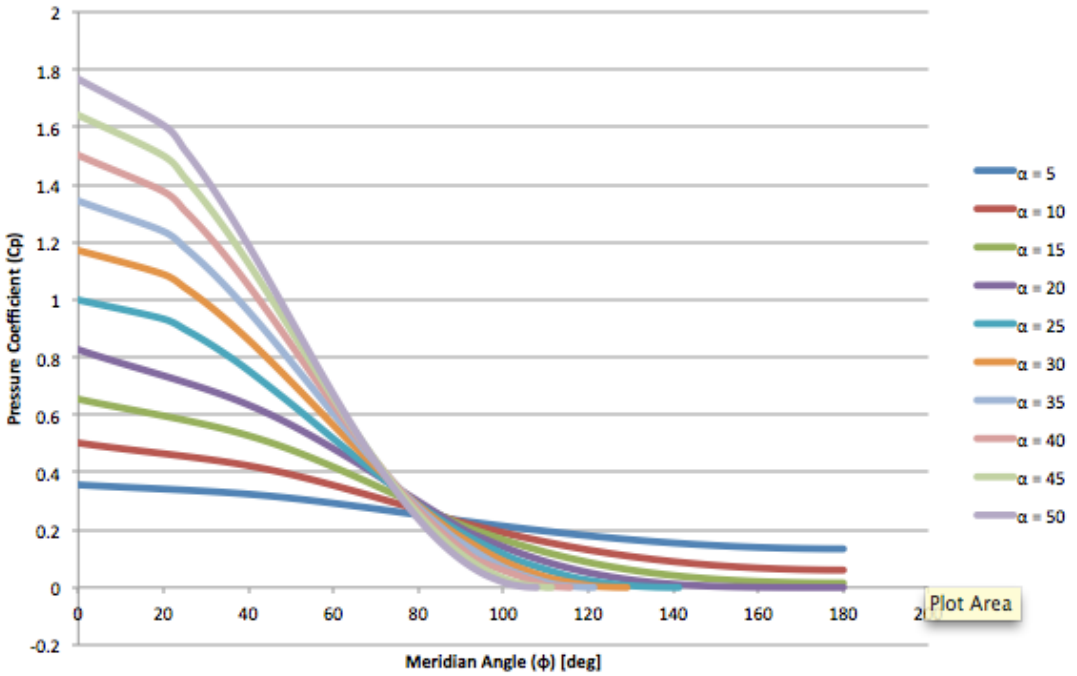

Figure 7: Pressure Coefficient distribution as a function of meridian angle (ϕ) for a twenty-degree semi-apex angle cone ($\varepsilon=20^{o}$) at various angles of attack (α)

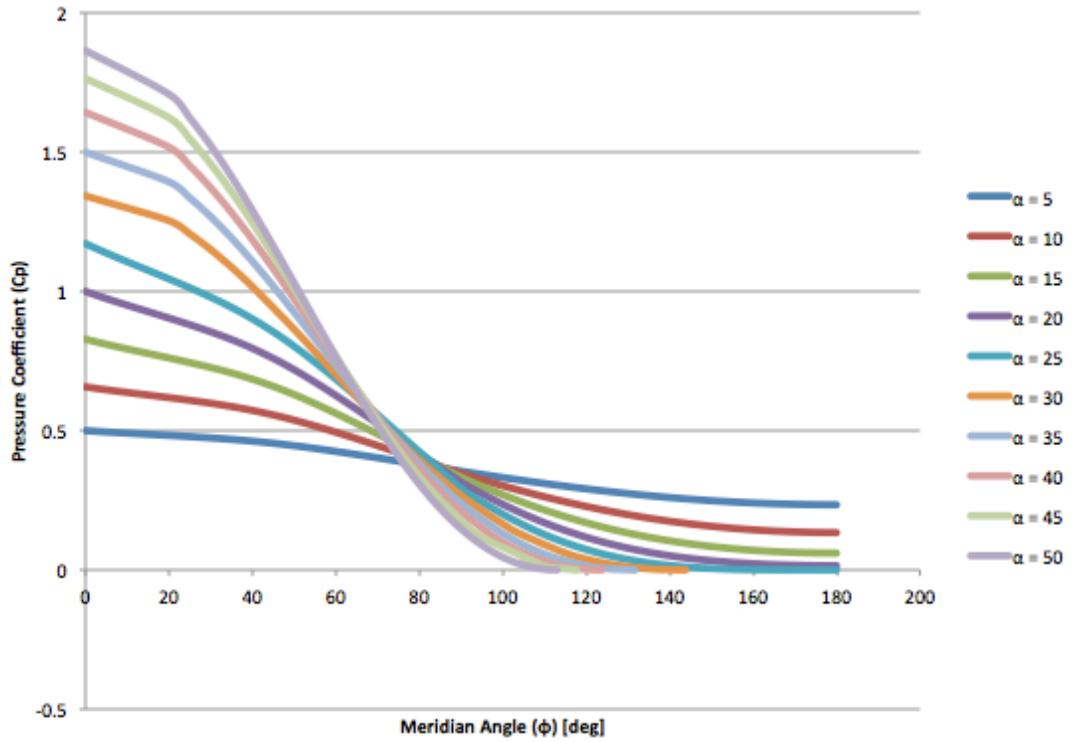

Figure 8: Pressure Coefficient distribution as a function of meridian angle (ϕ) for a twenty five-degree semi-apex angle cone ($\varepsilon=25^{o}$) at various angles of attack (α)

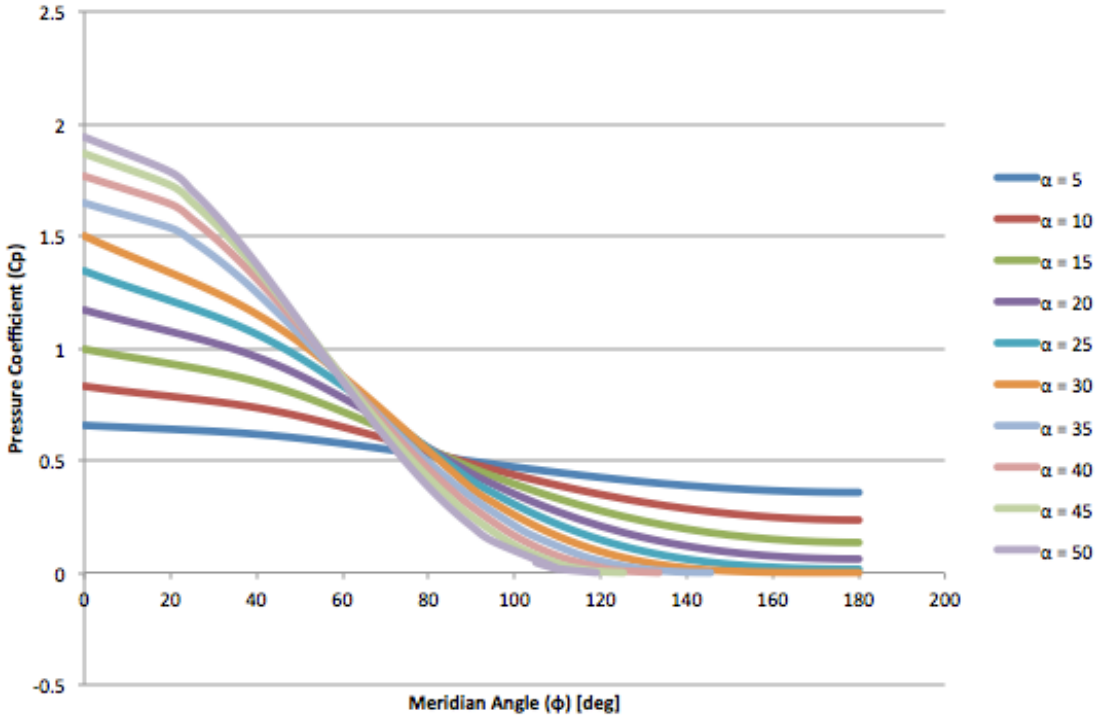

Figure 9: Pressure Coefficient distribution as a function of meridian angle (ϕ) for a thirty-degree semi-apex angle cone ($\varepsilon=30^{o}$) at various angles of attack (α)

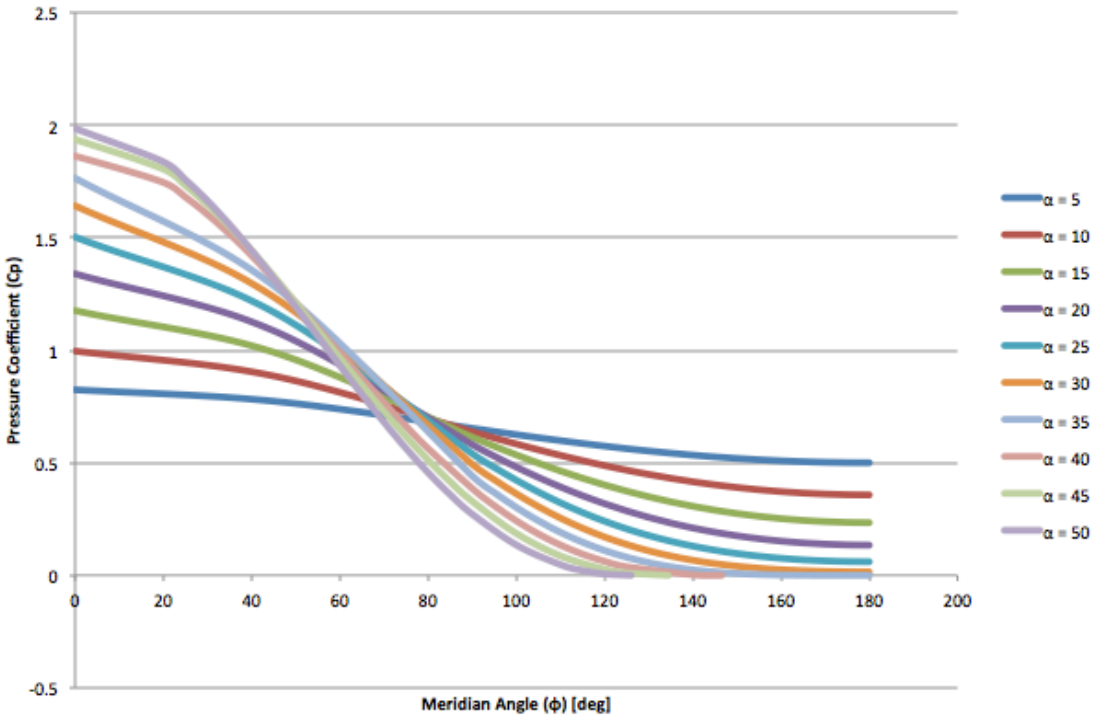

Figure 10: Pressure Coefficient distribution as a function of meridian angle (ϕ) for a thirty five-degree semi-apex angle cone ($\varepsilon=35^{o}$) at various angles of attack (α)

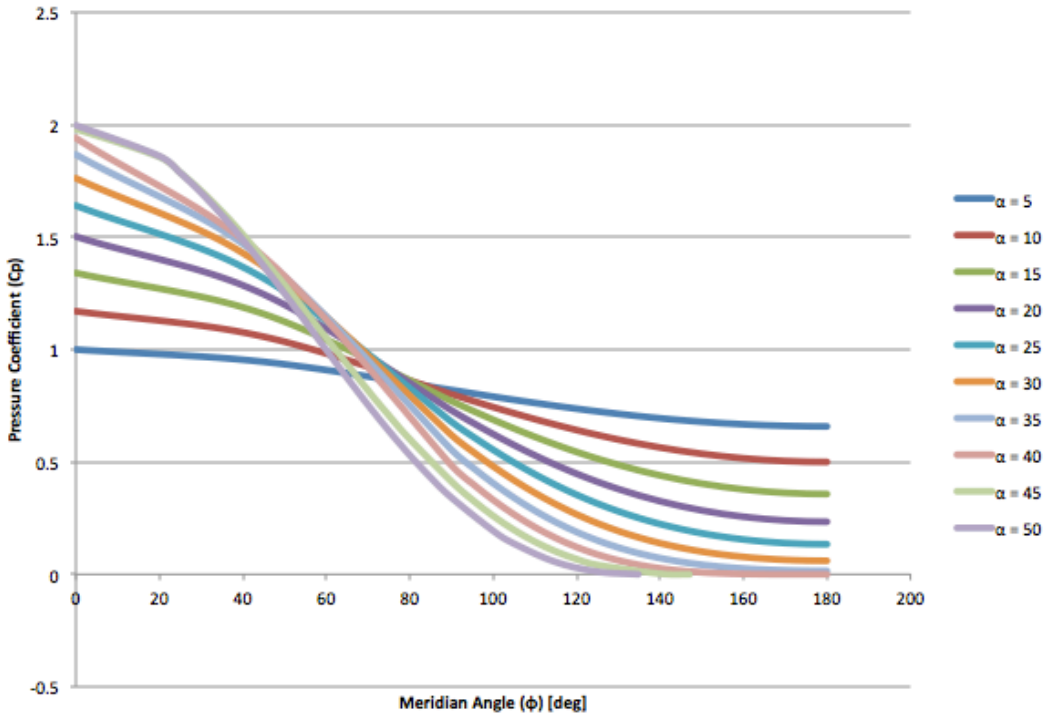

Figure 11: Pressure Coefficient distribution as a function of meridian angle (ϕ) for a forty-degree semi-apex angle cone ($\varepsilon=40^{o}$) at various angles of attack (α)

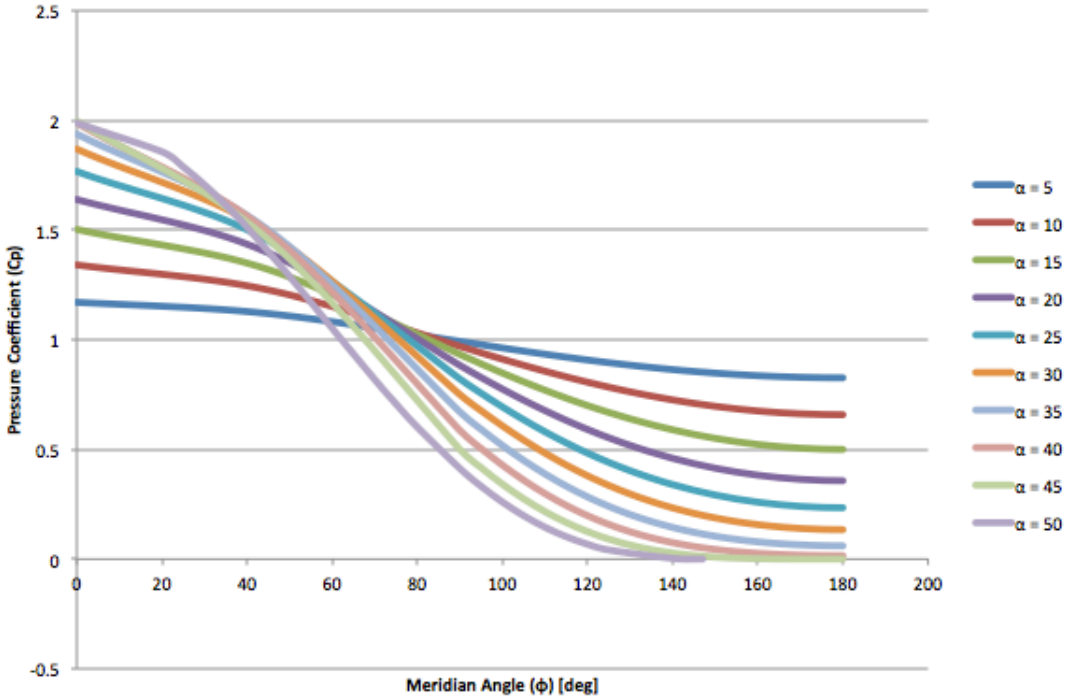

Figure 12: Pressure Coefficient distribution as a function of meridian angle (ϕ) for a forty five-degree semi-apex angle cone ($\varepsilon=45^{o}$) at various angles of attack (α)

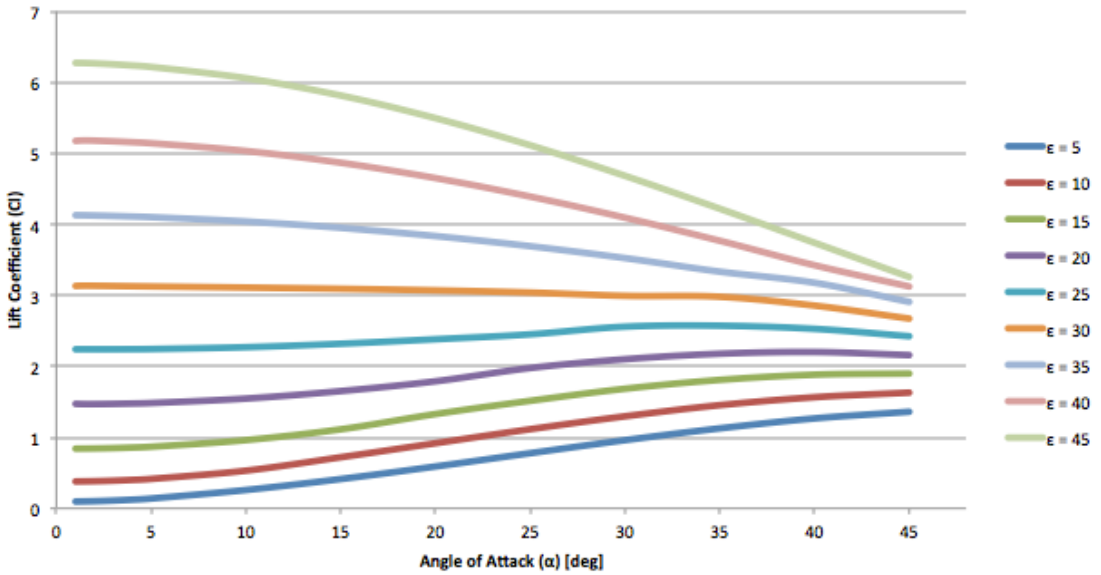

Figure 13: Lift Coefficient as a function of increasing angle of attack (α) for various semi-apex angles (ε) in a sharp cone

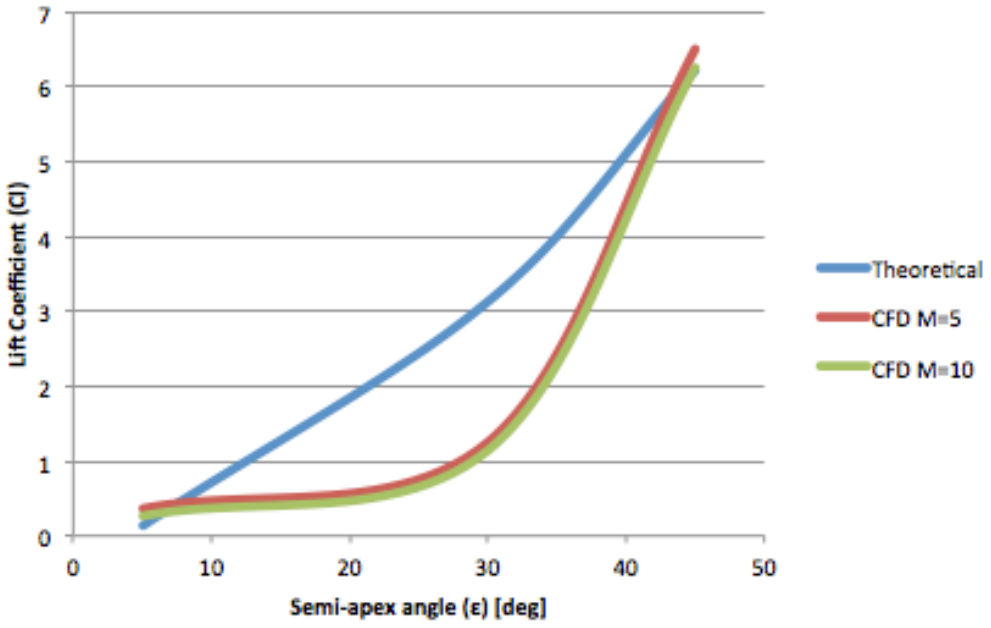

Figure 14: Lift Coefficient as a function of sharp cone semi-apex angle (ε), theoretical and CFD comparison at five-degree angle of attack ($\alpha=5^{o}$)

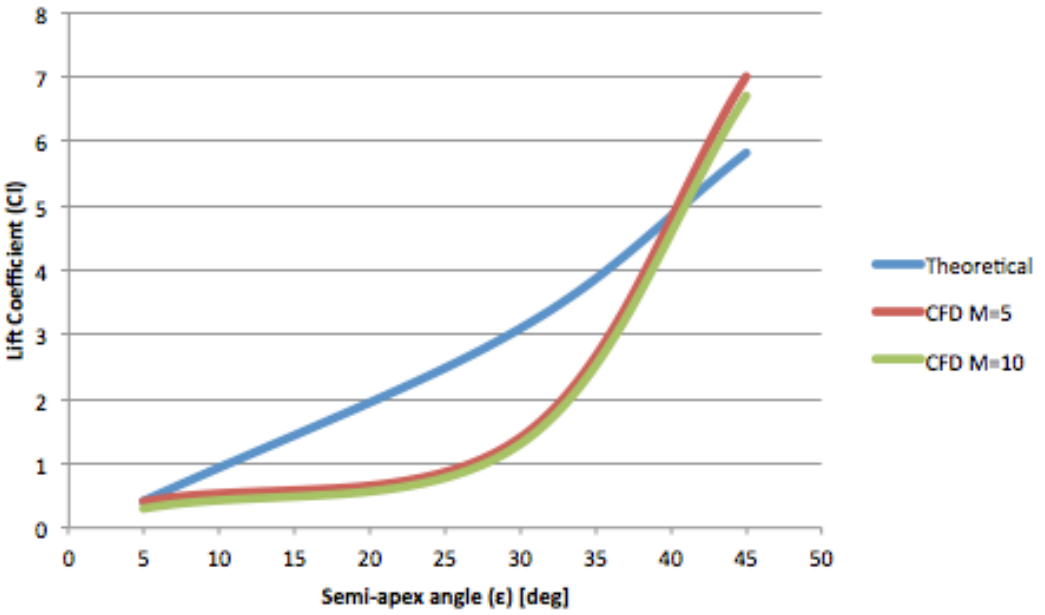

Figure 15: Lift Coefficient as a function of sharp cone semi-apex angle (ε), theoretical and CFD comparison at fifteen-degree angle of attack ($\alpha=15^{o}$)

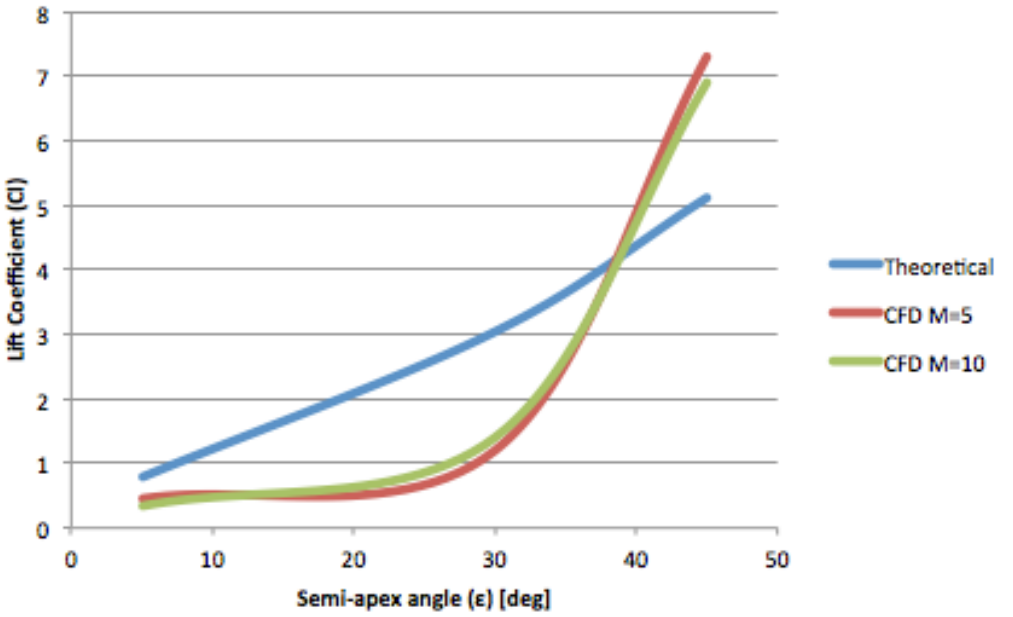

Figure 16: Lift Coefficient as a function of sharp cone semi-apex angle (ε), theoretical and CFD comparison at twenty-five-degree angle of attack ($\alpha=25^{o}$)

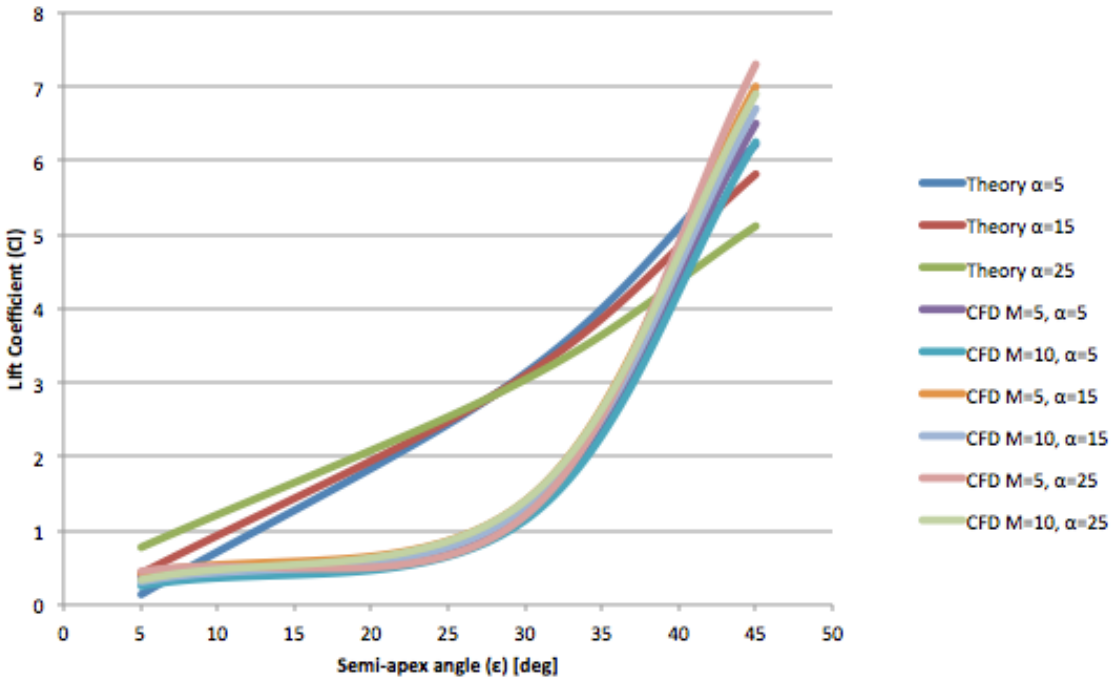

Figure 17: Lift Coefficient as a function of sharp cone semi-apex angle (ε), theoretical and CFD comparison at five, fifteen, and twenty five-degree angle of attack ($\alpha=5^o$, 15^o, 25^o)

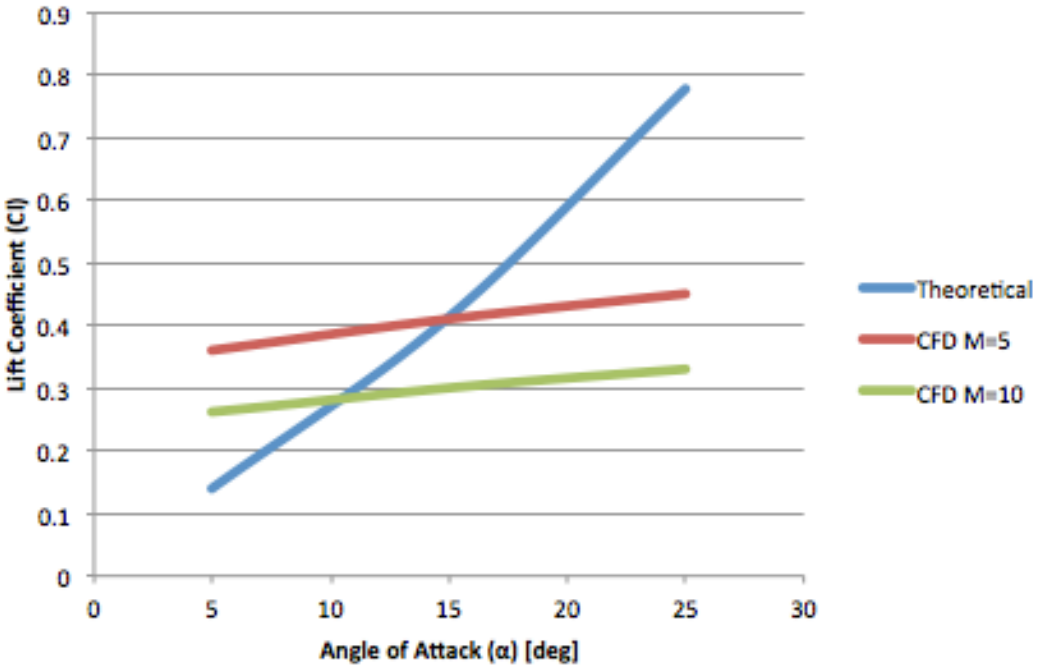

Figure 18: Lift Coefficient as a function of angle of attack (α), theoretical and CFD comparison for a five-degree sharp cone semi-apex angle ($\varepsilon=5^o$)

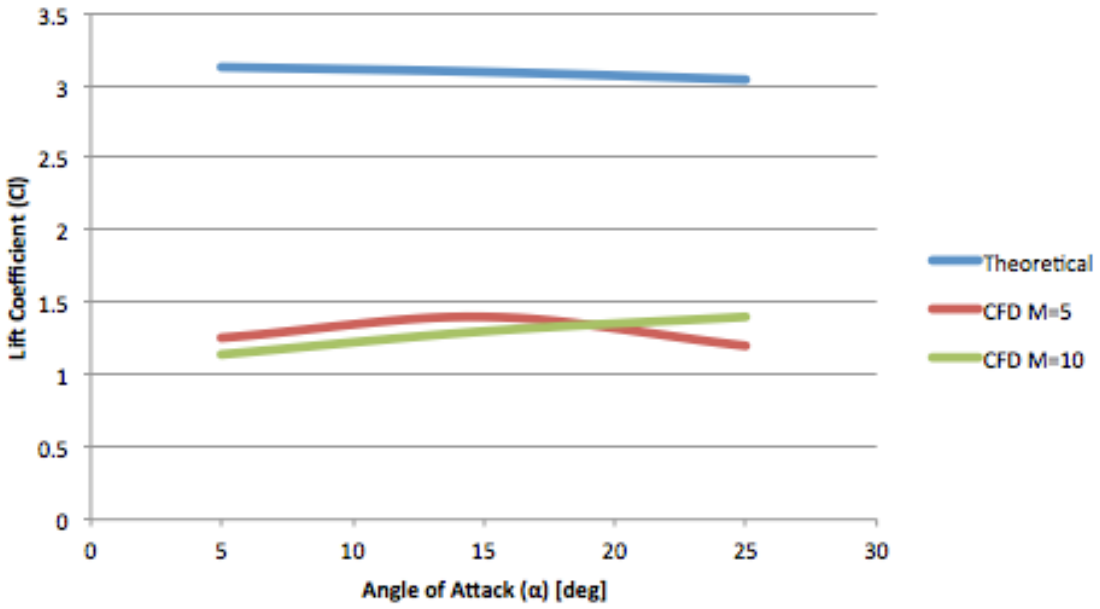

Figure 19: Lift Coefficient as a function of angle of attack (α), theoretical and CFD comparison for a thirty-degree sharp cone semi-apex angle ($\varepsilon=30^{o}$)

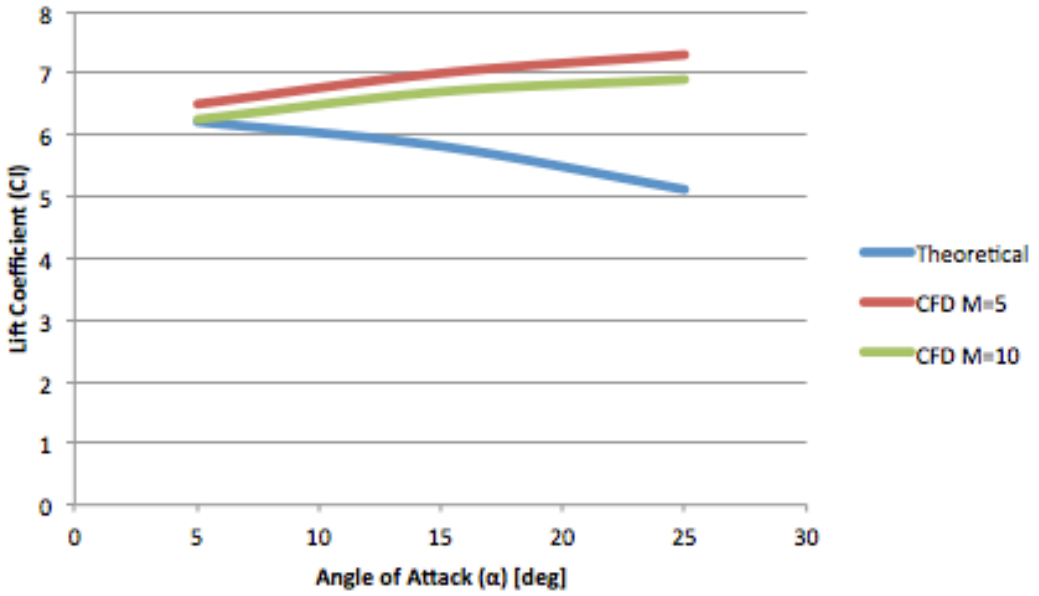

Figure 20: Lift Coefficient as a function of angle of attack (α), theoretical and CFD comparison for a forty five-degree sharp cone semi-apex angle ($\varepsilon=45^{o}$)

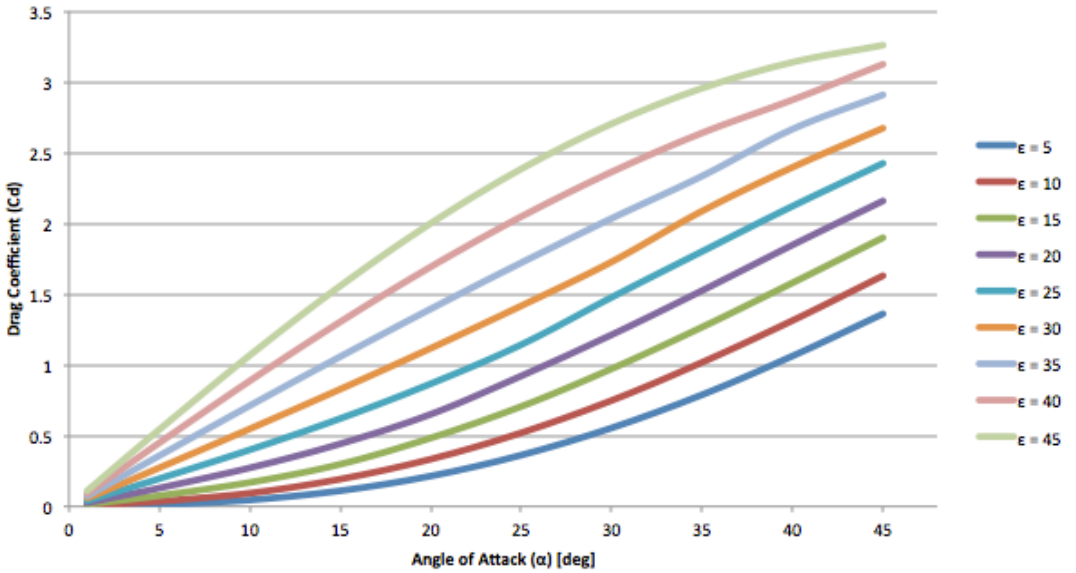

Figure 21: Drag Coefficient as a function of increasing angle of attack (α) for various semi-apex angles (ε) in a sharp cone

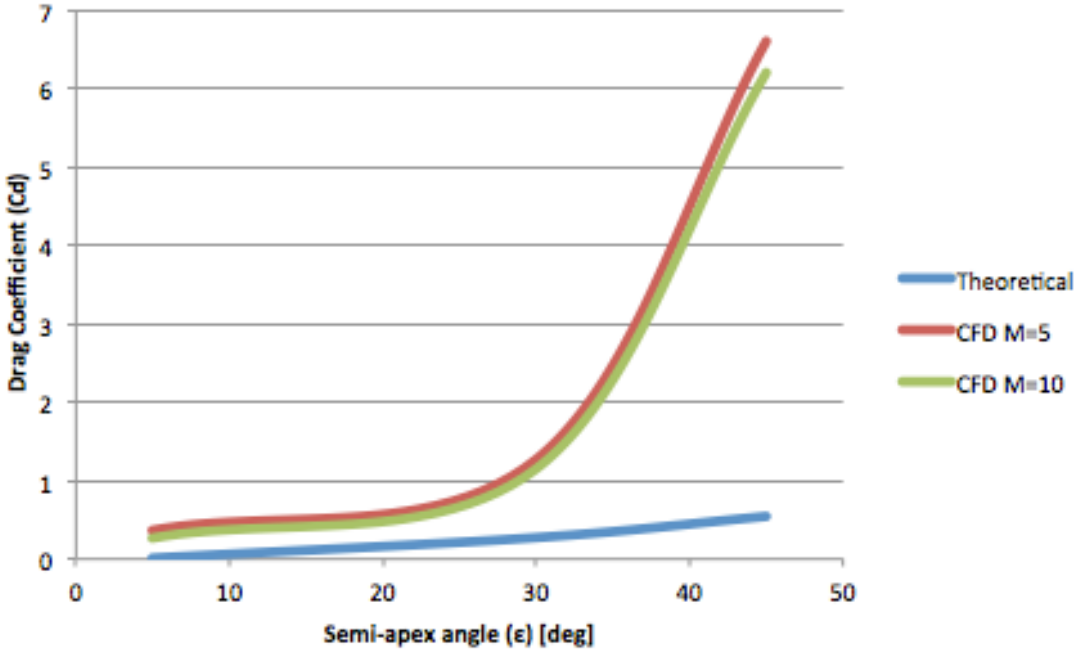

Figure 22: Drag Coefficient as a function of sharp cone semi-apex angle (ε), theoretical and CFD comparison at five-degree angle of attack ($\alpha=5^{o}$)

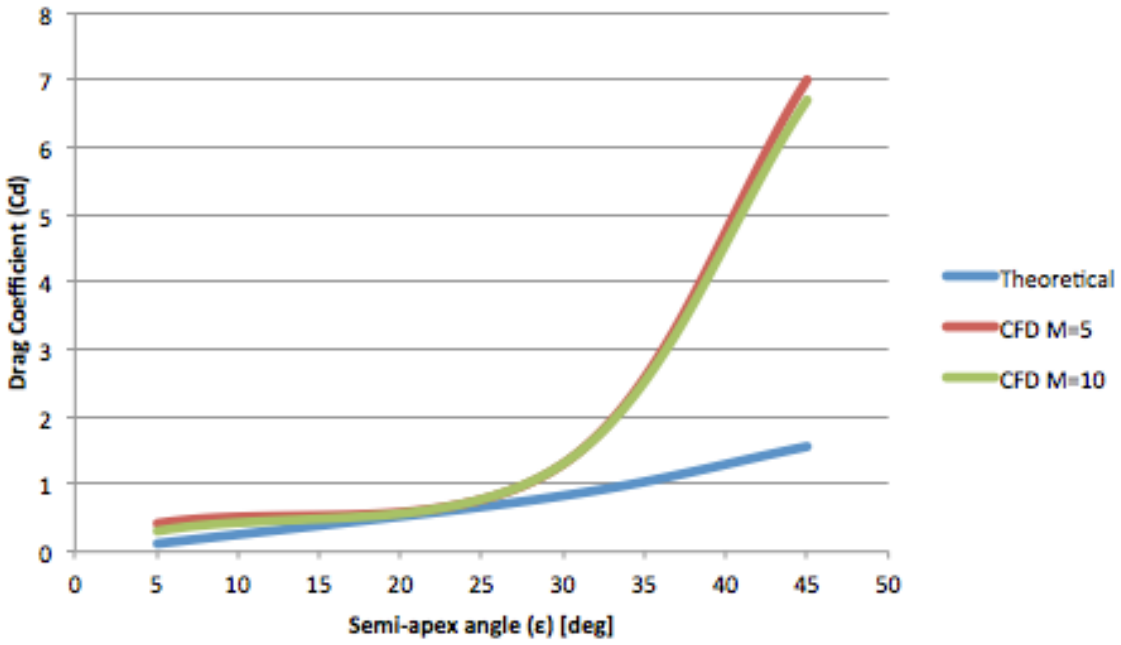

Figure 23: Lift Coefficient as a function of sharp cone semi-apex angle (ε), theoretical and CFD comparison at fifteen-degree angle of attack ($\alpha=15^{o}$)

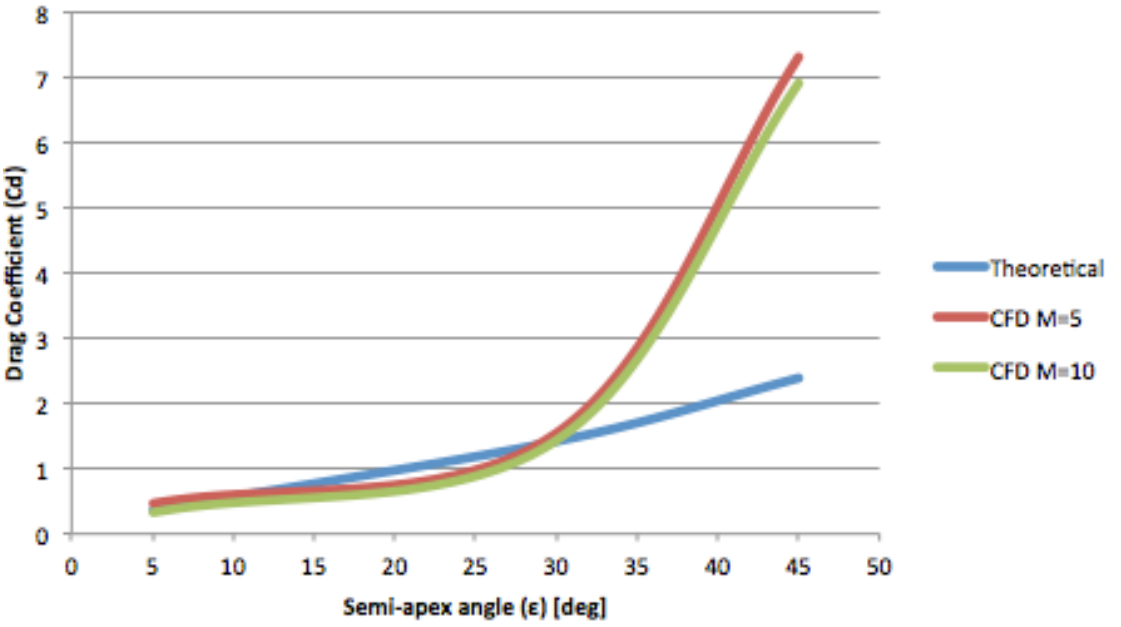

Figure 24: Lift Coefficient as a function of sharp cone semi-apex angle (ε), theoretical and CFD comparison at twenty-five-degree angle of attack ($\alpha=25^{o}$)

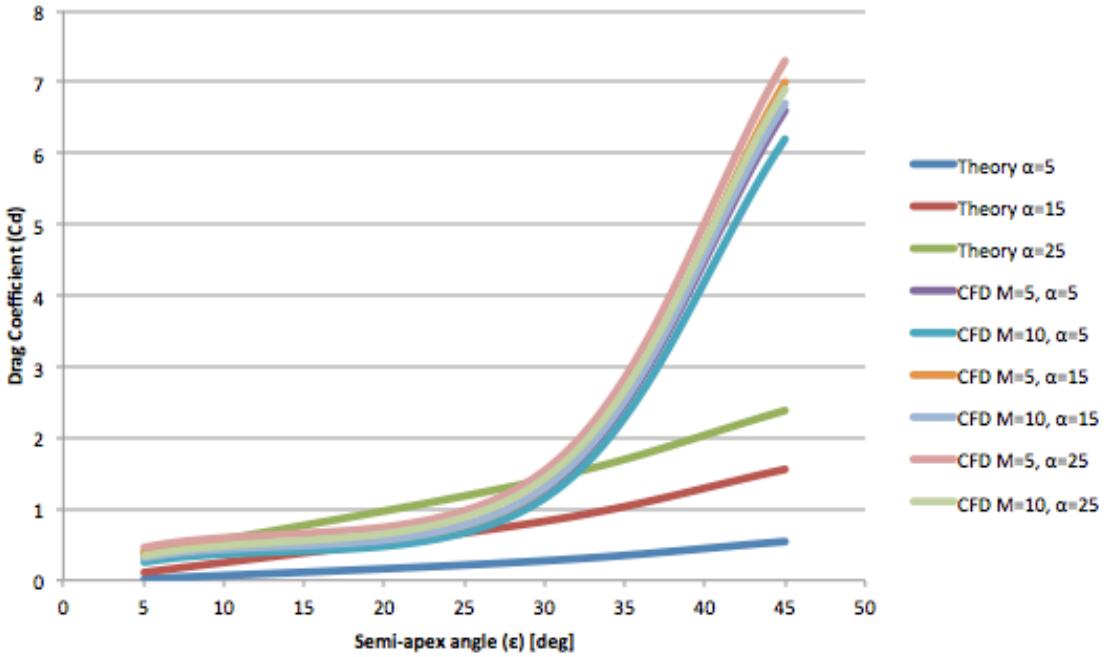

Figure 25: Drag Coefficient as a function of sharp cone semi-apex angle (ε), theoretical and CFD comparison at five, fifteen, and twenty five-degree angle of attack ($\alpha=5^{o}$, 15^{o}, 25^{o})

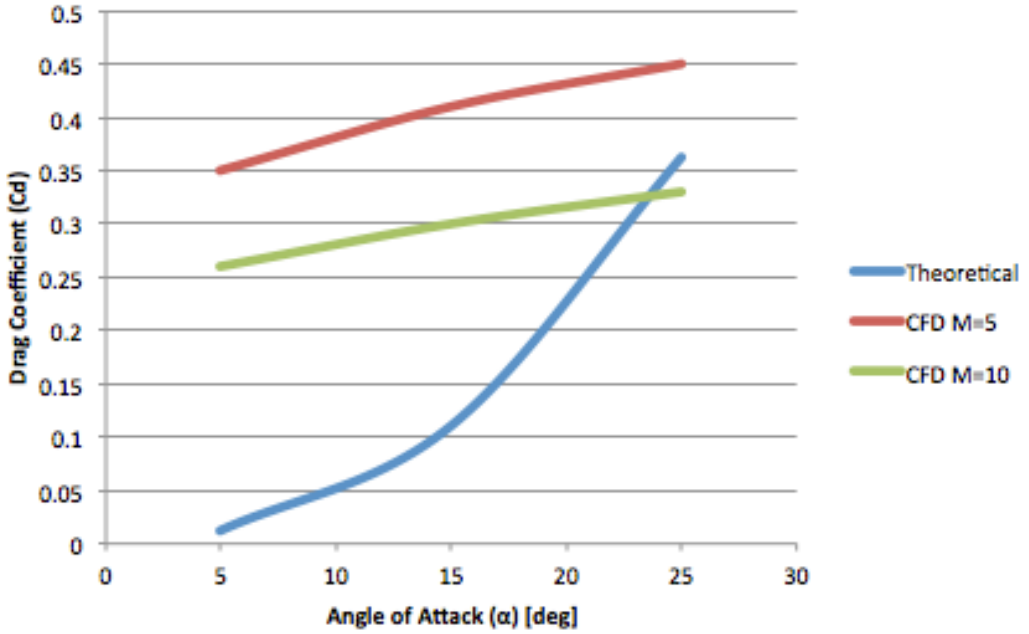

Figure 26: Drag Coefficient as a function of angle of attack (α), theoretical and CFD comparison for a five-degree sharp cone semi-apex angle ($\varepsilon=5^{o}$)

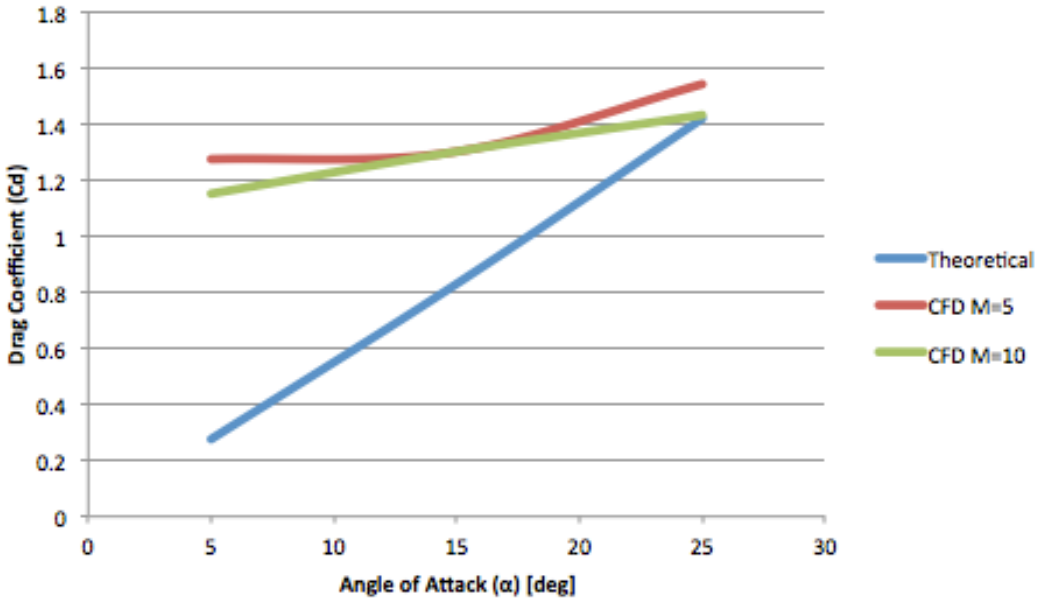

Figure 27: Drag Coefficient as a function of angle of attack (α), theoretical and CFD comparison for a thirty-degree sharp cone semi-apex angle ($\varepsilon=30^{o}$)

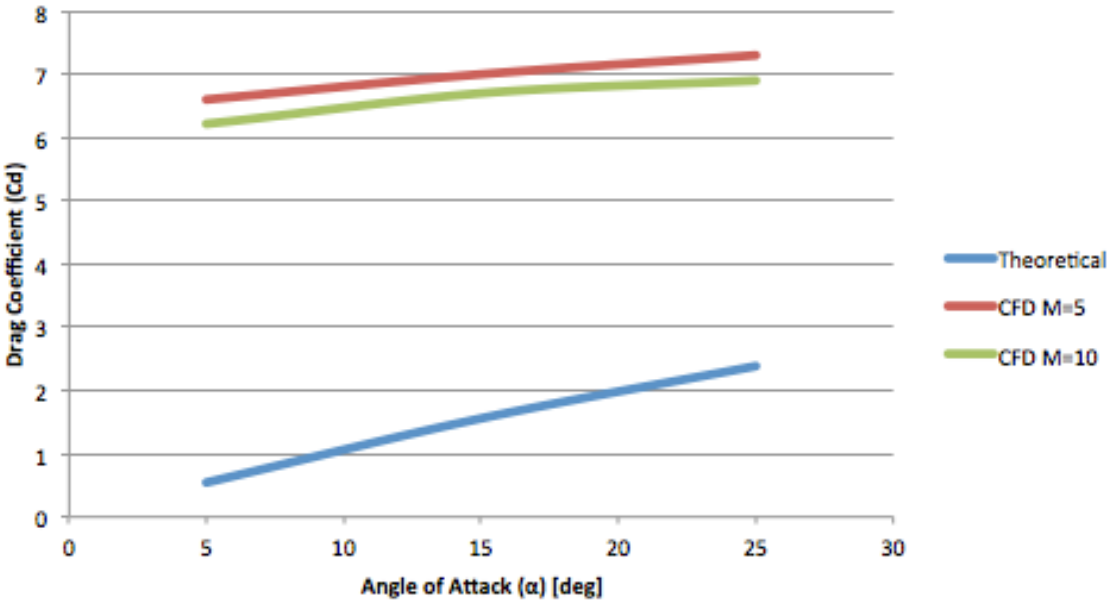

Figure 28: Drag Coefficient as a function of angle of attack (α), theoretical and CFD comparison for a forty five-degree sharp cone semi-apex angle ($\varepsilon=45^{o}$)

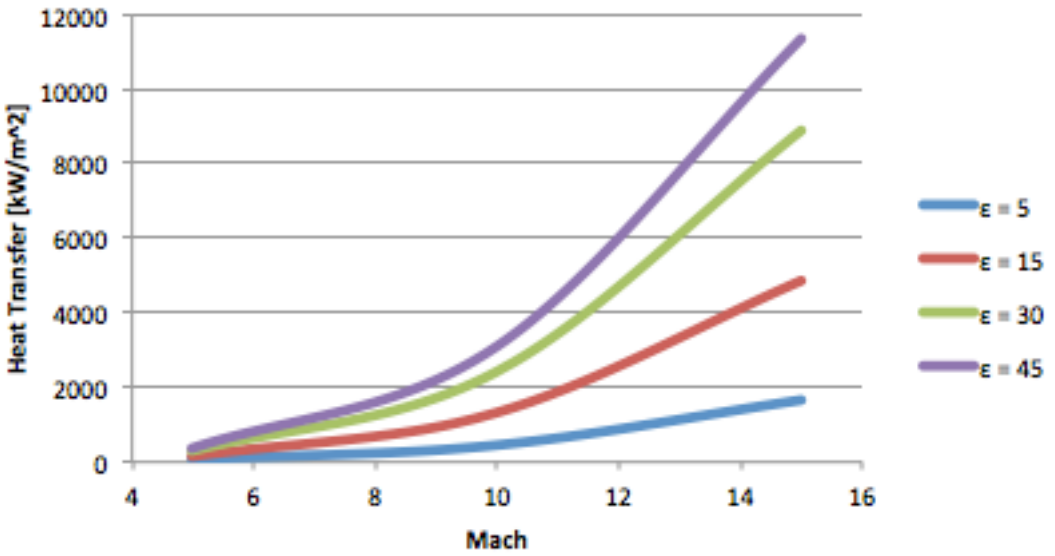

Figure 29: Theoretical Heat Transfer as a function of Mach number and semi-apex angles (ε), for a cone

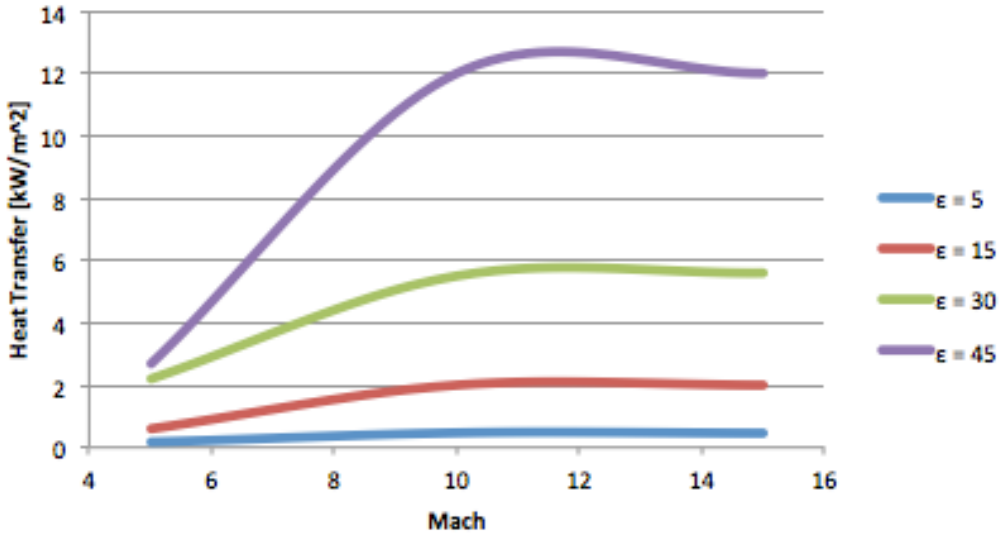

Figure 30: CFD Simulation Heat Transfer as a function of Mach number and semi-apex angles (ε), for a cone

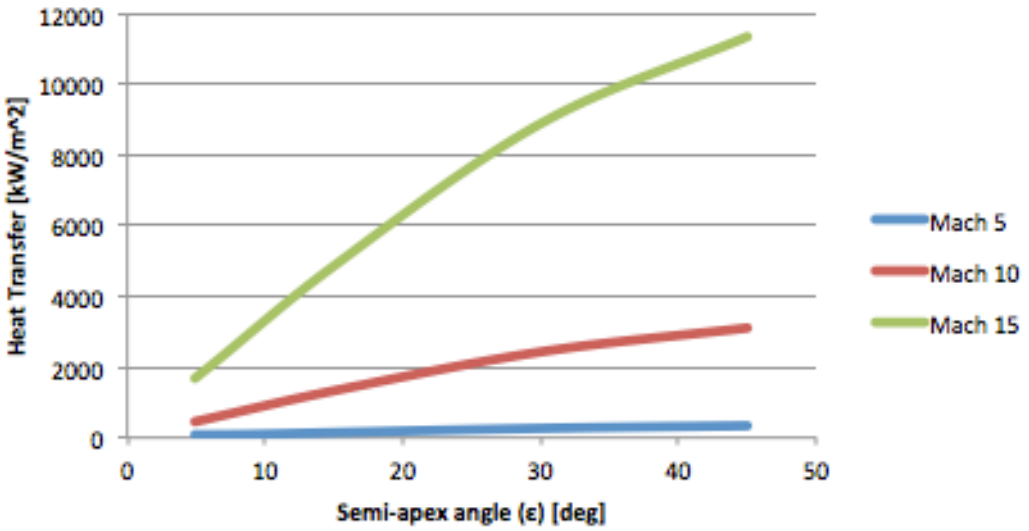

Figure 31: Theoretical Heat Transfer as a function of semi-apex angle (ε) for various Mach numbers

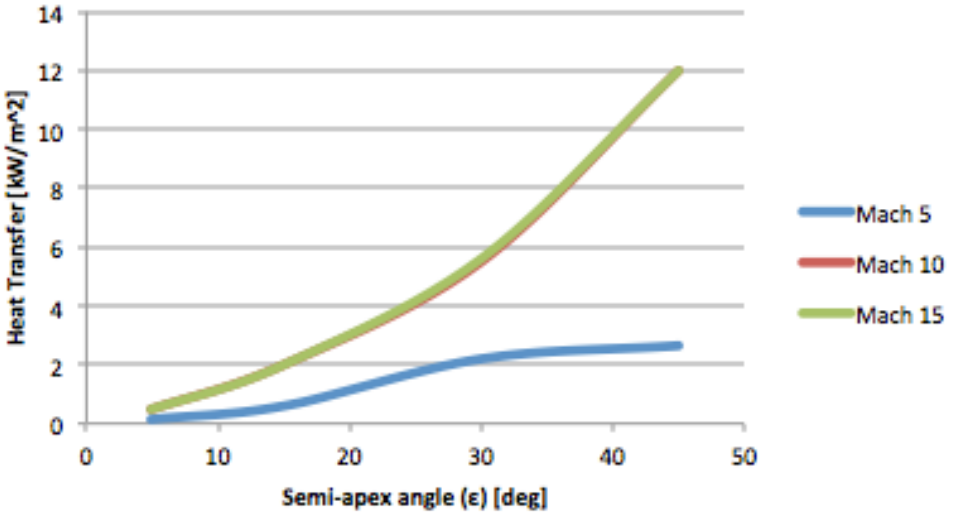

Figure 32: CFD Simulation Heat Transfer as a function of semi-apex angle (ε) for various Mach numbers

SPHERE

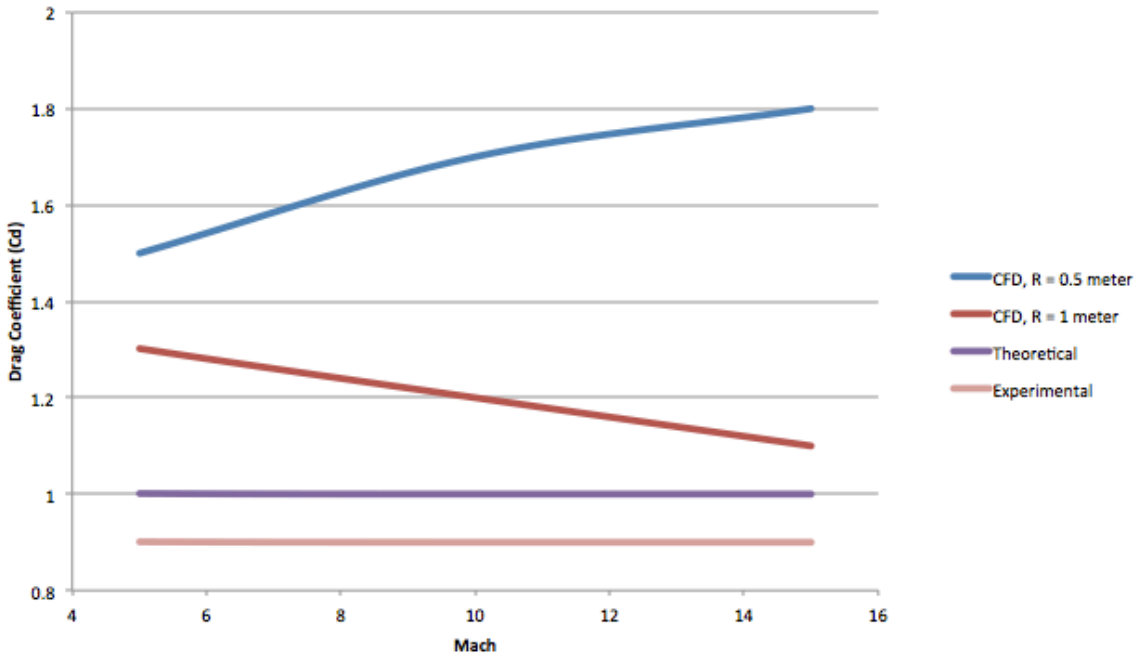

Figure 33: Drag Coefficient as a function of Mach number, theoretical and CFD comparison for 1-meter and 2-meter diameter sphere

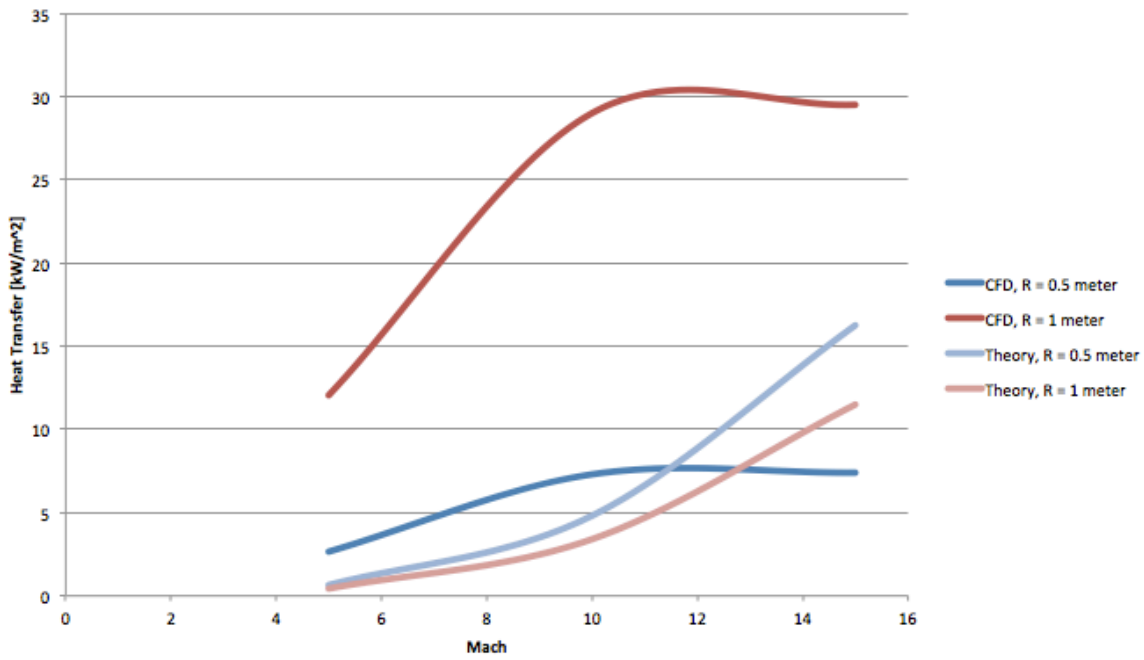

Figure 34: Heat Transfer as a function of Mach number, theoretical and CFD comparison for 1-meter and 2-meter diameter sphere

Table 1: Pressure coefficient distribution for a cone at zero angle of attack at different semi-apex angles (Figure 3)

ε	Theory	Experimental	CFD, M=5	CFD, M=10	CFD, M=15
5	0.0152	0.02	0.01	0.006	0.005
10	0.0603	0.07			
15	0.1339	0.15	0.1	0.065	0.065
20	0.2339	0.25			
25	0.3572	0.33			
30	0.5		1.15	1.05	1.1
35	0.6579				
40	0.8263				
45	1		1.5	5.8	6.25

Table 2: Theoretical lift and drag coefficients for a cone (Figure 18-20, 26-28)

ε	α	C_l	C_d
5	5	0.1384	0.0121
5	10	0.413	0.1106
5	25	0.7772	0.3624
30	5	3.126	0.2734
30	10	3.093	0.8287
30	25	3.0397	1.417
45	5	6.217	0.5439
45	10	5.816	1.558
45	25	5.114	2.385

(Figure 14-16, 22-24)

α	ε	C_l	C_d
5	5	0.1384	0.0121
5	30	3.126	0.273
5	45	6.217	0.543
15	5	0.413	0.110
15	30	3.093	0.828
15	45	5.816	1.558
25	5	0.777	0.3624
25	30	3.039	1.417
25	45	5.11	2.385

Table 3: CFD lift and drag coefficients for a cone at Mach 5 (Figure 18-20, 26-28)

ε	α	C_l	C_d
5	5	0.36	0.35
5	15	0.41	0.42
5	25	0.45	0.45
30	5	1.25	1.27
30	15	1.4	1.3
30	25	1.2	1.54

45	5	6.5	6.6
45	15	7	7
45	25	7.3	7.3

(Figure 14-16, 22-24)

α	**ε**	**C_l**	**C_d**
5	5	0.36	0.35
5	30	1.25	1.27
5	45	6.5	6.6
15	5	0.41	0.41
15	30	1.4	1.3
15	45	7	7
25	5	0.45	0.45
25	30	1.2	1.54
25	45	7.3	7.3

Table 4: CFD lift and drag coefficients for a cone at Mach 10 (Figure 18-20, 26-28)

ε	**α**	**C_l**	**C_d**
5	5	0.26	0.26
5	10	0.3	0.3
5	25	0.33	0.33
30	5	1.14	1.15
30	10	1.3	1.3
30	25	1.4	1.43
45	5	6.25	6.2
45	10	6.7	6.7
45	25	6.9	6.9

(Figure 14-16, 22-24)

α	**ε**	**C_l**	**C_d**
5	5	0.26	0.26
5	30	1.14	1.15
5	45	6.25	6.2
15	5	0.3	0.3
15	30	1.3	1.3
15	45	6.7	6.7
25	5	0.33	0.33
25	30	1.4	1.43
25	45	6.9	6.9

Table 5: Heat transfer data for cone at various semi-apex angles and Mach numbers (Figure 29 & 30)

ε	M	CFD	Theory
5	5	0.14	49.3
5	10	0.47	453.8
5	15	0.46	1661.2
15	5	0.6	144.3
15	10	2	1326.9
15	15	2	4857
30	5	2.2	263.9
30	10	5.5	2426.1
30	15	5.6	8880
45	5	2.65	337.6
45	10	12	3102.6
45	15	12	11339.6

(Figure 31 & 32)

M	ε	CFD	Theory
5	5	0.14	49.3
5	15	0.6	144.3
5	30	2.2	263.9
5	45	2.65	337.6
10	5	0.47	453.8
10	15	2	1326.9
10	30	5.5	2426.1
10	45	12	3102.6
15	5	0.46	1661.2
15	15	2	4857.2
15	30	5.6	8880
15	45	12	11339.6

Table 6: Drag coefficient for a sphere (Figure 33)

M	Theory	Experimental	R = 0.5	R = 1
5	1	~ 0.9	1.5	1.3
10	1	~ 0.9	1.7	1.1
15	1	~ 0.9	1.8	1.1

Table 7: Heat transfer for a sphere (Figure 34)

M	Theory, R = 0.5	Theory, R = 1	CFD, R = 0.5	CFD, R = 1
5	0.601	0.425	2.65	12
10	4.814	3.404	7.3	29
15	16.25	11.49	7.4	29.5

Discussion

Figure 3 shows the pressure coefficient comparison of theoretical and CFD simulation results. The comparison is for a sharp cone at $\alpha = 0$, as ε increases. The theoretical results do not account for Mach number, assuming Newtonian theory for hypersonic flow; hence, the results are valid for hypersonic Mach velocities. The CFD simulation results were calculated at Mach 5, 10 and 15. Where the pressure coefficient obtained at Mach 5 is fairly closed to the theoretical results, with the CFD value being about 30 percent higher and converging towards the theoretical result value as ε increases. The values obtained at Mach 10 and 15 are identical with theoretical results up to $\varepsilon = 25^o$, once ε increases beyond 25^o the CFD results increase very rapidly being over 6 times higher at $\varepsilon = 45^o$. Figure 36 illustrates experimental results, which are also being compared to Newtonian theory. Where experimental results are fairly similar to Newtonian theory and CFD results at high hypersonic Mach values. This comparison shows that Newtonian theory for hypersonic flow is only valid for slender bodies (cones), and it increases in accuracy as Mach increases, since it was not very accurate for Mach 5.

Figures 4-12 illustrate the pressure coefficient variation along the meridian angle, ϕ, in a sharp cone at increasing α. The pressure coefficient is calculated only over the surface where the flow impacts the cone directly, as stated by Newtonian theory for hypersonic flow. The pressure coefficient varies around the cone at every ϕ, as α increases. The change in pressure coefficient also occurs as the cone varies ε. When $\alpha > \varepsilon$, the top part of the cone will not be impacted by the free stream flow, and the bottom section of the cone will be impacted with higher pressure since it becomes the front part of the cone. Therefore, the area not being impacted is not accounted for when

determining pressure coefficient on the cone. As a result, the pressure force on the bottom section increases, as it can be see on the figures for $\phi = 0^o$, and it decreases as ϕ approaches 180^o. The pressure coefficient is not greatly affected at $\phi = 90^o$ since that is the angle on the side of the cone. As ε increases, the flow impacts the whole surface of the cone at $\alpha < \varepsilon$. Hence the plots show how the pressure coefficient is calculated all around the cone. For high α ($\alpha > \varepsilon$), where the pressure coefficient disappears before $\phi = 180^o$, the pressure coefficient is assumed to be zero after that point up to $\phi = 180^o$. Figure 6 illustrates pressure coefficient distribution along ϕ of a $\varepsilon = 15^o$ cone at $\alpha = 6^o$, 12^o, 18^o and 24^o, which can be compared to Figure 37 that displays experimental results of the same ϕ, ε and α values with very close results. The experimental results are also being compared to Newtonian theory, where it can be deduced that as α increases Newtonian theory over predicts the results, in comparison to experimental values.

Figures 13 & 21 show the aerodynamic force coefficients of lift, and drag as a function α, from $\varepsilon = 5^o$ to $\varepsilon = 60^o$. The aerodynamic coefficients were calculated after determining the pressure coefficient over the surface of the cone, Figure 4-12. Once the pressure coefficient is integrated over the surface area that was impacted by the flow, the normal force coefficient can be determined. The normal force coefficient is then used to determine the coefficients of lift and drag. As shown in Figure 13, lift coefficient increases as α increases if $\varepsilon \leq 20^o$. When $20^o < \varepsilon < 30^o$ the lift coefficient begins to decrease after $\alpha = 30^o$. Once $\varepsilon > 30^o$ the lift coefficient decreases as α decreases, due to a major increase in surface area of the cone being impacted causing more drag. Figure 21 illustrates that the drag coefficient increases as α and ε increases. As α increases the surface area being impacted by the flow increases as well, hence, causing an increase in

drag. For a cone with $\varepsilon > 45^o$ the drag coefficient peaks at $\alpha = 35 - 40^o$, having a small decrease for $\alpha \cong 60^o$.

Figures 14-16 show the comparison of lift coefficient as a function of ε between the theoretical and CFD simulation results for $\alpha = 5^o$, 15^o and 25^o. The CFD simulations were performed at Mach 5 & 10. As ε increases the theoretical results yield a lower maximum lift coefficient for high ε, such as $\varepsilon > 35^o$, as α increases where the lift coefficient increases slowly for $\varepsilon \leq 25^o$, and increases very rapidly for $\varepsilon > 30^o$. Meanwhile, the CFD results at Mach 5 & 10 are very similar; a small increase in lift coefficient is noticeable as α increases. It is clear that Mach value does not have much of an effect in the lift coefficient as ε and α vary. A small increase in lift coefficient is seen as α increases, but the major increase is seen as ε increases in cones with $\varepsilon > 30^o$.

Figure 17 compiles all the theoretical and CFD results at $\alpha = 5^o$, 15^o and 25^o for lift coefficient as a function of ε, up to $\varepsilon = 45^o$. Where Mach 5 & 10 results are very close together with a lift coefficient much lower than the theoretical for $\varepsilon \leq 40^o$. At $\varepsilon \cong 40^o$ the theoretical and CFD results converge together for all ε values with CFD lift coefficient results exceeding the theoretical for $\varepsilon > 40^o$.

Figures 18-20 illustrate the comparison of lift coefficient as a function of α between the theoretical and CFD simulation for $\varepsilon = 5^o$, 30^o and 45^o. In Figure 18 the theoretical lift coefficient for $\varepsilon = 5^o$ cone is the same as the CFD results for Mach 5 & 10 at $\alpha = 15^o$ & 10^o respectively. In Figure 19, results for a cone with $\varepsilon = 30^o$, the theoretical result is double than the CFD results. In Figure 20, results for a cone with $\varepsilon = 45^o$, the theoretical result are higher than the theoretical and increasing in difference as α increases with similar results only for $\alpha = 5^o$.

Figures 22-24 show the comparison of drag coefficient as a function of ε between the theoretical and CFD simulation for $\alpha = 5^o$, 15^o and 25^o. The CFD results for $\alpha = 5^o$ are higher than the theoretical, where the drag increases very rapidly for $\varepsilon > 30^o$ resulting in higher CFD drag coefficient than the theoretical. For $\alpha = 15^o$ the CFD drag coefficient results are very similar to the theoretical value up to $\varepsilon = 25^o$, with drag value increasing very rapidly for $\varepsilon > 25^o$. The CFD results for $\alpha = 25^o$ drag coefficient is very similar to the theoretical value up to $\varepsilon = 30^o$, with drag value increasing very rapidly for $\varepsilon > 30^o$. The CFD results at Mach 5 & 10 are very similar, with Mach value not displaying much of an effect on the drag coefficient.

Figure 25 compiles all the theoretical and CFD results at $\alpha = 5^o$, 15^o and 25^o for drag coefficient as a function of ε, up to $\varepsilon = 45^o$. Where Mach 5 & 10 results are not very different, where the CFD drag coefficient results are very similar to the theoretical results for $\varepsilon \leq 30^o$, with CFD drag coefficient results exceeding the theoretical results for $\varepsilon > 30^o$.

Figure 26-28 illustrate the comparison of drag coefficient as a function of α between the theoretical and CFD simulation for $\varepsilon = 5^o$, 30^o and 45^o. In Figure 26 the theoretical drag coefficient for a $\varepsilon = 5^o$ cone is much lower than the CFD results for Mach 5 & 10, with equal results only at $\alpha = 23^o$ for Mach 10. In Figure 27, results for a cone with $\varepsilon = 30^o$, the theoretical results are lower than the CFD results, with equal results only at $\alpha = 25^o$ for Mach 10. In Figure 28, results for a cone with $\varepsilon = 45^o$, the CFD results yield a drag coefficient much higher than the theoretical results, with CFD results more than six times higher than theoretical for $\alpha < 12^o$, and about three times higher for $\alpha > 15^o$.

Figures 29 & 30 illustrate the heat flux [kW/m^2] as a function of Mach for theoretical calculations assuming Newtonian flow and CFD simulation for $\varepsilon = 5^o$, 15^o, 30^o and 45^o. The theoretical calculations show that as ε increases the heat flux increases as Mach increases, with approximate values of 1900, 5000, 9000, and 11300 [kW/m^2] for $\varepsilon = 5^o$, 15^o, 30^o and 45^o respectively, at Mach 15. Similarly, the CFD results show that as ε increases the heat flux also increases as Mach increases, with approximate values of 0.5, 2, 6, and 12 [kW/m^2] for $\varepsilon = 5^o$, 15^o, 30^o and 45^o respectively, at Mach 15. The theoretical results yield a much higher heat flux transfer into the body than the CFD results. This shows how using exact methods to calculate the heat flux is not an accurate method for hypersonic flow heat transfer approximation.

Figures 31 & 32 illustrate the heat flux [kW/m^2] as a function of ε for a sharp cone for theoretical calculations assuming Newtonian flow and CFD simulation for Mach 5, 10 &15. The theoretical calculations show that as ε increases the heat flux increases as Mach increases, with approximate values of 300, 3200, and 11300 [kW/m^2] for Mach 5, 10 and 15 respectively, at $\varepsilon = 45^o$. Likewise, the CFD results show that as ε increases the heat flux also increases as Mach increases, with approximate values of 2.5, 12, and 12 [kW/m^2] for Mach 5, 10 and 15 respectively, at $\varepsilon = 45^o$. The theoretical results yield a much higher heat flux transfer into the body than the CFD results.

Figure 33 shows the theoretical and CFD drag coefficient results for a sphere of two different diameters. The theoretical results yield a drag coefficient of about one, as shown in Figure 35, where the CFD results yield a higher drag value, which increases as Mach increases. For a one-meter diameter sphere, the drag coefficient diverges as Mach increases, where as for a two-meter diameter sphere, the drag coefficient converges

towards the value calculated as Mach increases, assuming Newtonian theory. Consequently, showing that Newtonian theory's accuracy increases as Mach increases to very high hypersonic Mach values. A potential discrepancy in the CFD results for a one-meter diameter sphere is the probability of cavitation, the reduction of local pressure in intense turbulence Eddys, in turbulent flow. This phenomenon occurs as Mach increases where the wake area appears to be filled with bubbles and eventually the flow becomes a true cavity flow (turbulent wake). As cavitation develops drag rises and flow is unsteady; particularly where Reynolds numbers is not taking into account when varying the size of the sphere being simulated at higher Mach with the same Reynolds number.

Figure 34 illustrates the theoretical calculations and CFD results of heat flux [kW/m^2] as a function of Mach number for a one-meter and two-meter diameter sphere. The CFD one-meter diameter sphere results are higher than the theoretical results for Mach values up to about 11.5, where the CFD and theoretical results yield the same heat flux into the sphere with about 7 [kW/m^2]. After Mach 12 the theoretical results increase, as the CFD results settle at about 7 [kW/m^2] as Mach keeps increasing. For a two-meter diameter sphere the CFD results are significantly higher than the theoretical with 12 [kW/m^2] for the theoretical and 29 [kW/m^2] for CFD at Mach 15.

Conclusion

As seen in the results section, Newtonian theory for hypersonic flow accurately predicts the pressure coefficient for a slender sharp cone, $\varepsilon \leq 25^o$, at any ϕ around the cone, and for $\alpha \leq 25^o$. The comparison in between CFD, theoretical and experimental can be seen in Figures 3, 6 and 37. The lift coefficient is over predicted by Newtonian theory in comparison to CFD simulation results for cones up to $\varepsilon \approx 40^o$, at $\alpha = 5^o, 15^o, 25^o$. Meanwhile, the drag coefficient was under predicted by Newtonian theory, in comparison to CFD results, at $\alpha = 5^o$, with very similar results for $\varepsilon \leq 25^o$ at $\alpha \leq 25^o$. Lift and drag coefficient results obtained at Mach 10 are comparable to the theoretical values, better than the Mach 5 values. This comparison shows that Newtonian theory for hypersonic flow is only valid for slender bodies (cones), and it increases in accuracy as Mach increases, since it was not very accurate for Mach 5.

The heat flux calculated theoretically is extremely higher than the results yield by CFD simulation for a sharp cone of increasing ε. The CFD and theoretical results conclude that as ε increases the heat flux also increases due to the increase in surface area. The theoretical method used to calculate the heat flux makes use of exact methods to determine certain temperatures in the flow, as an oblique shock wave occurs, having a major over prediction in heat transfers to the cone in comparison to CFD results (Figures 29 & 30). In theoretical approximations the heat transfer increases as Mach increases, while the CFD results show that for Mach 10 & 15, the heat transfer remains very close. This could potentially be a discrepancy in the CFD set up, since a real gas model was used instead of chemically reacting flow.

The drag coefficient results yielded by Newtonian theory and experimental data seem to be similar to a two-meter diameter sphere at high hypersonic Mach numbers. As seen in Figure 33, the CFD results converge towards the theoretical value of $C_d = 1$, as Mach increases past Mach = 15. While for a smaller, one-meter diameter sphere, the CFD results diverge away from the theoretical results. This may be a discrepancy from the CFD set up, where Reynolds number was not taken into account, as the diameter was varied, causing a turbulent flow phenomenon known as cavitation, where drag rises in unsteady flow.

The heat transfer yielded by CFD results increase as diameter increases as well as Mach number. Meanwhile, the theoretical results are higher for a one-meter diameter sphere at Mach < 12, and equaling the CFD results at about Mach 12. As the radius increases, two-meter diameter sphere, theoretical results show that heat transfer decreases and CFD results show an increase in heat transfer.

References

[1] K. P. J. Reddy, et al. "Simultaneous Measurement Of Aerodynamic And Heat Transfer Data For Large Angle Blunt Cones In Hypersonic Shock Tunnel." Sadhana 31.5 (2006): 557-581. Academic Search Premier.

[2] Braun, Robert D., Grant, Michael J. "Analytic Hypersonic Aerodynamics For Conceptual Design of Entry Vehicles." AIAA Aerospace Sciences Meeting; Including the New Horizons Forum and Aerospace Exposition 4 - 7 January 2010, Orlando, Florida.

[3] Anderson, John D., Jr., *Hypersonic and High Temperature Gas Dynamics*, McGraw-Hill, New York 1989; reprinted by the American Institute of Aeronautics and Astronautics, Reston, VA, 2000.

[4] Anderson, John D., Jr., *Fundamentals of Aerodynamics*, 5th ed., McGraw-Hill, New York 2010.

[5] Anderson, John D., Jr., *Modern Compressible Flow with Historical perspective*, 3rd ed., McGraw-Hill Book Company, New York 2003.

[6] Hayes, Wallace D., Probstein, Ronald F., *Hypersonic Flow Theory*, Academic Press Inc, 2nd ed., New York 1966.

[7] Peckham, D. H. "Experiments at Hypersonic Speeds on Circular Cones at Incidence." Ministry of Aviation, Aeronautical research council current papers. London, 1965.

[8] Dorrance, William, H. *Viscous Hypersonic Flow: Theory of Reacting and Hypersonic Boundary Layer.* McGraw-Hill Book Company, Inc. New York 1962.

[9] Tauber, Michael, E. "A Review of High-Speed Convective Heat-Transfer Computation Methods." NASA Technical Paper, 1989.

[10] Crabtree, L. F., Dommett, R. L., Farmborough, R. A. E., Woodley, J.G. "Estimations of Heat Transfer to Flat Plate, Cones and Blunt Bodies." Aeronautical Research Council Reports and Memoranda No. 3637 July 1965.

[11] STAR CCM+ user guide

Appendix 1 – Analytical Calculations

Drag coefficient – Sphere

$$C_{p\ surface} = 2\sin^2\theta$$

$$C_{p\ surface} = \frac{P_s - P_\infty}{\frac{1}{2}\rho_\infty V_\infty^2}$$

Setting this two equation equal to each other gives:

$$P_s - P_\infty = \rho_\infty V_\infty^2 \sin^2\theta$$

The drag of the sphere is determined by integrating over the frontal area of the sphere:

$$D = \int_0^{\pi/2} (P_s - P_\infty) * (2\pi r sin\theta * rd\theta) * cos\theta$$

Where the first term is the pressure differences, the second term is the area on which the pressure differences act on, and the third term is the x-component of the pressure force.

$$D = 2\pi r^2 \int_0^{\pi/2} sin\theta * cos\theta * (P_s - P_\infty) d\theta$$

After substituting for $(P_s - P_\infty)$:

$$D = 2\pi r^2 \int_0^{\pi/2} \rho_\infty V_\infty^2 * sin^3\theta * cosd\theta$$

$$D = 2\pi r^2 \rho_\infty V_\infty^2 \int_0^{\pi/2} sin^3\theta * cosd\theta$$

$$D = 2\pi r^2 \rho_\infty V_\infty^2 [\frac{sin^4\theta}{4}]_0^{\pi/2}$$

$$D = 2\pi r^2 \rho_\infty V_\infty^2 * 1/4$$

$$D = 1/2\pi r^2 \rho_\infty V_\infty^2$$

$$C_d = \frac{D}{q_\infty S} = \frac{\frac{1}{2}\pi r^2 \rho V^2}{\frac{1}{2}\rho V^2 * \pi r^2} = 1$$

Where C_d is the non dimensional drag coefficient, D is the drag determined by integrating the pressure differences defined using Newtonian theory over the frontal area of the sphere, q_∞ is the dynamic pressure and S is the area of a circle which is seen as the impact surface area of the flow.

Drag coefficient – Cone

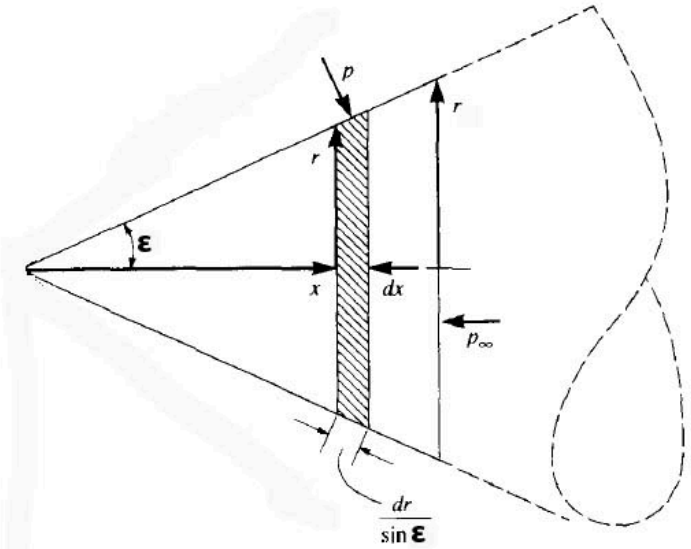

Assuming pressure to be the same as ambient pressure, $p = p_\infty$, and neglecting the effects of friction. The drag force on the shaded strip of surface area can be determined by:

$$(P\sin\varepsilon)(2\pi r)(dr/\sin\varepsilon) = 2\pi r p dr$$

Where ε is the semi apex angle of the cone, r is the radius, P is the pressure on the surface and dr/sinε is the y component of the force.

The total drag due to the pressure acting over the total surface area of cone is determined by:

$$D = \int_0^r 2\pi r P dr - \int_0^r 2\pi r p_\infty dr$$

Where the first integral is the horizontal force on the inclined surface of the cone and the second integral is the force on the base of the cone. Combining both the integrals yields:

$$D = \int_0^r 2\pi r(P - P_\infty)dr = \pi(p - p_\infty)r^2$$

Using the base area $S = \pi r^2$ the drag coefficient can be determined by:

$$C_d = \frac{D}{q_\infty S} = \frac{\pi(p - p_\infty)r^2}{\frac{1}{2}\rho V^2 * \pi r^2} = C_p$$

Therefore the drag coefficient for a cone is equal to its surface pressure coefficient, and in Newtonian Theory that is $C_d = 2\sin^2\varepsilon$

Lift coefficient – Cone at an angle of attack

Starting with the Newtonian Theory pressure coefficient definition, $C_p = 2\sin^2\theta$ and substituting sinθ with Eq. (17) it yields:

$$C_p = 2(\sin\varepsilon * \cos\alpha + \cos\varepsilon * \sin\alpha * \cos\phi)^2$$

Using this equation yields the pressure coefficient at any angle, ϕ, which is the meridional angle along the cone measured windward to leeward as a function of semi apex angle and angle of attack. The normal force coefficient can be determined by integrating the coefficient of pressure.

If $\alpha \leq \varepsilon$

$$C_n = \int_0^\pi C_p d\phi = 2\int_0^\pi (\sin\varepsilon * \cos\alpha + \cos\varepsilon * \sin\alpha * \cos\phi)^2 d\phi$$

If $\alpha > \varepsilon$

$$C_n = \int_0^b C_p d\phi = 2\int_0^b (\sin\varepsilon * \cos\alpha + \cos\varepsilon * \sin\alpha * \cos\phi)^2 d\phi$$

Where b is determined by Eq. (18) and that is the angle at which the cones surface is not being impacted by the fluid flow. The lift coefficient is calculated by: $C_l = C_n * \cos\alpha$.

Appendix 2 - Experimental data

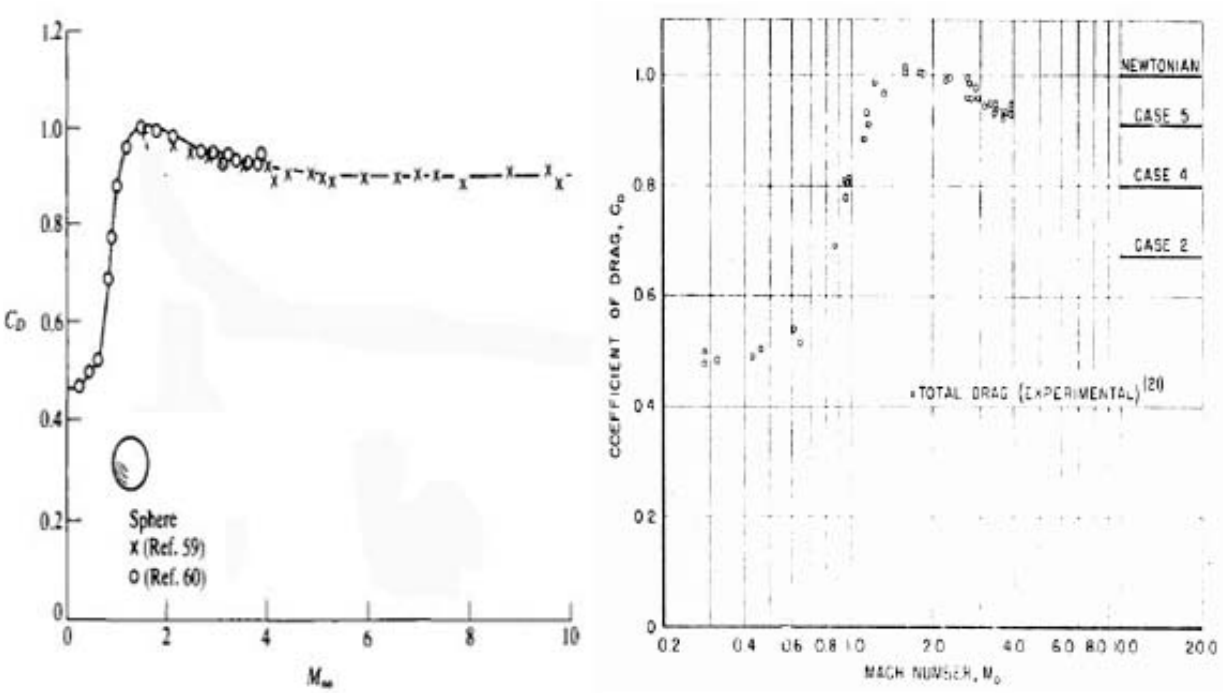

Figure 35: Drag Coefficient as a function of Mach number for a sphere

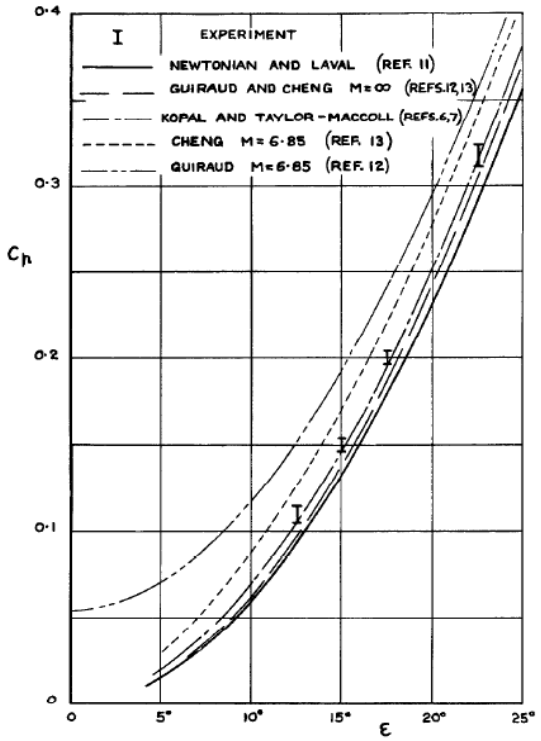

Figure 36: Pressure coefficient as a function of semi-apex angle (ε)

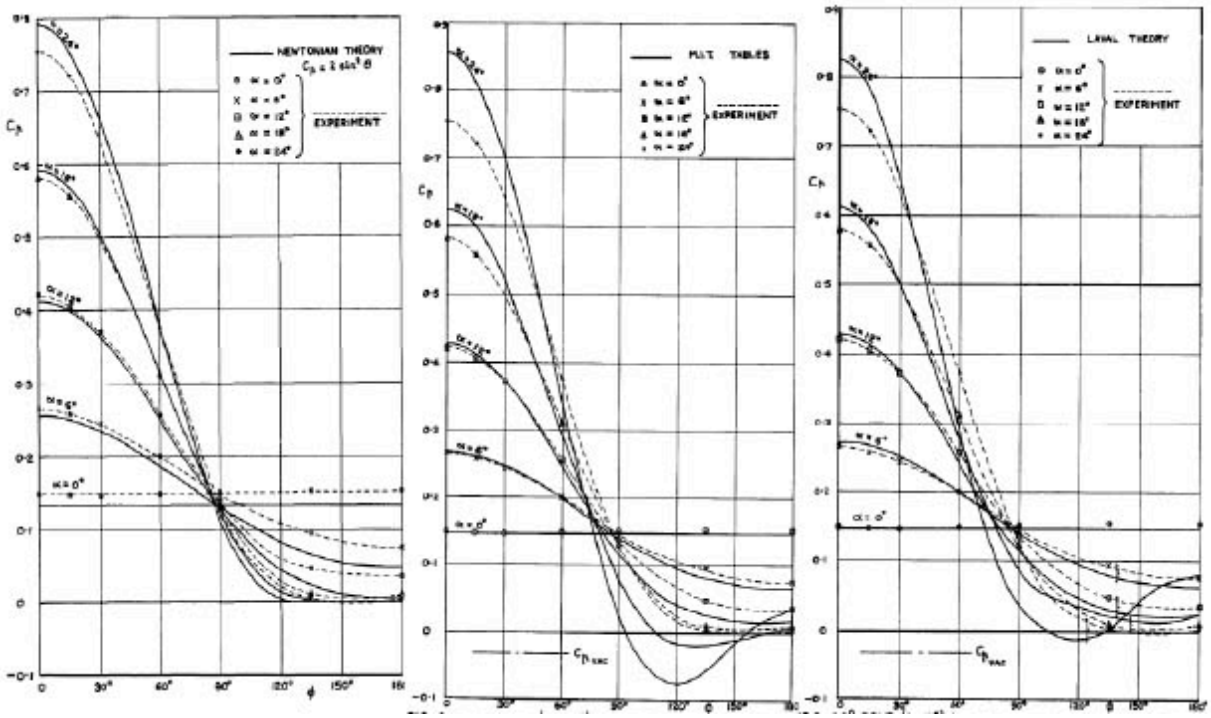

Figure 37: Pressure coefficient as a function of meridian angle (ϕ) and angle of attack (α) for a cone [7]

Appendix 3 – Calculation for pressure coefficient distribution (Fig 4-12)

semi	semi[rad]	AoA	meridian	cp
5	0.087266463	0	0	0.015192247
5	0.087266463	0	45	0.015192247
5	0.087266463	0	90	0.015192247
5	0.087266463	0	95	0.015192247
5	0.087266463	0	100	0.015192247
5	0.087266463	0	105	0.015192247
5	0.087266463	0	110	0.015192247
5	0.087266463	0	115	0.015192247
5	0.087266463	0	120	0.015192247
5	0.087266463	0	125	0.015192247
5	0.087266463	0	130	0.015192247
5	0.087266463	0	135	0.015192247
5	0.087266463	0	140	0.015192247
5	0.087266463	0	145	0.015192247
5	0.087266463	0	150	0.015192247
5	0.087266463	0	155	0.015192247
5	0.087266463	0	160	0.015192247
5	0.087266463	0	165	0.015192247
5	0.087266463	0	170	0.015192247
5	0.087266463	0	175	0.015192247
5	0.087266463	0	180	0.015192247
5	0.087266463	5	0	0.060307379
5	0.087266463	5	45	0.043937146
5	0.087266463	5	90	0.015076845
5	0.087266463	5	95	0.012563303
5	0.087266463	5	100	0.010295334
5	0.087266463	5	105	0.008282453
5	0.087266463	5	110	0.006527331
5	0.087266463	5	115	0.005026163
5	0.087266463	5	120	0.003769211
5	0.087266463	5	125	0.002741529
5	0.087266463	5	130	0.001923816
5	0.087266463	5	135	0.001293389
5	0.087266463	5	140	0.000825234
5	0.087266463	5	145	0.000493103
5	0.087266463	5	150	0.000270617
5	0.087266463	5	155	0.000132348
5	0.087266463	5	160	5.48342E-05

5	0.087266463	5	165	1.7505E-05
5	0.087266463	5	170	3.4798E-06
5	0.087266463	5	175	2.18318E-07
5	0.087266463	5	180	0
5	0.087266463	10	0	0.133974596
5	0.087266463	10	20	0.123391835
5	0.087266463	10	30	0.111055368
5	0.087266463	10	35	0.103544014
5	0.087266463	10	40	0.095351421
5	0.087266463	10	45	0.086654685
5	0.087266463	10	50	0.077638335
5	0.087266463	10	55	0.068489332
5	0.087266463	10	60	0.059392051
5	0.087266463	10	65	0.050523391
5	0.087266463	10	70	0.042048158
5	0.087266463	10	75	0.034114853
5	0.087266463	10	80	0.02685199
5	0.087266463	10	90	0.014734145
5	0.087266463	10	95	0.010012485
5	0.087266463	10	100	0.006225652
5	0.087266463	10	105	0.003371719
5	0.087266463	10	110	0.001422202
5	0.087266463	10	115	0.000323801
5	0.087266463	10	118	4.26701E-05
5	0.087266463	10	119.74	6.9679E-10
5	0.087266463	15	0	0.233955557
5	0.087266463	15	20	0.21316642
5	0.087266463	15	30	0.189084107
5	0.087266463	15	35	0.174512114
5	0.087266463	15	40	0.158707987
5	0.087266463	15	45	0.142046916
5	0.087266463	15	50	0.1249186
5	0.087266463	15	55	0.107716295
5	0.087266463	15	60	0.090825831
5	0.087266463	15	65	0.074614932
5	0.087266463	15	70	0.059423151
5	0.087266463	15	75	0.045552711
5	0.087266463	15	80	0.033260546
5	0.087266463	15	85	0.022751734

5	0.087266463	15	90	0.014174559
5	0.087266463	15	95	0.007617299
5	0.087266463	15	100	0.003106856
5	0.087266463	15	105	0.000609256
5	0.087266463	15	106	0.000344125
5	0.087266463	15	107	0.00015497
5	0.087266463	15	109.05	1.88237E-09
5	0.087266463	20	0	0.35721239
5	0.087266463	20	20	0.323321234
5	0.087266463	20	30	0.284213693
5	0.087266463	20	45	0.208430771
5	0.087266463	20	50	0.181092858
5	0.087266463	20	55	0.153821417
5	0.087266463	20	60	0.127269141
5	0.087266463	20	65	0.102055777
5	0.087266463	20	70	0.078750716
5	0.087266463	20	75	0.057857192
5	0.087266463	20	80	0.039798545
5	0.087266463	20	85	0.024906975
5	0.087266463	20	90	0.013415092
5	0.087266463	20	95	0.00545052
5	0.087266463	20	96	0.004284567
5	0.087266463	20	97	0.003260515
5	0.087266463	20	98	0.002377842
5	0.087266463	20	100	0.001033709
5	0.087266463	20	101	0.00057037
5	0.087266463	20	102	0.000244657
5	0.087266463	20	103.908	2.11742E-11
5	0.087266463	25	0	0.5
5	0.087266463	25	20	0.450509278
5	0.087266463	25	30	0.393553661
5	0.087266463	25	40	0.322408281
5	0.087266463	25	45	0.283789213
5	0.087266463	25	50	0.244454285
5	0.087266463	25	55	0.205403817
5	0.087266463	25	60	0.167614669
5	0.087266463	25	65	0.132012148
5	0.087266463	25	70	0.099443598
5	0.087266463	25	75	0.070654429

5	0.087266463	25	80	0.046267336
5	0.087266463	25	85	0.026765286
5	0.087266463	25	90	0.012478818
5	0.087266463	25	92	0.00826818
5	0.087266463	25	94	0.004924636
5	0.087266463	25	96	0.002447536
5	0.087266463	25	98	0.000832047
5	0.087266463	25	99	0.000344765
5	0.087266463	25	99.5	0.000180623
5	0.087266463	30	0	0.657979857
5	0.087266463	30	20	0.590866007
5	0.087266463	30	30	0.513781772
5	0.087266463	30	35	0.467537826
5	0.087266463	30	40	0.417778059
5	0.087266463	30	45	0.365832512
5	0.087266463	30	50	0.313077674
5	0.087266463	30	55	0.260896191
5	0.087266463	30	60	0.210636536
5	0.087266463	30	65	0.163573837
5	0.087266463	30	70	0.120873052
5	0.087266463	30	75	0.083555587
5	0.087266463	30	80	0.052470366
5	0.087266463	30	85	0.028270202
5	0.087266463	30	90	0.011394185
5	0.087266463	30	92	0.00675023
5	0.087266463	30	94	0.003318448
5	0.087266463	30	95	0.00205659
5	0.087266463	30	96	0.001096406
5	0.087266463	30	97	0.000436678
5	0.087266463	30	98.715	1.14766E-10
5	0.087266463	35	0	0.826351822
5	0.087266463	35	20	0.740126755
5	0.087266463	35	25	0.694436922
5	0.087266463	35	30	0.641244955
5	0.087266463	35	35	0.58201737
5	0.087266463	35	40	0.518379577
5	0.087266463	35	45	0.452067824
5	0.087266463	35	50	0.384877938
5	0.087266463	35	55	0.318612431
5	0.087266463	35	60	0.255027546

5	0.087266463	35	65	0.195781858
5	0.087266463	35	70	0.142387955
5	0.087266463	35	75	0.096168668
5	0.087266463	35	80	0.05821916
5	0.087266463	35	85	0.029375999
5	0.087266463	35	90	0.010194151
5	0.087266463	35	92	0.005294709
5	0.087266463	35	94	0.001988961
5	0.087266463	35	96	0.000272233
5	0.087266463	35	97	6.18406E-06
5	0.087266463	35	97.17	1.1553E-08

5	0.087266463	40	0	1
5	0.087266463	40	15	0.939238381
5	0.087266463	40	20	0.893756308
5	0.087266463	40	25	0.837507257
5	0.087266463	40	30	0.772070307
5	0.087266463	40	35	0.699276844
5	0.087266463	40	40	0.621156111
5	0.087266463	40	45	0.539874934
5	0.087266463	40	50	0.457673465
5	0.087266463	40	55	0.376798858
5	0.087266463	40	60	0.2994389
5	0.087266463	40	65	0.227657587
5	0.087266463	40	70	0.163334588
5	0.087266463	40	75	0.108110432
5	0.087266463	40	80	0.063339043
5	0.087266463	40	85	0.030049075
5	0.087266463	40	90	0.008915176
5	0.087266463	40	92	0.003945842
5	0.087266463	40	94	0.000976572
5	0.087266463	40	95	0.000240056
5	0.087266463	40	95.9848	7.69068E-14

5	0.087266463	45	0	1.173648178
5	0.087266463	45	15	1.101252805
5	0.087266463	45	20	1.04708671
5	0.087266463	45	25	0.980129215
5	0.087266463	45	30	0.902282764
5	0.087266463	45	35	0.81575338
5	0.087266463	45	40	0.722984846

5	0.087266463	45	45	0.626585866
5	0.087266463	45	50	0.529252396
5	0.087266463	45	55	0.433687507
5	0.087266463	45	60	0.342521181
5	0.087266463	45	65	0.258232495
5	0.087266463	45	70	0.183076499
5	0.087266463	45	75	0.119018033
5	0.087266463	45	80	0.067674452
5	0.087266463	45	85	0.030268982
5	0.087266463	45	90	0.007596123
5	0.087266463	45	92	0.002744612
5	0.087266463	45	94	0.000312042
5	0.087266463	45	95	1.09994E-07
5	0.087266463	45	95.0191	6.94031E-13

semi	semi[rad]	AoA	meridian	cp
10	0.174532925	0	0	0.060307379
10	0.174532925	0	45	0.060307379
10	0.174532925	0	90	0.060307379
10	0.174532925	0	95	0.060307379
10	0.174532925	0	100	0.060307379
10	0.174532925	0	105	0.060307379
10	0.174532925	0	110	0.060307379
10	0.174532925	0	115	0.060307379
10	0.174532925	0	120	0.060307379
10	0.174532925	0	125	0.060307379
10	0.174532925	0	130	0.060307379
10	0.174532925	0	135	0.060307379
10	0.174532925	0	140	0.060307379
10	0.174532925	0	145	0.060307379
10	0.174532925	0	150	0.060307379
10	0.174532925	0	155	0.060307379
10	0.174532925	0	160	0.060307379
10	0.174532925	0	165	0.060307379
10	0.174532925	0	170	0.060307379
10	0.174532925	0	175	0.060307379
10	0.174532925	0	180	0.060307379
10	0.174532925	5	0	0.133974596
10	0.174532925	5	45	0.109212252
10	0.174532925	5	90	0.059849277
10	0.174532925	5	95	0.054784917
10	0.174532925	5	100	0.049980396

10	0.174532925	5	105	0.04546471
10	0.174532925	5	110	0.041259866
10	0.174532925	5	115	0.037381091
10	0.174532925	5	120	0.033837226
10	0.174532925	5	125	0.030631284
10	0.174532925	5	130	0.027761159
10	0.174532925	5	135	0.025220447
10	0.174532925	5	140	0.022999349
10	0.174532925	5	145	0.021085634
10	0.174532925	5	150	0.019465619
10	0.174532925	5	155	0.018125128
10	0.174532925	5	160	0.017050406
10	0.174532925	5	165	0.016228952
10	0.174532925	5	170	0.015650244
10	0.174532925	5	175	0.015306326
10	0.174532925	5	180	0.015192247
10				
10	0.174532925	10	0	0.233955557
10	0.174532925	10	45	0.170449114
10	0.174532925	10	90	0.058488889
10	0.174532925	10	95	0.048737893
10	0.174532925	10	100	0.039939567
10	0.174532925	10	105	0.032130825
10	0.174532925	10	110	0.025322033
10	0.174532925	10	115	0.019498422
10	0.174532925	10	120	0.014622222
10	0.174532925	10	125	0.010635447
10	0.174532925	10	130	0.007463223
10	0.174532925	10	135	0.005017553
10	0.174532925	10	140	0.003201401
10	0.174532925	10	145	0.001912937
10	0.174532925	10	150	0.001049828
10	0.174532925	10	155	0.000513429
10	0.174532925	10	160	0.000212723
10	0.174532925	10	165	6.79085E-05
10	0.174532925	10	170	1.34995E-05
10	0.174532925	10	175	8.46938E-07
10	0.174532925	10	180	0
10				
10				
10	0.174532925	15	0	0.35721239
10	0.174532925	15	20	0.331699741
10	0.174532925	15	30	0.301817693

10	0.174532925	15	40	0.263517718
10	0.174532925	15	45	0.242157316
10	0.174532925	15	50	0.219876622
10	0.174532925	15	60	0.174256279
10	0.174532925	15	70	0.129955921
10	0.174532925	15	80	0.089881151
10	0.174532925	15	90	0.056267551
10	0.174532925	15	95	0.042350042
10	0.174532925	15	100	0.030489976
10	0.174532925	15	105	0.020710866
10	0.174532925	15	110	0.012978142
10	0.174532925	15	115	0.007202726
10	0.174532925	15	120	0.003246207
10	0.174532925	15	122	0.002133577
10	0.174532925	15	124	0.001270106
10	0.174532925	15	126	0.000641711
10	0.174532925	15	128	0.000233589
10	0.174532925	15	131.15	1.06633E-10
10				
10				
10	0.174532925	20	0	0.5
10	0.174532925	20	20	0.460199278
10	0.174532925	20	25	0.4388762
10	0.174532925	20	30	0.413820946
10	0.174532925	20	35	0.385593122
10	0.174532925	20	45	0.32215804
10	0.174532925	20	50	0.28831724
10	0.174532925	20	55	0.253999541
10	0.174532925	20	60	0.219901145
10	0.174532925	20	65	0.186689734
10	0.174532925	20	70	0.15498699
10	0.174532925	20	75	0.125352649
10	0.174532925	20	80	0.098270567
10	0.174532925	20	85	0.074137192
10	0.174532925	20	90	0.053252756
10	0.174532925	20	95	0.035815455
10	0.174532925	20	100	0.021918745
10	0.174532925	20	105	0.011551824
10	0.174532925	20	110	0.004603257
10	0.174532925	20	115	0.000867603
10	0.174532925	20	118.97	2.39757E-09
10				
10				

10	0.174532925	25	0	0.657979857
10	0.174532925	25	20	0.601653252
10	0.174532925	25	25	0.57155572
10	0.174532925	25	30	0.53626788
10	0.174532925	25	35	0.496621578
10	0.174532925	25	40	0.453541761
10	0.174532925	25	45	0.408020504
10	0.174532925	25	50	0.361089277
10	0.174532925	25	55	0.313790281
10	0.174532925	25	60	0.267147702
10	0.174532925	25	65	0.222139734
10	0.174532925	25	70	0.179672197
10	0.174532925	25	75	0.140554533
10	0.174532925	25	80	0.105478865
10	0.174532925	25	85	0.075002751
10	0.174532925	25	90	0.049536108
10	0.174532925	25	95	0.029332683
10	0.174532925	25	100	0.014486306
10	0.174532925	25	105	0.004931992
10	0.174532925	25	110	0.000451843
10	0.174532925	25	112.218	2.69946E-12
10				
10				
10	0.174532925	30	0	0.826351822
10	0.174532925	30	20	0.751763656
10	0.174532925	30	25	0.711990084
10	0.174532925	30	30	0.665438008
10	0.174532925	30	35	0.613250161
10	0.174532925	30	40	0.556696057
10	0.174532925	30	45	0.49713582
10	0.174532925	30	50	0.435981591
10	0.174532925	30	55	0.374657638
10	0.174532925	30	60	0.31456039
10	0.174532925	30	65	0.257019554
10	0.174532925	30	70	0.203261496
10	0.174532925	30	75	0.154375944
10	0.174532925	30	80	0.111287023
10	0.174532925	30	85	0.074729439
10	0.174532925	30	90	0.045230534
10	0.174532925	30	95	0.023098702
10	0.174532925	30	100	0.008418491
10	0.174532925	30	102	0.004609385
10	0.174532925	30	105	0.001052508

10	0.174532925	30	107.78	9.54187E-10
10				
10				
10	0.174532925	35	0	1
10	0.174532925	35	15	0.946301542
10	0.174532925	35	20	0.90596946
10	0.174532925	35	25	0.855912264
10	0.174532925	35	30	0.797406561
10	0.174532925	35	35	0.731935173
10	0.174532925	35	40	0.661144332
10	0.174532925	35	45	0.586796266
10	0.174532925	35	50	0.510718616
10	0.174532925	35	55	0.434752187
10	0.174532925	35	60	0.360698595
10	0.174532925	35	65	0.290269389
10	0.174532925	35	70	0.225038136
10	0.174532925	35	75	0.166396926
10	0.174532925	35	80	0.115518563
10	0.174532925	35	85	0.07332556
10	0.174532925	35	90	0.040466859
10	0.174532925	35	95	0.017302928
10	0.174532925	35	100	0.003899666
10	0.174532925	35	102	0.001230352
10	0.174532925	35	104.585	1.60948E-11
10				
10				
10	0.174532925	40	0	1.173648178
10	0.174532925	40	15	1.108485259
10	0.174532925	40	20	1.0595852
10	0.174532925	40	25	0.998949258
10	0.174532925	40	30	0.92816374
10	0.174532925	40	35	0.849070428
10	0.174532925	40	40	0.763712977
10	0.174532925	40	45	0.674277553
10	0.174532925	40	50	0.583029507
10	0.174532925	40	55	0.492247985
10	0.174532925	40	60	0.404160434
10	0.174532925	40	65	0.320878959
10	0.174532925	40	70	0.244340446
10	0.174532925	40	75	0.176252228
10	0.174532925	40	80	0.118044912
10	0.174532925	40	85	0.07083377
10	0.174532925	40	90	0.035389823

	10	0.174532925	40	95	0.012121463
	10	0.174532925	40	100	0.001067134
	10	0.174532925	40	102	3.97339E-06
	10	0.174532925	40	102.13	4.89154E-11
	10				
	10				
	10	0.174532925	45	0	1.342020143
	10	0.174532925	45	5	1.333351581
	10	0.174532925	45	10	1.307579644
	10	0.174532925	45	15	1.265398706
	10	0.174532925	45	20	1.207943338
	10	0.174532925	45	25	1.13675496
	10	0.174532925	45	30	1.053736555
	10	0.174532925	45	35	0.961096831
	10	0.174532925	45	40	0.861285497
	10	0.174532925	45	45	0.756921607
	10	0.174532925	45	50	0.650717133
	10	0.174532925	45	55	0.545398053
	10	0.174532925	45	60	0.443625339
	10	0.174532925	45	65	0.347918207
	10	0.174532925	45	70	0.260581935
	10	0.174532925	45	75	0.1836424
	10	0.174532925	45	80	0.118789309
	10	0.174532925	45	85	0.067329782
	10	0.174532925	45	90	0.03015369
	10	0.174532925	45	95	0.007711742
	10	0.174532925	45	100	6.9596E-06

semi	semi[rad]	AoA	meridian	cp
15	0.261799388	0	0	0.133974596
15	0.261799388	0	45	0.133974596
15	0.261799388	0	90	0.133974596
15	0.261799388	0	95	0.133974596
15	0.261799388	0	100	0.133974596
15	0.261799388	0	105	0.133974596
15	0.261799388	0	110	0.133974596
15	0.261799388	0	115	0.133974596
15	0.261799388	0	120	0.133974596
15	0.261799388	0	125	0.133974596
15	0.261799388	0	130	0.133974596
15	0.261799388	0	135	0.133974596
15	0.261799388	0	140	0.133974596
15	0.261799388	0	145	0.133974596

15	0.261799388	0	150	0.133974596
15	0.261799388	0	155	0.133974596
15	0.261799388	0	160	0.133974596
15	0.261799388	0	165	0.133974596
15	0.261799388	0	170	0.133974596
15	0.261799388	0	175	0.133974596
15	0.261799388	0	180	0.133974596
15				
15	0.261799388	5	0	0.233955557
15	0.261799388	5	45	0.20143809
15	0.261799388	5	90	0.132956909
15	0.261799388	5	95	0.125497362
15	0.261799388	5	100	0.118307479
15	0.261799388	5	105	0.111434696
15	0.261799388	5	110	0.10491943
15	0.261799388	5	115	0.098795127
15	0.261799388	5	120	0.093088504
15	0.261799388	5	125	0.087819944
15	0.261799388	5	130	0.083004047
15	0.261799388	5	135	0.078650286
15	0.261799388	5	140	0.074763771
15	0.261799388	5	145	0.071346051
15	0.261799388	5	150	0.068395962
15	0.261799388	5	155	0.065910456
15	0.261799388	5	160	0.063885404
15	0.261799388	5	165	0.062316323
15	0.261799388	5	170	0.061199017
15	0.261799388	5	175	0.060530099
15	0.261799388	5	180	0.060307379
15				
15	0.261799388	6	0	0.256855175
15	0.261799388	6	45	0.216212929
15	0.261799388	6	90	0.132510763
15	0.261799388	6	95	0.123605288
15	0.261799388	6	100	0.11507381
15	0.261799388	6	105	0.106970785
15	0.261799388	6	110	0.099340779
15	0.261799388	6	115	0.092218649
15	0.261799388	6	120	0.085629982
15	0.261799388	6	125	0.079591773
15	0.261799388	6	130	0.074113298
15	0.261799388	6	135	0.069197163
15	0.261799388	6	140	0.064840467

15	0.261799388	6	145	0.061036053
15	0.261799388	6	150	0.057773785
15	0.261799388	6	155	0.055041813
15	0.261799388	6	160	0.052827779
15	0.261799388	6	165	0.051119918
15	0.261799388	6	170	0.049908016
15	0.261799388	6	179	0.048953107
15				
15	0.261799388	12	0	0.412214748
15	0.261799388	12	45	0.312317952
15	0.261799388	12	90	0.12818324
15	0.261799388	12	95	0.11107125
15	0.261799388	12	100	0.095300994
15	0.261799388	12	105	0.080951054
15	0.261799388	12	110	0.068062978
15	0.261799388	12	115	0.056643018
15	0.261799388	12	120	0.046664876
15	0.261799388	12	125	0.038073339
15	0.261799388	12	130	0.030788688
15	0.261799388	12	135	0.024711714
15	0.261799388	12	140	0.019729168
15	0.261799388	12	145	0.015719474
15	0.261799388	12	150	0.012558497
15	0.261799388	12	155	0.010125188
15	0.261799388	12	160	0.008306915
15	0.261799388	12	165	0.007004303
15	0.261799388	12	170	0.006135434
15	0.261799388	12	175	0.005639255
15	0.261799388	12	180	0.005478105
15				
15				
15	0.261799388	18	0	0.593263357
15	0.261799388	18	20	0.554695243
15	0.261799388	18	25	0.533902145
15	0.261799388	18	30	0.509341818
15	0.261799388	18	35	0.481490902
15	0.261799388	18	40	0.450881906
15	0.261799388	18	45	0.418089415
15	0.261799388	18	50	0.383715337
15	0.261799388	18	55	0.34837362
15	0.261799388	18	60	0.312674866
15	0.261799388	18	65	0.277211313
15	0.261799388	18	70	0.242542579

	15	0.261799388	18	80	0.177588153
	15	0.261799388	18	90	0.121181161
	15	0.261799388	18	100	0.075520315
	15	0.261799388	18	110	0.041508183
	15	0.261799388	18	120	0.01878224
	15	0.261799388	18	125	0.011233849
	15	0.261799388	18	130	0.00589426
	15	0.261799388	18	135	0.002462477
	15	0.261799388	18	137.4	0.001397699
	15				
	15	0.261799388	25	0	0.826351822
	15	0.261799388	25	20	0.764265969
	15	0.261799388	25	30	0.69171565
	15	0.261799388	25	35	0.647436057
	15	0.261799388	25	40	0.59903685
	15	0.261799388	25	45	0.547525362
	15	0.261799388	25	50	0.493952637
	15	0.261799388	25	55	0.439385404
	15	0.261799388	25	60	0.384877938
	15	0.261799388	25	70	0.280034005
	15	0.261799388	25	80	0.186606747
	15	0.261799388	25	85	0.145960154
	15	0.261799388	25	90	0.110045903
	15	0.261799388	25	95	0.079194981
	15	0.261799388	25	100	0.053584526
	15	0.261799388	25	105	0.033238232
	15	0.261799388	25	110	0.018031375
	15	0.261799388	25	115	0.007700251
	15	0.261799388	25	120	0.001855717
	15	0.261799388	25	122	0.00066592
	15	0.261799388	25	125.07	5.90897E-10

semi		semi[rad]	AoA		meridian	cp
	20	0.34906585		0	0	0.233955557
	20	0.34906585		0	45	0.233955557
	20	0.34906585		0	90	0.233955557
	20	0.34906585		0	95	0.233955557
	20	0.34906585		0	100	0.233955557
	20	0.34906585		0	105	0.233955557
	20	0.34906585		0	110	0.233955557
	20	0.34906585		0	115	0.233955557
	20	0.34906585		0	120	0.233955557
	20	0.34906585		0	125	0.233955557

20	0.34906585	0	130	0.233955557
20	0.34906585	0	135	0.233955557
20	0.34906585	0	140	0.233955557
20	0.34906585	0	145	0.233955557
20	0.34906585	0	150	0.233955557
20	0.34906585	0	155	0.233955557
20	0.34906585	0	160	0.233955557
20	0.34906585	0	165	0.233955557
20	0.34906585	0	170	0.233955557
20	0.34906585	0	175	0.233955557
20	0.34906585	0	180	0.233955557
20				
20	0.34906585	5	0	0.35721239
20	0.34906585	5	45	0.317812426
20	0.34906585	5	90	0.232178402
20	0.34906585	5	95	0.222552076
20	0.34906585	5	100	0.213200498
20	0.34906585	5	105	0.204187946
20	0.34906585	5	110	0.195571758
20	0.34906585	5	115	0.187402236
20	0.34906585	5	120	0.179722726
20	0.34906585	5	125	0.172569862
20	0.34906585	5	130	0.16597395
20	0.34906585	5	135	0.159959468
20	0.34906585	5	140	0.154545665
20	0.34906585	5	145	0.149747216
20	0.34906585	5	150	0.14557492
20	0.34906585	5	155	0.142036399
20	0.34906585	5	160	0.139136772
20	0.34906585	5	165	0.136879277
20	0.34906585	5	170	0.135265824
20	0.34906585	5	175	0.134297437
20	0.34906585	5	180	0.133974596
20				
20	0.34906585	10	0	0.5
20	0.34906585	10	45	0.408982129
20	0.34906585	10	90	0.226900934
20	0.34906585	10	95	0.20814458
20	0.34906585	10	100	0.19033079
20	0.34906585	10	105	0.17356778
20	0.34906585	10	110	0.157938456
20	0.34906585	10	115	0.14350114
20	0.34906585	10	120	0.130290967

20	0.34906585	10	125	0.118321891
20	0.34906585	10	130	0.107589205
20	0.34906585	10	135	0.098072495
20	0.34906585	10	140	0.089738889
20	0.34906585	10	145	0.082546515
20	0.34906585	10	150	0.076448011
20	0.34906585	10	155	0.071393994
20	0.34906585	10	160	0.067336345
20	0.34906585	10	165	0.064231202
20	0.34906585	10	170	0.062041572
20	0.34906585	10	175	0.060739446
20	0.34906585	10	180	0.060307379
20				
20	0.34906585	15	0	0.657979857
20	0.34906585	15	45	0.504694518
20	0.34906585	15	90	0.218283506
20	0.34906585	15	95	0.191170831
20	0.34906585	15	100	0.166041316
20	0.34906585	15	105	0.143025436
20	0.34906585	15	110	0.12219912
20	0.34906585	15	115	0.103586183
20	0.34906585	15	120	0.08716224
20	0.34906585	15	125	0.072859939
20	0.34906585	15	130	0.060575313
20	0.34906585	15	135	0.05017504
20	0.34906585	15	140	0.041504352
20	0.34906585	15	145	0.034395314
20	0.34906585	15	150	0.028675216
20	0.34906585	15	155	0.024174776
20	0.34906585	15	160	0.020735896
20	0.34906585	15	165	0.018218707
20	0.34906585	15	170	0.016507683
20	0.34906585	15	175	0.015516607
20	0.34906585	15	180	0.015192247
20				
20	0.34906585	20	0	0.826351822
20	0.34906585	20	45	0.602041422
20	0.34906585	20	90	0.206587956
20	0.34906585	20	95	0.17214657
20	0.34906585	20	100	0.141070101
20	0.34906585	20	105	0.11348893
20	0.34906585	20	110	0.089439671
20	0.34906585	20	115	0.068870159

20	0.34906585	20	120	0.051646989
20	0.34906585	20	125	0.037565346
20	0.34906585	20	130	0.026360766
20	0.34906585	20	135	0.017722445
20	0.34906585	20	140	0.011307634
20	0.34906585	20	145	0.006756662
20	0.34906585	20	150	0.003708087
20	0.34906585	20	155	0.001813477
20	0.34906585	20	160	0.000751356
20	0.34906585	20	165	0.000239859
20	0.34906585	20	170	4.76814E-05
20	0.34906585	20	175	2.99146E-06
20	0.34906585	20	180	0
20				
20	0.34906585	25	0	1
20	0.34906585	25	20	0.933406524
20	0.34906585	25	25	0.897528468
20	0.34906585	25	30	0.85517377
20	0.34906585	25	35	0.807177631
20	0.34906585	25	40	0.754472754
20	0.34906585	25	50	0.639007378
20	0.34906585	25	60	0.517228203
20	0.34906585	25	70	0.397479578
20	0.34906585	25	75	0.340742714
20	0.34906585	25	80	0.287185953
20	0.34906585	25	90	0.192169645
20	0.34906585	25	100	0.116175881
20	0.34906585	25	105	0.085855711
20	0.34906585	25	115	0.040407898
20	0.34906585	25	120	0.024824326
20	0.34906585	25	125	0.013510519
20	0.34906585	25	130	0.005985157
20	0.34906585	25	135	0.001700764
20	0.34906585	25	138	0.000441014
20	0.34906585	25	141.309	2.05709E-11
20				
20	0.34906585	30	0	1.173648178
20	0.34906585	30	20	1.088429856
20	0.34906585	30	25	1.042635876
20	0.34906585	30	30	0.988690708
20	0.34906585	30	35	0.927722765
20	0.34906585	30	40	0.860990289
20	0.34906585	30	45	0.789847637

20	0.34906585	30	50	0.715709258
20	0.34906585	30	55	0.6400124
20	0.34906585	30	60	0.564179645
20	0.34906585	30	65	0.489582364
20	0.34906585	30	70	0.417506146
20	0.34906585	30	75	0.349119205
20	0.34906585	30	80	0.285444657
20	0.34906585	30	85	0.227337463
20	0.34906585	30	90	0.175466668
20	0.34906585	30	100	0.092115056
20	0.34906585	30	110	0.036721167
20	0.34906585	30	120	0.007509246
20	0.34906585	30	125	0.001426353
20	0.34906585	30	129.08	4.46868E-11
20				
20	0.34906585	35	0	1.342020143
20	0.34906585	35	20	1.237627756
20	0.34906585	35	25	1.181655778
20	0.34906585	35	30	1.115843727
20	0.34906585	35	35	1.041637147
20	0.34906585	35	40	0.960645978
20	0.34906585	35	45	0.874600552
20	0.34906585	35	50	0.785304571
20	0.34906585	35	55	0.694586478
20	0.34906585	35	60	0.60425063
20	0.34906585	35	65	0.516029724
20	0.34906585	35	70	0.431539847
20	0.34906585	35	75	0.352239478
20	0.34906585	35	80	0.279393609
20	0.34906585	35	85	0.214044019
20	0.34906585	35	90	0.156986535
20	0.34906585	35	100	0.069618701
20	0.34906585	35	110	0.018363936
20	0.34906585	35	115	0.005487615
20	0.34906585	35	120	0.000227857
20	0.34906585	35	121.319	5.04672E-13
20				
20	0.34906585	40	0	1.5
20	0.34906585	40	20	1.376466922
20	0.34906585	40	25	1.310364125
20	0.34906585	40	30	1.232769348
20	0.34906585	40	35	1.145459544
20	0.34906585	40	40	1.050411833

20	0.34906585	40	45	0.949748573
20	0.34906585	40	50	0.845678697
20	0.34906585	40	55	0.740437068
20	0.34906585	40	60	0.636223623
20	0.34906585	40	65	0.53514413
20	0.34906585	40	70	0.439154274
20	0.34906585	40	75	0.350008725
20	0.34906585	40	80	0.269216668
20	0.34906585	40	85	0.198005071
20	0.34906585	40	90	0.137290756
20	0.34906585	40	95	0.087662027
20	0.34906585	40	110	0.006141572
20	0.34906585	40	105	0.022332312
20	0.34906585	40	110	0.006141572
20	0.34906585	40	115.7	7.85435E-09
20				
20	0.34906585	45	0	1.64278761
20	0.34906585	45	20	1.500728796
20	0.34906585	45	25	1.424850177
20	0.34906585	45	30	1.335914844
20	0.34906585	45	35	1.236035367
20	0.34906585	45	40	1.127560366
20	0.34906585	45	45	1.013008367
20	0.34906585	45	50	0.894997201
20	0.34906585	45	55	0.776171022
20	0.34906585	45	60	0.659127139
20	0.34906585	45	65	0.5463448
20	0.34906585	45	70	0.440118067
20	0.34906585	45	75	0.342494727
20	0.34906585	45	80	0.255223053
20	0.34906585	45	85	0.179707956
20	0.34906585	45	90	0.116977778
20	0.34906585	45	95	0.067662693
20	0.34906585	45	100	0.031985259
20	0.34906585	45	105	0.009763376
20	0.34906585	45	110	0.000425446
20	0.34906585	45	111.34	4.16143E-09

semi	semi[rad]	AoA	meridian	cp
25	0.436332313	0	0	0.35721239
25	0.436332313	4	45	0.434857701
25	0.436332313	4	90	0.355474207
25	0.436332313	4	95	0.346243013

25	0.436332313	4	100	0.337202133
25	0.436332313	4	105	0.328416269
25	0.436332313	4	110	0.319945579
25	0.436332313	4	115	0.311845432
25	0.436332313	4	120	0.304166254
25	0.436332313	4	125	0.296953491
25	0.436332313	4	130	0.290247657
25	0.436332313	4	135	0.284084461
25	0.436332313	4	140	0.278495003
25	0.436332313	4	145	0.273506015
25	0.436332313	4	150	0.269140142
25	0.436332313	4	155	0.265416229
25	0.436332313	4	160	0.262349621
25	0.436332313	4	165	0.259952437
25	0.436332313	4	170	0.258233821
25	0.436332313	4	175	0.257200147
25	0.436332313	4	180	0.256855175
25				
25	0.436332313	5	0	0.5
25	0.436332313	5	45	0.454799285
25	0.436332313	5	90	0.354498961
25	0.436332313	5	95	0.343000101
25	0.436332313	5	100	0.331776177
25	0.436332313	5	105	0.320906199
25	0.436332313	5	110	0.310462426
25	0.436332313	5	115	0.300510135
25	0.436332313	5	120	0.291107554
25	0.436332313	5	125	0.282305954
25	0.436332313	5	130	0.274149872
25	0.436332313	5	135	0.266677455
25	0.436332313	5	140	0.259920898
25	0.436332313	5	145	0.253906948
25	0.436332313	5	150	0.248657451
25	0.436332313	5	155	0.244189909
25	0.436332313	5	160	0.240518034
25	0.436332313	5	165	0.237652257
25	0.436332313	5	170	0.235600181
25	0.436332313	5	175	0.234366956
25	0.436332313	5	180	0.233955557
25				
25	0.436332313	10	0	0.657979857
25	0.436332313	10	45	0.556473009
25	0.436332313	10	90	0.346441119

25	0.436332313	10	95	0.323982367
25	0.436332313	10	100	0.302438536
25	0.436332313	10	105	0.281948138
25	0.436332313	10	110	0.262625565
25	0.436332313	10	115	0.244561478
25	0.436332313	10	120	0.227823831
25	0.436332313	10	125	0.212459464
25	0.436332313	10	130	0.198496201
25	0.436332313	10	135	0.185945336
25	0.436332313	10	140	0.174804441
25	0.436332313	10	145	0.165060356
25	0.436332313	10	150	0.156692266
25	0.436332313	10	155	0.149674747
25	0.436332313	10	160	0.143980664
25	0.436332313	10	165	0.139583829
25	0.436332313	10	170	0.136461308
25	0.436332313	10	175	0.134595313
25	0.436332313	10	180	0.133974596
25				
25	0.436332313	15	0	0.826351822
25	0.436332313	15	45	0.659144259
25	0.436332313	15	90	0.333283697
25	0.436332313	15	95	0.300737033
25	0.436332313	15	100	0.270090877
25	0.436332313	15	105	0.24152193
25	0.436332313	15	110	0.215155308
25	0.436332313	15	115	0.191066392
25	0.436332313	15	120	0.169284062
25	0.436332313	15	125	0.14979517
25	0.436332313	15	130	0.132550076
25	0.436332313	15	135	0.117469039
25	0.436332313	15	140	0.10444924
25	0.436332313	15	145	0.093372171
25	0.436332313	15	150	0.084111151
25	0.436332313	15	155	0.076538699
25	0.436332313	15	160	0.07053352
25	0.436332313	15	165	0.065986867
25	0.436332313	15	170	0.062808057
25	0.436332313	15	175	0.060928972
25	0.436332313	15	180	0.060307379
25				
25	0.436332313	20	0	1
25	0.436332313	20	45	0.759693421

25	0.436332313	20	90	0.315426478
25	0.436332313	20	95	0.273970397
25	0.436332313	20	100	0.235716066
25	0.436332313	20	105	0.200855903
25	0.436332313	20	110	0.169494012
25	0.436332313	20	115	0.141650297
25	0.436332313	20	120	0.117266951
25	0.436332313	20	125	0.096217095
25	0.436332313	20	130	0.078315236
25	0.436332313	20	135	0.063329181
25	0.436332313	20	140	0.050993002
25	0.436332313	20	145	0.041020604
25	0.436332313	20	150	0.033119446
25	0.436332313	20	155	0.027003967
25	0.436332313	20	160	0.022408256
25	0.436332313	20	165	0.019097577
25	0.436332313	20	170	0.016878344
25	0.436332313	20	175	0.015606248
25	0.436332313	20	180	0.015192247
25				
25	0.436332313	25	0	1.173648178
25	0.436332313	25	45	0.855065359
25	0.436332313	25	90	0.293412044
25	0.436332313	25	95	0.244495749
25	0.436332313	25	100	0.200358566
25	0.436332313	25	105	0.161185674
25	0.436332313	25	110	0.127029075
25	0.436332313	25	115	0.097814677
25	0.436332313	25	120	0.073353011
25	0.436332313	25	125	0.053353182
25	0.436332313	25	130	0.03743958
25	0.436332313	25	135	0.025170774
25	0.436332313	25	140	0.016059968
25	0.436332313	25	145	0.009596329
25	0.436332313	25	150	0.005266509
25	0.436332313	25	155	0.002575639
25	0.436332313	25	160	0.001067134
25	0.436332313	25	165	0.000340666
25	0.436332313	25	170	6.77208E-05
25	0.436332313	25	175	4.2487E-06
25	0.436332313	25	180	0
25				
25	0.436332313	30	0	1.342020143

25	0.436332313	30	20	1.253968976
25	0.436332313	30	25	1.206510411
25	0.436332313	30	30	1.150465302
25	0.436332313	30	35	1.086927943
25	0.436332313	30	40	1.017120697
25	0.436332313	30	50	0.864033626
25	0.436332313	30	60	0.702290492
25	0.436332313	30	70	0.542852638
25	0.436332313	30	75	0.467124933
25	0.436332313	30	80	0.395493943
25	0.436332313	30	90	0.267909293
25	0.436332313	30	100	0.165092697
25	0.436332313	30	105	0.123716604
25	0.436332313	30	115	0.060891454
25	0.436332313	30	120	0.038876544
25	0.436332313	30	125	0.022505829
25	0.436332313	30	130	0.011165094
25	0.436332313	30	135	0.004153242
25	0.436332313	30	138	0.001709859
25	0.436332313	30	143.868	2.54199E-11
25				
25	0.436332313	35	0	1.5
25	0.436332313	35	20	1.393366078
25	0.436332313	35	25	1.336026399
25	0.436332313	35	30	1.268443737
25	0.436332313	35	35	1.19201118
25	0.436332313	35	40	1.108282664
25	0.436332313	35	45	1.018931608
25	0.436332313	35	50	0.925706693
25	0.436332313	35	55	0.83038608
25	0.436332313	35	60	0.734731411
25	0.436332313	35	65	0.640442916
25	0.436332313	35	70	0.549116928
25	0.436332313	35	75	0.46220704
25	0.436332313	35	80	0.380989992
25	0.436332313	35	85	0.306537257
25	0.436332313	35	90	0.239693112
25	0.436332313	35	100	0.130989992
25	0.436332313	35	110	0.056713051
25	0.436332313	35	120	0.014885101
25	0.436332313	35	125	0.004612317
25	0.436332313	35	131.755	4.96354E-11
25				

25	0.436332313	40	0	1.64278761
25	0.436332313	40	20	1.517891462
25	0.436332313	40	25	1.450874806
25	0.436332313	40	30	1.372026236
25	0.436332313	40	35	1.283049443
25	0.436332313	40	40	1.185842623
25	0.436332313	40	45	1.082446926
25	0.436332313	40	50	0.974991383
25	0.436332313	40	55	0.865635923
25	0.436332313	40	60	0.756514156
25	0.436332313	40	65	0.649677591
25	0.436332313	40	70	0.547042925
25	0.436332313	40	75	0.450343924
25	0.436332313	40	80	0.361089277
25	0.436332313	40	85	0.280527642
25	0.436332313	40	90	0.209620835
25	0.436332313	40	100	0.099086647
25	0.436332313	40	110	0.030998482
25	0.436332313	40	115	0.012025658
25	0.436332313	40	120	0.002107649
25	0.436332313	40	123.76	4.885E-11
25				
25	0.436332313	45	0	1.766044443
25	0.436332313	45	20	1.623761488
25	0.436332313	45	25	1.547566022
25	0.436332313	45	30	1.458065497
25	0.436332313	45	35	1.357276583
25	0.436332313	45	40	1.247443955
25	0.436332313	45	45	1.130978318
25	0.436332313	45	50	1.010390205
25	0.436332313	45	55	0.888221526
25	0.436332313	45	60	0.766976868
25	0.436332313	45	65	0.649056588
25	0.436332313	45	70	0.536693648
25	0.436332313	45	75	0.431896038
25	0.436332313	45	80	0.336396471
25	0.436332313	45	85	0.251610776
25	0.436332313	45	90	0.178606195
25	0.436332313	45	95	0.118080432
25	0.436332313	45	110	0.012688387
25	0.436332313	45	105	0.035362256
25	0.436332313	45	110	0.012688387
25	0.436332313	45	117.794	1.53122E-10

semi	semi[rad]	AoA	meridian	cp
30	0.523598776	0	0	0.5
30	0.523598776	3	45	0.564695113
30	0.523598776	3	90	0.498630474
30	0.523598776	3	95	0.49077197
30	0.523598776	3	100	0.483034982
30	0.523598776	3	105	0.475476282
30	0.523598776	3	110	0.468149951
30	0.523598776	3	115	0.461107067
30	0.523598776	3	120	0.454395466
30	0.523598776	3	125	0.448059547
30	0.523598776	3	130	0.442140138
30	0.523598776	3	135	0.436674413
30	0.523598776	3	140	0.431695846
30	0.523598776	3	145	0.427234202
30	0.523598776	3	150	0.42331556
30	0.523598776	3	155	0.419962353
30	0.523598776	3	160	0.417193419
30	0.523598776	3	165	0.415024066
30	0.523598776	3	170	0.413466127
30	0.523598776	3	175	0.412528011
30	0.523598776	3	180	0.412214748
30				
30	0.523598776	5	0	0.657979857
30	0.523598776	5	45	0.608236388
30	0.523598776	5	90	0.496201938
30	0.523598776	5	95	0.483181684
30	0.523598776	5	100	0.470431654
30	0.523598776	5	105	0.45804303
30	0.523598776	5	110	0.446100539
30	0.523598776	5	115	0.434682098
30	0.523598776	5	120	0.423858618
30	0.523598776	5	125	0.413693945
30	0.523598776	5	130	0.404244941
30	0.523598776	5	135	0.395561673
30	0.523598776	5	140	0.387687697
30	0.523598776	5	145	0.380660409
30	0.523598776	5	150	0.374511444
30	0.523598776	5	155	0.369267103
30	0.523598776	5	160	0.364948773
30	0.523598776	5	165	0.361573326

30	0.523598776	5	170	0.35915348
30	0.523598776	5	175	0.357698094
30	0.523598776	5	180	0.35721239
30				
30	0.523598776	10	0	0.826351822
30	0.523598776	10	45	0.716982131
30	0.523598776	10	90	0.484923155
30	0.523598776	10	95	0.459451364
30	0.523598776	10	100	0.434852757
30	0.523598776	10	105	0.411291309
30	0.523598776	10	110	0.388908395
30	0.523598776	10	115	0.367822869
30	0.523598776	10	120	0.348131722
30	0.523598776	10	125	0.329911276
30	0.523598776	10	130	0.313218833
30	0.523598776	10	135	0.298094714
30	0.523598776	10	140	0.284564589
30	0.523598776	10	145	0.272641993
30	0.523598776	10	150	0.262330949
30	0.523598776	10	155	0.253628562
30	0.523598776	10	160	0.246527523
30	0.523598776	10	165	0.241018392
30	0.523598776	10	170	0.237091605
30	0.523598776	10	175	0.234739103
30	0.523598776	10	180	0.233955557
30				
30	0.523598776	15	0	1
30	0.523598776	15	45	0.822933042
30	0.523598776	15	90	0.466506351
30	0.523598776	15	95	0.429530073
30	0.523598776	15	100	0.394344356
30	0.523598776	15	105	0.361165364
30	0.523598776	15	110	0.330161323
30	0.523598776	15	115	0.301453795
30	0.523598776	15	120	0.275120237
30	0.523598776	15	125	0.251197688
30	0.523598776	15	130	0.229687458
30	0.523598776	15	135	0.210560607
30	0.523598776	15	140	0.193764017
30	0.523598776	15	145	0.179226839
30	0.523598776	15	150	0.166867061
30	0.523598776	15	155	0.156597995
30	0.523598776	15	160	0.148334419

30	0.523598776	15	165	0.141998199
30	0.523598776	15	170	0.137523161
30	0.523598776	15	175	0.134859075
30	0.523598776	15	180	0.133974596
30				
30	0.523598776	20	0	1.173648178
30	0.523598776	20	45	0.922869859
30	0.523598776	20	90	0.441511111
30	0.523598776	20	95	0.394326955
30	0.523598776	20	100	0.350137278
30	0.523598776	20	105	0.309188248
30	0.523598776	20	110	0.271644322
30	0.523598776	20	115	0.237591468
30	0.523598776	20	120	0.207042578
30	0.523598776	20	125	0.179944853
30	0.523598776	20	130	0.156188876
30	0.523598776	20	135	0.13561903
30	0.523598776	20	140	0.118044912
30	0.523598776	20	145	0.103253316
30	0.523598776	20	150	0.091020404
30	0.523598776	20	155	0.081123627
30	0.523598776	20	160	0.073353011
30	0.523598776	20	165	0.067521425
30	0.523598776	20	170	0.063473486
30	0.523598776	20	175	0.061092812
30	0.523598776	20	180	0.060307379
30				
30	0.523598776	25	0	1.342020143
30	0.523598776	25	45	1.01375605
30	0.523598776	25	90	0.410696902
30	0.523598776	25	95	0.354911639
30	0.523598776	25	100	0.303574733
30	0.523598776	25	105	0.256939258
30	0.523598776	25	110	0.215135403
30	0.523598776	25	115	0.178176312
30	0.523598776	25	120	0.145967252
30	0.523598776	25	125	0.118317753
30	0.523598776	25	130	0.094956303
30	0.523598776	25	135	0.075547047
30	0.523598776	25	140	0.059707961
30	0.523598776	25	145	0.047029844
30	0.523598776	25	150	0.03709554
30	0.523598776	25	155	0.029498708

30	0.523598776	25	160	0.02386157
30	0.523598776	25	165	0.019851009
30	0.523598776	25	170	0.017192542
30	0.523598776	25	175	0.015681665
30	0.523598776	25	180	0.015192247
30				
30	0.523598776	30	0	1.5
30	0.523598776	30	45	1.092830086
30	0.523598776	30	90	0.375
30	0.523598776	30	95	0.312481739
30	0.523598776	30	100	0.2560715
30	0.523598776	30	105	0.206005953
30	0.523598776	30	110	0.162351559
30	0.523598776	30	115	0.125013627
30	0.523598776	30	120	0.09375
30	0.523598776	30	125	0.068188896
30	0.523598776	30	130	0.047850259
30	0.523598776	30	135	0.032169914
30	0.523598776	30	140	0.020525701
30	0.523598776	30	145	0.012264744
30	0.523598776	30	150	0.006730947
30	0.523598776	30	155	0.003291837
30	0.523598776	30	160	0.001363867
30	0.523598776	30	165	0.000435393
30	0.523598776	30	170	8.65516E-05
30	0.523598776	30	175	5.43012E-06
30	0.523598776	30	180	0
30				
30	0.523598776	35	0	1.64278761
30	0.523598776	35	20	1.535982838
30	0.523598776	35	25	1.478401645
30	0.523598776	35	30	1.410388171
30	0.523598776	35	35	1.333262403
30	0.523598776	35	40	1.24849905
30	0.523598776	35	50	1.062500172
30	0.523598776	35	60	0.8657751
30	0.523598776	35	70	0.671567002
30	0.523598776	35	75	0.579188594
30	0.523598776	35	80	0.49169991
30	0.523598776	35	90	0.335505036
30	0.523598776	35	100	0.209070942
30	0.523598776	35	105	0.157935917
30	0.523598776	35	115	0.079718733

30	0.523598776	35	120	0.051977418
30	0.523598776	35	125	0.031081421
30	0.523598776	35	130	0.01630204
30	0.523598776	35	135	0.006805623
30	0.523598776	35	140	0.001688667
30	0.523598776	35	145.542	1.09714E-13
30				
30	0.523598776	40	0	1.766044443
30	0.523598776	40	20	1.642111577
30	0.523598776	40	25	1.575443637
30	0.523598776	40	30	1.496840759
30	0.523598776	40	35	1.407908843
30	0.523598776	40	40	1.31043961
30	0.523598776	40	45	1.2063631
30	0.523598776	40	50	1.09769687
30	0.523598776	40	55	0.986493408
30	0.523598776	40	60	0.874787277
30	0.523598776	40	65	0.764543527
30	0.523598776	40	70	0.657608862
30	0.523598776	40	75	0.55566697
30	0.523598776	40	80	0.460199278
30	0.523598776	40	85	0.372452238
30	0.523598776	40	90	0.293412044
30	0.523598776	40	100	0.164001145
30	0.523598776	40	110	0.074212427
30	0.523598776	40	120	0.021918745
30	0.523598776	40	125	0.008122821
30	0.523598776	40	133.476	4.56916E-11
30				
30	0.523598776	45	0	1.866025404
30	0.523598776	45	20	1.726064348
30	0.523598776	45	25	1.650930921
30	0.523598776	45	30	1.5625
30	0.523598776	45	35	1.462664034
30	0.523598776	45	40	1.353532015
30	0.523598776	45	45	1.237372436
30	0.523598776	45	50	1.116552333
30	0.523598776	45	55	0.993474211
30	0.523598776	45	60	0.870512702
30	0.523598776	45	65	0.749952797
30	0.523598776	45	70	0.633931467
30	0.523598776	45	75	0.524384342
30	0.523598776	45	80	0.422999

	30	0.523598776	45	85	0.33117618
	30	0.523598776	45	90	0.25
	30	0.523598776	45	100	0.122231534
	30	0.523598776	45	110	0.041535201
	30	0.523598776	45	115	0.017956496
	30	0.523598776	45	120	0.004487298
	30	0.523598776	45	125.264	2.31286E-11

semi		semi[rad]	AoA	meridian	cp
	35	0.610865238	0	0	0.657979857
	35	0.610865238	4	45	0.750518641
	35	0.610865238	4	90	0.654778149
	35	0.610865238	4	95	0.643429531
	35	0.610865238	4	100	0.632265362
	35	0.610865238	4	105	0.621367253
	35	0.610865238	4	110	0.610812668
	35	0.610865238	4	115	0.600674499
	35	0.610865238	4	120	0.591020737
	35	0.610865238	4	125	0.581914238
	35	0.610865238	4	130	0.573412558
	35	0.610865238	4	135	0.565567882
	35	0.610865238	4	140	0.558426999
	35	0.610865238	4	145	0.552031343
	35	0.610865238	4	150	0.54641707
	35	0.610865238	4	155	0.54161516
	35	0.610865238	4	160	0.537651541
	35	0.610865238	4	165	0.534547213
	35	0.610865238	4	170	0.532318368
	35	0.610865238	4	175	0.53097649
	35	0.610865238	4	180	0.530528437
	35				
	35	0.610865238	5	0	0.826351822
	35	0.610865238	5	45	0.773461629
	35	0.610865238	5	90	0.65298176
	35	0.610865238	5	95	0.638837479
	35	0.610865238	5	100	0.624953952
	35	0.610865238	5	105	0.611431606
	35	0.610865238	5	110	0.598364801
	35	0.610865238	5	115	0.585841379
	35	0.610865238	5	120	0.573942343
	35	0.610865238	5	125	0.562741676
	35	0.610865238	5	130	0.552306284

35	0.610865238	5	135	0.542696042
35	0.610865238	5	140	0.533963934
35	0.610865238	5	145	0.526156257
35	0.610865238	5	150	0.519312889
35	0.610865238	5	155	0.513467574
35	0.610865238	5	160	0.508648222
35	0.610865238	5	165	0.504877206
35	0.610865238	5	170	0.502171617
35	0.610865238	5	175	0.500543498
35	0.610865238	5	180	0.5
35				
35	0.610865238	10	0	1
35	0.610865238	10	45	0.885632505
35	0.610865238	10	90	0.638139336
35	0.610865238	10	95	0.610435412
35	0.610865238	10	100	0.583550113
35	0.610865238	10	105	0.557667264
35	0.610865238	10	110	0.532949904
35	0.610865238	10	115	0.509540077
35	0.610865238	10	120	0.487559149
35	0.610865238	10	125	0.467108612
35	0.610865238	10	130	0.448271312
35	0.610865238	10	135	0.431113027
35	0.610865238	10	140	0.415684326
35	0.610865238	10	145	0.402022614
35	0.610865238	10	150	0.390154281
35	0.610865238	10	155	0.380096855
35	0.610865238	10	160	0.371861085
35	0.610865238	10	165	0.365452853
35	0.610865238	10	170	0.360874859
35	0.610865238	10	175	0.358128
35	0.610865238	10	180	0.35721239
35				
35	0.610865238	15	0	1.173648178
35	0.610865238	15	45	0.991084228
35	0.610865238	15	90	0.613903564
35	0.610865238	15	95	0.573636638
35	0.610865238	15	100	0.535026374
35	0.610865238	15	105	0.498320435
35	0.610865238	15	110	0.463722765
35	0.610865238	15	115	0.431394327
35	0.610865238	15	120	0.401454985
35	0.610865238	15	125	0.373986428

35	0.610865238	15	130	0.349035991
35	0.610865238	15	135	0.326621203
35	0.610865238	15	140	0.306734899
35	0.610865238	15	145	0.289350665
35	0.610865238	15	150	0.274428451
35	0.610865238	15	155	0.261920104
35	0.610865238	15	160	0.251774653
35	0.610865238	15	165	0.243943137
35	0.610865238	15	170	0.238382813
35	0.610865238	15	175	0.235060585
35	0.610865238	15	180	0.233955557
35				
35	0.610865238	20	0	1.342020143
35	0.610865238	20	45	1.086612701
35	0.610865238	20	90	0.581010835
35	0.610865238	20	95	0.52955927
35	0.610865238	20	100	0.480857104
35	0.610865238	20	105	0.435194341
35	0.610865238	20	110	0.392786815
35	0.610865238	20	115	0.353778548
35	0.610865238	20	120	0.318246082
35	0.610865238	20	125	0.286204594
35	0.610865238	20	130	0.257615535
35	0.610865238	20	135	0.232395503
35	0.610865238	20	140	0.210426026
35	0.610865238	20	145	0.191563891
35	0.610865238	20	150	0.17565167
35	0.610865238	20	155	0.162528059
35	0.610865238	20	160	0.152037691
35	0.610865238	20	165	0.144040069
35	0.610865238	20	170	0.138417336
35	0.610865238	20	175	0.135080596
35	0.610865238	20	180	0.133974596
35				
35	0.610865238	25	0	1.5
35	0.610865238	25	45	1.169315341
35	0.610865238	25	90	0.540460578
35	0.610865238	25	95	0.479542577
35	0.610865238	25	100	0.42268821
35	0.610865238	25	105	0.370207037
35	0.610865238	25	110	0.322297407
35	0.610865238	25	115	0.279051056
35	0.610865238	25	120	0.240460701

35	0.610865238	25	125	0.206430316
35	0.610865238	25	130	0.176787709
35	0.610865238	25	135	0.151298926
35	0.610865238	25	140	0.129684004
35	0.610865238	25	145	0.111633493
35	0.610865238	25	150	0.09682522
35	0.610865238	25	155	0.084940698
35	0.610865238	25	160	0.075680656
35	0.610865238	25	165	0.068779154
35	0.610865238	25	170	0.06401583
35	0.610865238	25	175	0.061225873
35	0.610865238	25	180	0.060307379
35				
35	0.610865238	30	0	1.64278761
35	0.610865238	30	45	1.236679269
35	0.610865238	30	90	0.493484893
35	0.610865238	30	95	0.425106289
35	0.610865238	30	100	0.362287123
35	0.610865238	30	105	0.30533313
35	0.610865238	30	110	0.254396327
35	0.610865238	30	115	0.209482409
35	0.610865238	30	120	0.170462311
35	0.610865238	30	125	0.137087496
35	0.610865238	30	130	0.109008425
35	0.610865238	30	135	0.085795551
35	0.610865238	30	140	0.066962138
35	0.610865238	30	145	0.051988116
35	0.610865238	30	150	0.040344204
35	0.610865238	30	155	0.031515475
35	0.610865238	30	160	0.025023619
35	0.610865238	30	165	0.020447155
35	0.610865238	30	170	0.017438948
35	0.610865238	30	175	0.015740455
35	0.610865238	30	180	0.015192247
35				
35	0.610865238	35	0	1.766044443
35	0.610865238	35	45	1.286657667
35	0.610865238	35	90	0.441511111
35	0.610865238	35	95	0.367904426
35	0.610865238	35	100	0.3014891
35	0.610865238	35	105	0.242543779
35	0.610865238	35	110	0.191146713
35	0.610865238	35	115	0.147186414

35	0.610865238	35	120	0.110377778
35	0.610865238	35	125	0.08028308
35	0.610865238	35	130	0.056337123
35	0.610865238	35	135	0.037875665
35	0.610865238	35	140	0.0241662
35	0.610865238	35	145	0.014440055
35	0.610865238	35	150	0.007924768
35	0.610865238	35	155	0.003875686
35	0.610865238	35	160	0.001605767
35	0.610865238	35	165	0.000512616
35	0.610865238	35	170	0.000101903
35	0.610865238	35	175	6.39322E-06
35	0.610865238	35	180	0
35				
35	0.610865238	40	0	1.866025404
35	0.610865238	40	20	1.745352901
35	0.610865238	40	25	1.680285657
35	0.610865238	40	30	1.603420492
35	0.610865238	40	35	1.516243952
35	0.610865238	40	40	1.420416978
35	0.610865238	40	50	1.210066815
35	0.610865238	40	60	0.987449318
35	0.610865238	40	70	0.767492595
35	0.610865238	40	75	0.662777678
35	0.610865238	40	80	0.563535264
35	0.610865238	40	90	0.38611843
35	0.610865238	40	95	0.309675038
35	0.610865238	40	100	0.242141459
35	0.610865238	40	105	0.183746808
35	0.610865238	40	110	0.134470374
35	0.610865238	40	115	0.094055904
35	0.610865238	40	120	0.06203274
35	0.610865238	40	125	0.037743042
35	0.610865238	40	140	0.002596524
35	0.610865238	40	146.56	7.32986E-11
35				
35	0.610865238	45	0	1.939692621
35	0.610865238	45	20	1.804528954
35	0.610865238	45	25	1.731804184
35	0.610865238	45	30	1.646045163
35	0.610865238	45	35	1.548995576
35	0.610865238	45	40	1.442601113
35	0.610865238	45	45	1.328957989

	35	0.610865238	45	50	1.2102579
	35	0.610865238	45	55	1.088731028
	35	0.610865238	45	60	0.966588757
	35	0.610865238	45	65	0.845967746
	35	0.610865238	45	70	0.728877001
	35	0.610865238	45	75	0.617149427
	35	0.610865238	45	80	0.512399269
	35	0.610865238	45	85	0.415986612
	35	0.610865238	45	90	0.328989928
	35	0.610865238	45	100	0.186047447
	35	0.610865238	45	110	0.086089391
	35	0.610865238	45	120	0.026896136
	35	0.610865238	45	125	0.010759939
	35	0.610865238	45	134.44	1.39357E-09

semi	semi[rad]	AoA	meridian	cp
40	0.698131701	0	0	0.826351822
40	0.698131701	4	45	0.922101459
40	0.698131701	4	90	0.822330823
40	0.698131701	4	95	0.810428747
40	0.698131701	4	100	0.798703026
40	0.698131701	4	105	0.787239968
40	0.698131701	4	110	0.776122022
40	0.698131701	4	115	0.7654273
40	0.698131701	4	120	0.755229181
40	0.698131701	4	125	0.745595993
40	0.698131701	4	130	0.736590777
40	0.698131701	4	135	0.728271118
40	0.698131701	4	140	0.720689042
40	0.698131701	4	145	0.713890961
40	0.698131701	4	150	0.707917663
40	0.698131701	4	155	0.702804335
40	0.698131701	4	160	0.698580607
40	0.698131701	4	165	0.695270609
40	0.698131701	4	170	0.69289303
40	0.698131701	4	175	0.691461175
40	0.698131701	4	180	0.690983006
40				
40	0.698131701	5	0	1
40	0.698131701	5	45	0.945454721
40	0.698131701	5	90	0.820074752
40	0.698131701	5	95	0.805237963

40	0.698131701	5	100	0.79064799
40	0.698131701	5	105	0.776411292
40	0.698131701	5	110	0.76262874
40	0.698131701	5	115	0.749395078
40	0.698131701	5	120	0.73679851
40	0.698131701	5	125	0.724920408
40	0.698131701	5	130	0.713835133
40	0.698131701	5	135	0.703609959
40	0.698131701	5	140	0.694305077
40	0.698131701	5	145	0.685973675
40	0.698131701	5	150	0.678662068
40	0.698131701	5	155	0.672409863
40	0.698131701	5	160	0.667250148
40	0.698131701	5	165	0.66320968
40	0.698131701	5	170	0.660309058
40	0.698131701	5	175	0.658562881
40	0.698131701	5	180	0.657979857
40				
40	0.698131701	10	0	1.173648178
40	0.698131701	10	45	1.057299775
40	0.698131701	10	90	0.801434266
40	0.698131701	10	95	0.772346938
40	0.698131701	10	100	0.74401251
40	0.698131701	10	105	0.716628446
40	0.698131701	10	110	0.690373466
40	0.698131701	10	115	0.665407097
40	0.698131701	10	120	0.641869677
40	0.698131701	10	125	0.619882801
40	0.698131701	10	130	0.599550137
40	0.698131701	10	135	0.58095858
40	0.698131701	10	140	0.564179645
40	0.698131701	10	145	0.549271053
40	0.698131701	10	150	0.536278416
40	0.698131701	10	155	0.525236953
40	0.698131701	10	160	0.516173155
40	0.698131701	10	165	0.509106334
40	0.698131701	10	170	0.504049981
40	0.698131701	10	175	0.501012892
40	0.698131701	10	180	0.5
40				
40	0.698131701	15	0	1.342020143
40	0.698131701	15	45	1.158488627
40	0.698131701	15	90	0.770996746

40	0.698131701	15	95	0.728678124
40	0.698131701	15	100	0.687862379
40	0.698131701	15	105	0.648819755
40	0.698131701	15	110	0.611781439
40	0.698131701	15	115	0.57693981
40	0.698131701	15	120	0.544449688
40	0.698131701	15	125	0.514430516
40	0.698131701	15	130	0.486969328
40	0.698131701	15	135	0.462124386
40	0.698131701	15	140	0.439929321
40	0.698131701	15	145	0.420397594
40	0.698131701	15	150	0.403527121
40	0.698131701	15	155	0.389304866
40	0.698131701	15	160	0.377711241
40	0.698131701	15	165	0.368724136
40	0.698131701	15	170	0.362322443
40	0.698131701	15	175	0.358488932
40	0.698131701	15	180	0.35721239
40				
40	0.698131701	20	0	1.5
40	0.698131701	20	45	1.245946706
40	0.698131701	20	90	0.729687022
40	0.698131701	20	95	0.675558378
40	0.698131701	20	100	0.62390369
40	0.698131701	20	105	0.575045552
40	0.698131701	20	110	0.529240639
40	0.698131701	20	115	0.486681251
40	0.698131701	20	120	0.4474986
40	0.698131701	20	125	0.411767668
40	0.698131701	20	130	0.379513415
40	0.698131701	20	135	0.350718095
40	0.698131701	20	140	0.32532939
40	0.698131701	20	145	0.303269055
40	0.698131701	20	150	0.284441764
40	0.698131701	20	155	0.26874383
40	0.698131701	20	160	0.2560715
40	0.698131701	20	165	0.246328529
40	0.698131701	20	170	0.239432764
40	0.698131701	20	175	0.23532152
40	0.698131701	20	180	0.233955557
40				
40	0.698131701	25	0	1.64278761
40	0.698131701	25	45	1.317016642

40	0.698131701	25	90	0.678760267
40	0.698131701	25	95	0.614601714
40	0.698131701	25	100	0.554079794
40	0.698131701	25	105	0.497547429
40	0.698131701	25	110	0.445259026
40	0.698131701	25	115	0.397373881
40	0.698131701	25	120	0.353962223
40	0.698131701	25	125	0.315013615
40	0.698131701	25	130	0.280447392
40	0.698131701	25	135	0.250124729
40	0.698131701	25	140	0.223861911
40	0.698131701	25	145	0.201444327
40	0.698131701	25	150	0.182640694
40	0.698131701	25	155	0.167217031
40	0.698131701	25	160	0.154949896
40	0.698131701	25	165	0.145638441
40	0.698131701	25	170	0.139114885
40	0.698131701	25	175	0.135253035
40	0.698131701	25	180	0.133974596
40				
40	0.698131701	30	0	1.766044443
40	0.698131701	30	45	1.369539011
40	0.698131701	30	90	0.619763867
40	0.698131701	30	95	0.547660271
40	0.698131701	30	100	0.480512256
40	0.698131701	30	105	0.418680128
40	0.698131701	30	110	0.362388338
40	0.698131701	30	115	0.311731259
40	0.698131701	30	120	0.266682612
40	0.698131701	30	125	0.227108181
40	0.698131701	30	130	0.192781331
40	0.698131701	30	135	0.163400767
40	0.698131701	30	140	0.138609923
40	0.698131701	30	145	0.118017302
40	0.698131701	30	150	0.101217085
40	0.698131701	30	155	0.08780931
40	0.698131701	30	160	0.077418956
40	0.698131701	30	165	0.06971329
40	0.698131701	30	170	0.064416913
40	0.698131701	30	175	0.061324007
40	0.698131701	30	180	0.060307379
40				
40	0.698131701	35	0	1.866025404

40	0.698131701	35	45	1.401917948
40	0.698131701	35	90	0.554490396
40	0.698131701	35	95	0.47676803
40	0.698131701	35	100	0.405436388
40	0.698131701	35	105	0.340839991
40	0.698131701	35	110	0.283146561
40	0.698131701	35	115	0.232355593
40	0.698131701	35	120	0.188311714
40	0.698131701	35	125	0.150722327
40	0.698131701	35	130	0.119178919
40	0.698131701	35	135	0.093181272
40	0.698131701	35	140	0.072163764
40	0.698131701	35	145	0.055522869
40	0.698131701	35	150	0.042644952
40	0.698131701	35	155	0.03293343
40	0.698131701	35	160	0.025834419
40	0.698131701	35	165	0.020860022
40	0.698131701	35	170	0.017608509
40	0.698131701	35	175	0.015780733
40	0.698131701	35	180	0.015192247
40				
40	0.698131701	40	0	1.939692621
40	0.698131701	40	45	1.413169636
40	0.698131701	40	90	0.484923155
40	0.698131701	40	95	0.404079016
40	0.698131701	40	100	0.331133333
40	0.698131701	40	105	0.266392151
40	0.698131701	40	110	0.209941415
40	0.698131701	40	115	0.161658673
40	0.698131701	40	120	0.121230789
40	0.698131701	40	125	0.088176999
40	0.698131701	40	130	0.06187653
40	0.698131701	40	135	0.04159983
40	0.698131701	40	140	0.026542367
40	0.698131701	40	145	0.015859889
40	0.698131701	40	150	0.008703979
40	0.698131701	40	155	0.004256767
40	0.698131701	40	160	0.001763656
40	0.698131701	40	165	0.00056302
40	0.698131701	40	170	0.000111922
40	0.698131701	40	175	7.02184E-06
40	0.698131701	40	180	0
40				

40	0.698131701	45	0	1.984807753
40	0.698131701	45	20	1.8567712
40	0.698131701	45	25	1.787728518
40	0.698131701	45	30	1.70616251
40	0.698131701	45	35	1.613648069
40	0.698131701	45	40	1.511944929
40	0.698131701	45	50	1.28865971
40	0.698131701	45	60	1.05228581
40	0.698131701	45	70	0.818645378
40	0.698131701	45	75	0.707372674
40	0.698131701	45	80	0.601880894
40	0.698131701	45	90	0.413175911
40	0.698131701	45	95	0.331801848
40	0.698131701	45	100	0.259860751
40	0.698131701	45	105	0.197598669
40	0.698131701	45	110	0.144997201
40	0.698131701	45	115	0.101788588
40	0.698131701	45	120	0.067478057
40	0.698131701	45	125	0.041372605
40	0.698131701	45	140	0.003131916
40	0.698131701	45	147.04	1.41114E-09

semi	semi[rad]	AoA	meridian	cp
45	0.785398163	0	0	1
45	0.785398163	4	45	1.095977261
45	0.785398163	4	90	0.995134034
45	0.785398163	4	95	0.983041262
45	0.785398163	4	100	0.971113606
45	0.785398163	4	105	0.959439343
45	0.785398163	4	110	0.94810324
45	0.785398163	4	115	0.937186032
45	0.785398163	4	120	0.926763975
45	0.785398163	4	125	0.916908477
45	0.785398163	4	130	0.907685789
45	0.785398163	4	135	0.899156774
45	0.785398163	4	140	0.89137672
45	0.785398163	4	145	0.884395216
45	0.785398163	4	150	0.878256068
45	0.785398163	4	155	0.872997243
45	0.785398163	4	160	0.868650854
45	0.785398163	4	165	0.86524315
45	0.785398163	4	170	0.862794524

45	0.785398163	4	175	0.861319532
45	0.785398163	4	180	0.860826899
45				
45	0.785398163	5	0	1.173648178
45	0.785398163	5	45	1.118989742
45	0.785398163	5	90	0.992403877
45	0.785398163	5	95	0.977327142
45	0.785398163	5	100	0.962479238
45	0.785398163	5	105	0.947969265
45	0.785398163	5	110	0.93390128
45	0.785398163	5	115	0.9203737
45	0.785398163	5	120	0.907478819
45	0.785398163	5	125	0.895302422
45	0.785398163	5	130	0.883923515
45	0.785398163	5	135	0.873414134
45	0.785398163	5	140	0.863839243
45	0.785398163	5	145	0.855256692
45	0.785398163	5	150	0.847717236
45	0.785398163	5	155	0.84126459
45	0.785398163	5	160	0.835935511
45	0.785398163	5	165	0.831759897
45	0.785398163	5	170	0.828760877
45	0.785398163	5	175	0.826954905
45	0.785398163	5	180	0.826351822
45				
45	0.785398163	10	0	1.342020143
45	0.785398163	10	45	1.226767918
45	0.785398163	10	90	0.96984631
45	0.785398163	10	95	0.940266342
45	0.785398163	10	100	0.911364381
45	0.785398163	10	105	0.883344898
45	0.785398163	10	110	0.856395844
45	0.785398163	10	115	0.830687988
45	0.785398163	10	120	0.806374661
45	0.785398163	10	125	0.783591876
45	0.785398163	10	130	0.762458778
45	0.785398163	10	135	0.743078393
45	0.785398163	10	140	0.725538592
45	0.785398163	10	145	0.70991324
45	0.785398163	10	150	0.696263445
45	0.785398163	10	155	0.684638845
45	0.785398163	10	160	0.675078884
45	0.785398163	10	165	0.667613996

45	0.785398163	10	170	0.662266666
45	0.785398163	10	175	0.659052295
45	0.785398163	10	180	0.657979857
45				
45				
45	0.785398163	15	0	1.5
45	0.785398163	15	45	1.320059742
45	0.785398163	15	90	0.933012702
45	0.785398163	15	95	0.889943674
45	0.785398163	15	100	0.848208527
45	0.785398163	15	105	0.808090477
45	0.785398163	15	110	0.769838656
45	0.785398163	15	115	0.733667917
45	0.785398163	15	120	0.699759526
45	0.785398163	15	125	0.66826263
45	0.785398163	15	130	0.639296435
45	0.785398163	15	135	0.61295296
45	0.785398163	15	140	0.589300241
45	0.785398163	15	145	0.568385831
45	0.785398163	15	150	0.550240474
45	0.785398163	15	155	0.53488176
45	0.785398163	15	160	0.522317664
45	0.785398163	15	165	0.512549789
45	0.785398163	15	170	0.505576209
45	0.785398163	15	175	0.501393807
45	0.785398163	15	180	0.5
45				
45	0.785398163	20	0	1.64278761
45	0.785398163	20	45	1.396030588
45	0.785398163	20	90	0.883022222
45	0.785398163	20	95	0.827888168
45	0.785398163	20	100	0.774930636
45	0.785398163	20	105	0.724492572
45	0.785398163	20	110	0.676859712
45	0.785398163	20	115	0.632261395
45	0.785398163	20	120	0.590872861
45	0.785398163	20	125	0.552818906
45	0.785398163	20	130	0.518178711
45	0.785398163	20	135	0.486991633
45	0.785398163	20	140	0.459263723
45	0.785398163	20	145	0.434974705
45	0.785398163	20	150	0.414085156
45	0.785398163	20	155	0.396543628

45	0.785398163	20	160	0.382293426
45	0.785398163	20	165	0.371278822
45	0.785398163	20	170	0.363450467
45	0.785398163	20	175	0.358769814
45	0.785398163	20	180	0.35721239
45				
45	0.785398163	25	0	1.766044443
45	0.785398163	25	45	1.452372123
45	0.785398163	25	90	0.821393805
45	0.785398163	25	95	0.755985347
45	0.785398163	25	100	0.693757219
45	0.785398163	25	105	0.63509126
45	0.785398163	25	110	0.580284131
45	0.785398163	25	115	0.529549607
45	0.785398163	25	120	0.483023132
45	0.785398163	25	125	0.440768402
45	0.785398163	25	130	0.402785706
45	0.785398163	25	135	0.369021682
45	0.785398163	25	140	0.339380134
45	0.785398163	25	145	0.313733489
45	0.785398163	25	150	0.291934503
45	0.785398163	25	155	0.273827783
45	0.785398163	25	160	0.259260734
45	0.785398163	25	165	0.248093542
45	0.785398163	25	170	0.240207857
45	0.785398163	25	175	0.235513873
45	0.785398163	25	180	0.233955557
45				
45				
45	0.785398163	30	0	1.866025404
45	0.785398163	30	45	1.487372436
45	0.785398163	30	90	0.75
45	0.785398163	30	95	0.676419944
45	0.785398163	30	100	0.607154689
45	0.785398163	30	105	0.542602956
45	0.785398163	30	110	0.483046312
45	0.785398163	30	115	0.428653398
45	0.785398163	30	120	0.379487298
45	0.785398163	30	125	0.335515717
45	0.785398163	30	130	0.296623579
45	0.785398163	30	135	0.262627564
45	0.785398163	30	140	0.233292074
45	0.785398163	30	145	0.208346038

45	0.785398163	30	150	0.1875
45	0.785398163	30	155	0.170462884
45	0.785398163	30	160	0.156957874
45	0.785398163	30	165	0.146736872
45	0.785398163	30	170	0.139593046
45	0.785398163	30	175	0.135371053
45	0.785398163	30	180	0.133974596
45				
45				
45	0.785398163	35	0	1.939692621
45	0.785398163	35	45	1.49996806
45	0.785398163	35	90	0.671010072
45	0.785398163	35	95	0.591609511
45	0.785398163	35	100	0.517754421
45	0.785398163	35	105	0.449837871
45	0.785398163	35	110	0.388100778
45	0.785398163	35	115	0.332638449
45	0.785398163	35	120	0.283411243
45	0.785398163	35	125	0.2402589
45	0.785398163	35	130	0.202918012
45	0.785398163	35	135	0.171042011
45	0.785398163	35	140	0.144222976
45	0.785398163	35	145	0.122014496
45	0.785398163	35	150	0.103954837
45	0.785398163	35	155	0.089589621
45	0.785398163	35	160	0.078493267
45	0.785398163	35	165	0.070288482
45	0.785398163	35	170	0.064663161
45	0.785398163	35	175	0.061384145
45	0.785398163	35	180	0.060307379
45				
45				
45	0.785398163	40	0	1.984807753
45	0.785398163	40	45	1.489776285
45	0.785398163	40	90	0.586824089
45	0.785398163	40	95	0.504130973
45	0.785398163	40	100	0.428272795
45	0.785398163	40	105	0.359614625
45	0.785398163	40	110	0.2983324
45	0.785398163	40	115	0.244422126
45	0.785398163	40	120	0.19771419
45	0.785398163	40	125	0.157892281
45	0.785398163	40	130	0.124516201

45	0.785398163	40	135	0.097047804
45	0.785398163	40	140	0.07487916
45	0.785398163	40	145	0.057362002
45	0.785398163	40	150	0.04383749
45	0.785398163	40	155	0.033665287
45	0.785398163	40	160	0.026251021
45	0.785398163	40	165	0.02107122
45	0.785398163	40	170	0.017694911
45	0.785398163	40	175	0.015801203
45	0.785398163	40	180	0.015192247
45				
45				
45	0.785398163	45	0	2
45	0.785398163	45	45	1.457106781
45	0.785398163	45	90	0.5
45	0.785398163	45	95	0.416642319
45	0.785398163	45	100	0.341428667
45	0.785398163	45	105	0.274674604
45	0.785398163	45	110	0.216468746
45	0.785398163	45	115	0.166684836
45	0.785398163	45	120	0.125
45	0.785398163	45	125	0.090918528
45	0.785398163	45	130	0.063800346
45	0.785398163	45	135	0.042893219
45	0.785398163	45	140	0.027367601
45	0.785398163	45	145	0.016352992
45	0.785398163	45	150	0.008974596
45	0.785398163	45	155	0.004389115
45	0.785398163	45	160	0.00181849
45	0.785398163	45	165	0.000580525
45	0.785398163	45	170	0.000115402
45	0.785398163	45	175	7.24016E-06
45	0.785398163	45	180	0

Appendix 4 – Calculations for aerodynamic coefficients (Fig 13 & 21)

semi	AoA	AoA[rad]	Cn	Cl	Cd
5	1	0.017453293	0.0483	0.096585287	0.001685902
5	2	0.034906585	0.0508	0.101538108	0.003545789
5	3	0.052359878	0.0552	0.110248701	0.00577789
5	4	0.06981317	0.0614	0.122500865	0.008566095
5	5	0.087266463	0.0695	0.138471063	0.012114648
5	10	0.174532925	0.1314	0.258807477	0.045634741
5	15	0.261799388	0.2138	0.413029883	0.110671024
5	20	0.34906585	0.3138	0.589751089	0.214651842
5	25	0.436332313	0.4288	0.777249558	0.362437421
5	30	0.523598776	0.5546	0.960595378	0.5546
5	35	0.610865238	0.6878	1.126825552	0.789011746
5	40	0.698131701	0.8269	1.2668843	1.063042149
5	45	0.785398163	0.9623	1.360897711	1.360897711
5	50	0.872664626	1.0948	1.40744775	1.677330913

semi	AoA	AoA[rad]	Cn	Cl	Cd
10	1	0.017453293	0.1897	0.379342216	0.006621443
10	2	0.034906585	0.1917	0.383166443	0.013380467
10	3	0.052359878	0.1954	0.390264422	0.020452892
10	4	0.06981317	0.2009	0.400821235	0.028028151
10	5	0.087266463	0.2081	0.414616233	0.03627422
10	10	0.174532925	0.2696	0.53100834	0.093631097
10	15	0.261799388	0.3726	0.719807926	0.192871952
10	20	0.34906585	0.4882	0.917515875	0.333948468
10	25	0.436332313	0.6151	1.11493984	0.519904986
10	30	0.523598776	0.7487	1.29678644	0.7487
10	35	0.610865238	0.8874	1.453831048	1.017983459
10	40	0.698131701	1.0218	1.565488424	1.313600759
10	45	0.785398163	1.1528	1.630305395	1.630305395
10	50	0.872664626	1.2711	1.634094661	1.947438183

semi	AoA	AoA[rad]	Cn	Cl	Cd
15	1	0.017453293	0.4207	0.841271851	0.014684455
15	2	0.034906585	0.4221	0.843685736	0.029462155
15	3	0.052359878	0.425	0.848835105	0.044485563
15	4	0.06981317	0.4295	0.856907519	0.059920811
15	5	0.087266463	0.4355	0.867685582	0.075912652

	15	10	0.174532925	0.488	0.961172367	0.169480621
	15	15	0.261799388	0.5762	1.113132922	0.298263068
	15	20	0.34906585	0.7068	1.328349489	0.483479675
	15	25	0.436332313	0.8357	1.514802835	0.706364163
	15	30	0.523598776	0.9727	1.684765821	0.9727
	15	35	0.610865238	1.1046	1.809670696	1.267145063
	15	40	0.698131701	1.2292	1.883243659	1.58022906
	15	45	0.785398163	1.3428	1.899005972	1.899005972
	15	50	0.872664626	1.4428	1.854827927	2.210497845

semi	AoA		AoA[rad]	Cn	Cl	Cd
	20	1	0.017453293	0.7344	1.468576295	0.025634095
	20	2	0.034906585	0.7351	1.469304394	0.05130924
	20	3	0.052359878	0.7371	1.47217966	0.077153667
	20	4	0.06981317	0.7403	1.476993333	0.103281435
	20	5	0.087266463	0.7447	1.483732383	0.129809763
	20	10	0.174532925	0.7852	1.546542095	0.272697098
	20	15	0.261799388	0.855	1.651733163	0.442580567
	20	20	0.34906585	0.9523	1.789738566	0.651411565
	20	25	0.436332313	1.0907	1.977019807	0.921899476
	20	30	0.523598776	1.213	2.10097763	1.213
	20	35	0.610865238	1.3297	2.178452947	1.525369175
	20	40	0.698131701	1.4372	2.201918147	1.847628705
	20	45	0.785398163	1.5267	2.159079846	2.159079846
	20	50	0.872664626	1.6001	2.057048909	2.451495427

semi	AoA		AoA[rad]	Cn	Cl	Cd
	25	1	0.017453293	1.1212	2.242058472	0.039135276
	25	2	0.034906585	1.1212	2.241033991	0.078258631
	25	3	0.052359878	1.1221	2.241124402	0.117452353
	25	4	0.06981317	1.1238	2.242124959	0.15678465
	25	5	0.087266463	1.1264	2.244227416	0.196344457
	25	10	0.174532925	1.1527	2.270375794	0.400328509
	25	15	0.261799388	1.2002	2.318608353	0.621269236
	25	20	0.34906585	1.2675	2.382120794	0.867021063
	25	25	0.436332313	1.3525	2.451562564	1.143182398
	25	30	0.523598776	1.4777	2.559451478	1.4777
	25	35	0.610865238	1.5707	2.573284232	1.801833017
	25	40	0.698131701	1.6505	2.528712707	2.1218419

	25	45	0.785398163	1.7145	2.424669153	2.424669153
	25	50	0.872664626	1.7543	2.255284607	2.687743533

semi	AoA		AoA[rad]	Cn	Cl	Cd
	30	1	0.017453293	1.5694	3.138321946	0.054779613
	30	2	0.034906585	1.5686	3.135288903	0.109486701
	30	3	0.052359878	1.5683	3.132301399	0.16415696
	30	4	0.06981317	1.5684	3.129158913	0.218812107
	30	5	0.087266463	1.569	3.126058963	0.273494721
	30	10	0.174532925	1.5792	3.110416807	0.548450404
	30	15	0.261799388	1.6011	3.093087681	0.828790346
	30	20	0.34906585	1.6341	3.071103423	1.117790232
	30	25	0.436332313	1.677	3.039756318	1.41746165
	30	30	0.523598776	1.7286	2.994023026	1.7286
	30	35	0.610865238	1.8195	2.980894289	2.087244652
	30	40	0.698131701	1.8643	2.856273311	2.396697881
	30	45	0.785398163	1.8903	2.673287897	2.673287897
	30	50	0.872664626	1.8969	2.438607634	2.906219408

semi	AoA		AoA[rad]	Cn	Cl	Cd
	35	1	0.017453293	2.0654	4.130170859	0.072092401
	35	2	0.034906585	2.0637	4.124885699	0.144044183
	35	3	0.052359878	2.0621	4.118547927	0.215843951
	35	4	0.06981317	2.0605	4.110961451	0.287466428
	35	5	0.087266463	2.059	4.102329767	0.358907349
	35	10	0.174532925	2.0518	4.041257095	0.712582662
	35	15	0.261799388	2.0457	3.951988926	1.058932241
	35	20	0.34906585	2.0409	3.83563734	1.396057821
	35	25	0.436332313	2.0374	3.693022971	1.722084893
	35	30	0.523598776	2.0355	3.525589419	2.0355
	35	35	0.610865238	2.03526	3.334374779	2.334754356
	35	40	0.698131701	2.074	3.17755235	2.666283005
	35	45	0.785398163	2.0567	2.908613034	2.908613034
	35	50	0.872664626	2.0184	2.594805023	3.092368208

semi	AoA		AoA[rad]	Cn	Cl	Cd
	40	1	0.017453293	2.594	5.187209842	0.090543085

	40	2	0.034906585	2.5916	5.180042535	0.180891071
	40	3	0.052359878	2.5887	5.170304553	0.27096418
	40	4	0.06981317	2.5853	5.158004678	0.360682823
	40	5	0.087266463	2.5815	5.143353226	0.4499851
	40	10	0.174532925	2.556	5.034337233	0.887689484
	40	15	0.261799388	2.5203	4.86884572	1.304603279
	40	20	0.34906585	2.4755	4.652418166	1.69334173
	40	25	0.436332313	2.4229	4.391786274	2.047923573
	40	30	0.523598776	2.3641	4.094741314	2.3641
	40	35	0.610865238	2.301	3.769737708	2.63959876
	40	40	0.698131701	2.2353	3.424678287	2.873646288
	40	45	0.785398163	2.2095	3.124704866	3.124704866
	40	50	0.872664626	2.1236	2.730047536	3.253543959

semi	AoA		AoA[rad]	Cn	Cl	Cd
	45	1	0.017453293	3.1393	6.277643739	0.109576679
	45	2	0.034906585	3.1361	6.268379145	0.218896623
	45	3	0.052359878	3.1319	6.25521568	0.327821963
	45	4	0.06981317	3.1268	6.238366545	0.436229084
	45	5	0.087266463	3.1207	6.217649589	0.543973853
	45	10	0.174532925	3.0766	6.059719066	1.068491967
	45	15	0.261799388	3.0107	5.81622577	1.558452998
	45	20	0.34906585	2.9248	5.496825955	2.00068103
	45	25	0.436332313	2.8217	5.114657365	2.385003898
	45	30	0.523598776	2.7044	4.684158204	2.7044
	45	35	0.610865238	2.5766	4.221254315	2.955754092
	45	40	0.698131701	2.442	3.74136106	3.139374686
	45	45	0.785398163	2.3048	3.259479419	3.259479419
	45	50	0.872664626	2.2095	2.840478447	3.385150394

semi	AoA		AoA[rad]	Cn	Cl	Cd
	50	1	0.017453293	3.6846	7.368077635	0.128610274
	50	2	0.034906585	3.6806	7.356715756	0.256902175
	50	3	0.052359878	3.6752	7.340326532	0.384690213
	50	4	0.06981317	3.6684	7.318927924	0.511789297
	50	5	0.087266463	3.6602	7.292543668	0.638014899
	50	10	0.174532925	3.5978	7.086282668	1.249502827
	50	15	0.261799388	3.5018	6.764958117	1.812665064
	50	20	0.34906585	3.3751	6.343113129	2.308704371

	50	25	0.436332313	3.2217	5.839703595	2.723098508
	50	30	0.523598776	3.046	5.27582676	3.046
	50	35	0.610865238	2.8536	4.675064547	3.273515438
	50	40	0.698131701	2.6502	4.060341966	3.407031446
	50	45	0.785398163	2.442	3.453509519	3.453509519
	50	50	0.872664626	2.2353	2.873646288	3.424678287

semi	AoA		AoA[rad]	Cn	Cl	Cd
	55	1	0.017453293	4.2134	8.425516558	0.147067939
	55	2	0.034906585	4.2088	8.412472226	0.293770003
	55	3	0.052359878	4.2023	8.393081788	0.439862778
	55	4	0.06981317	4.1938	8.367168228	0.585089399
	55	5	0.087266463	4.1835	8.335161039	0.7292321
	55	10	0.174532925	4.1036	8.082514191	1.425165324
	55	15	0.261799388	3.9787	7.68625817	2.059526669
	55	20	0.34906585	3.8128	7.165720049	2.608108805
	55	25	0.436332313	3.6107	6.544811053	3.051895515
	55	30	0.523598776	3.3786	5.851906858	3.3786
	55	35	0.610865238	3.1237	5.117570481	3.583361428
	55	40	0.698131701	2.8536	4.371968846	3.668517446
	55	45	0.785398163	2.5766	3.643862665	3.643862665
	55	50	0.872664626	2.301	2.95810858	3.525336527

semi	AoA		AoA[rad]	Cn	Cl	Cd
	60	1	0.017453293	4.7096	9.41776541	0.164387707
	60	2	0.034906585	4.7045	9.403268291	0.328369364
	60	3	0.052359878	4.6969	9.380926124	0.491633506
	60	4	0.06981317	4.687	9.351165407	0.653897185
	60	5	0.087266463	4.6748	9.314021949	0.814871332
	60	10	0.174532925	4.5787	9.018278517	1.590165822
	60	15	0.261799388	4.4271	8.552500451	2.291635589
	60	20	0.34906585	4.2244	7.939275014	2.889659787
	60	25	0.436332313	3.9769	7.208590877	3.36142113
	60	30	0.523598776	3.6921	6.394904787	3.6921
	60	35	0.610865238	3.3786	5.535174194	3.875770696
	60	40	0.698131701	3.046	4.666742747	3.915862118
	60	45	0.785398163	2.7044	3.824599158	3.824599158
	60	50	0.872664626	2.3641	3.039228376	3.622011336